THE DESIGN AND FABRICATION OF AN OMNI-DIRECTIONAL VEHICLE PLATFORM

By

CHRISTOPHER ROBERT FULMER

A THESIS PRESENTED TO THE GRADUATE SCHOOL
OF THE UNIVERSITY OF FLORIDA IN PARTIAL FULFILLMENT
OF THE REQUIREMENTS FOR THE DEGREE OF
MASTER OF SCIENCE

UNIVERSITY OF FLORIDA

2003

ACKNOWLEDGMENTS

The author would like to thank all of those who made his years at the University of Florida a memorable and interesting experience. In particular the author would like to express his deepest gratitude to Dr. Carl Crane for the dedication he has for his students and the engineering program as a whole.

The author would also like to thank Dr. John Zigert and Shannon Ridgway for their guidance and many suggestions throughout the development of this project. Thanks go to all the people of the Center for Intelligent Machines and Robotics for their help and friendship.

The author would like to thank his parents, Craig and Patty Fulmer, for their support and encouragement throughout the years. To his fiancee, Cindy, he wishes to extend his most heartfelt love and gratitude for inspiring him to make the most out of this opportunity.

TABLE OF CONTENTS

page

LIST OF TABLES

LIST OF FIGURES

Abstract of Thesis Presented to the Graduate School
of the University of Florida in Partial Fulfillment of the
Requirements for the Degree of Master of Science

DESIGN AND FABRICATION OF AN OMNI-DIRECTIONAL
VEHICLE PLATFORM

By

Christopher Robert Fulmer

August 2003

Chair: Dr. Carl D. Crane III
Major Department: Mechanical and Aerospace Engineering

The recent development in the area of screw theory based vehicle control has warranted the design of a new omni-directional vehicle. This novel approach to vehicle control is not limited to tracked, steered or even land vehicles. The objective of this work is to design and fabricate a high mobility vehicle (HMV) to serve as a test bed for this ongoing research. This paper describes the design and development of this new vehicle and focuses on the unique drive system that is being employed.

The drive system for the HMV consists of four independently driven and independently steered wheels. Each wheel is driven by a brushless DC motor, which is fabricated as part of a double stage epicyclic gear train in order to completely contain the drive system within the hub of the wheel. The methodology used in the design of the drive wheel will be summarized and its performance specifications will be given from a series of load tests.

CHAPTER 1
INTRODUCTION

Researchers at the University of Florida have been investigating autonomous vehicle technologies under the sponsorship of the Air Force Research Laboratory (AFRL) at Tyndall Air Force Base in Panama City, Florida. Research is ongoing in the areas of path planning, positioning systems, vehicle control, obstacle detection and mapping, multiple cooperative vehicle systems and system architecture. The resulting hardware and software systems are tested on research vehicles such as the Navigation Test Vehicle (NTV) shown in Figure 1-1, before being transitioned to AFRL vehicle systems.

Figure 1-1. Navigation test vehicle

The architecture used to interface these hardware and software technologies together complies with the Joint Architecture for Unmanned Systems (JAUS) standard. JAUS is a component based, message-passing architecture that specifies data formats and component behaviors that are independent of technology, computer hardware, operator

use, and type of vehicle platform. JAUS is designed to be used with any air, land, surface or underwater unmanned system.

The flexibility of JAUS in regards to the vehicle platform is due to the generic nature of the data string sent to the Primitive Driver Component. With this architecture the vehicle is treated as a rigid body with an arbitrary system of forces and moments acting upon it. These forces and moments yield an equivalent force and torque about the vehicles origin that can be used to characterize the motion of the vehicle. The ability to characterize the motion of any rigid body with six values becomes very important when standardized messaging for all types of vehicles is needed. The equivalent set of forces and moments that is passed to the Primitive Driver Component in this type of architecture is known as a wrench.

The test vehicles currently used for the research and development of this system architecture at the University of Florida are for the most part comprised of Ackerman steered and tracked vehicles. These vehicle systems are limited in their mobility due to the non-holonomic constraints of their wheels. In terms of the coordinate system in Figure 1-2 these vehicles are constrained to a translation on the X-axis and a moment about the Z-axis.

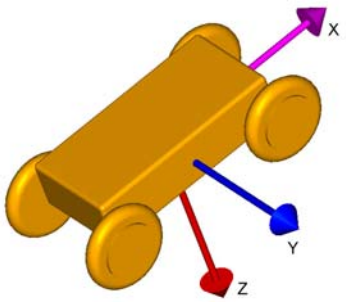

Figure 1-2. Vehicle coordinate system

A vehicle with the additional ability to translate along the Y-axis would be useful in traversing a heavily populated environment of obstacles. Figure 1-3 illustrates this point. The shaded circles to the right and left of the vehicle are inaccessible areas for Ackerman steered platforms due the mechanical limits that dictate the minimum turning radius. Tracked vehicles are also limited in their mobility because of the orientation change they must make to reach any point in this plane. A vehicle capable of translation to any point in a plane instantaneously is known as an omni-directional vehicle and would be valuable in the research of unmanned ground systems.

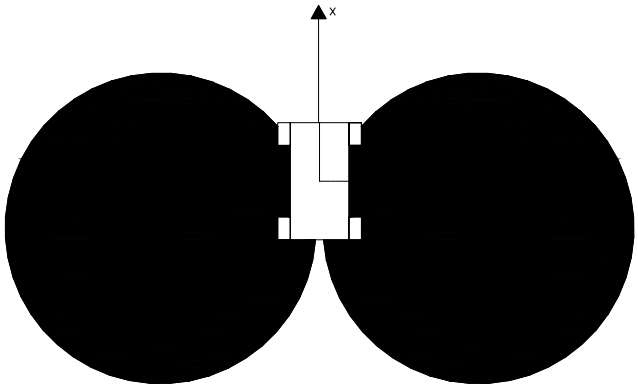

Figure 1-3. Mobility of Ackerman steered vehicle

Omni-directional Vehicle Platforms

The development of an omni-directional vehicle platform was pursued to further prove the effectiveness of this type of architecture and to add a ground vehicle platform that is capable of exceptional maneuverability. Omni directional vehicles are divided into two categories that describe the type of wheel arrangement they use for mobility. These two categories are summarized below.

Special Wheel Designs

Special wheel designs include the universal wheel, the Mecanum wheel, and the ball wheel mechanism. The universal wheel provides a combination of constrained and unconstrained motion during turning. The mechanism consists of small rollers located around the outer diameter of a wheel to allow for normal wheel rotation, yet be free to roll in the direction parallel to the wheels axis. The wheel is capable of this action because the rollers are mounted perpendicular to the axis of rotation of the wheel. When two or more of these wheels are mounted on a vehicle platform their combined constrained and unconstrained motion allows for omni-directional mobility. Figure 1-4 and 1-5 illustrate the mechanics of the universal wheel and a sample platform with two universal wheels. The traction wheel labeled (T) in the illustration is used to translate the platform while the rudder wheel (R) is used for steering. The other two wheels mounted parallel to the traction wheel are passive and provide platform stability.

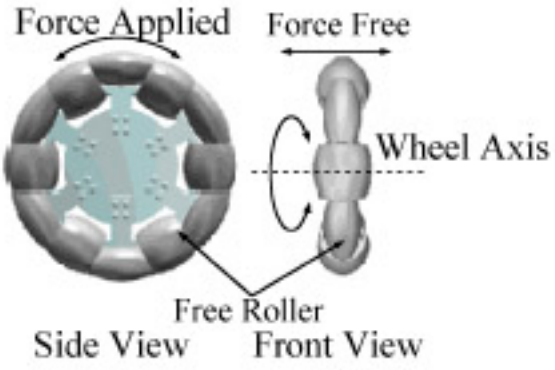

Figure 1-4. Universal wheel (Yamashita et al., 2001)

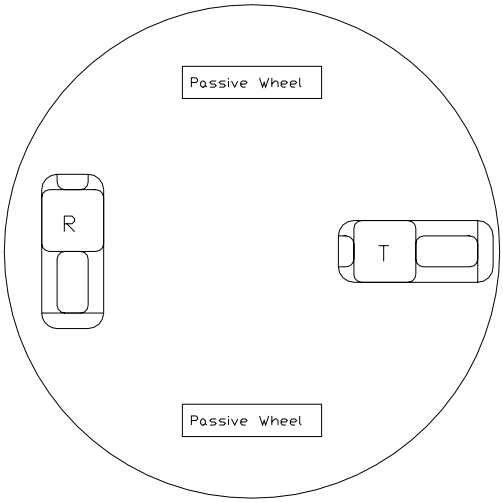

Figure 1-5. Universal wheel platform

The Mecanum wheel is similar to the universal wheel in design except that its rollers are mounted on angles as shown in Figure 1-6. This configuration transmits a portion of the force in the rotational direction of the wheel to a force normal to the direction of the wheel. The platform configuration consists of four wheels located similarly to that of an automobile. The forces due to the direction and speed of each of the four wheels can be summed into a total force vector, which allows for vehicle translation in any direction (Diegel et al., 2000).

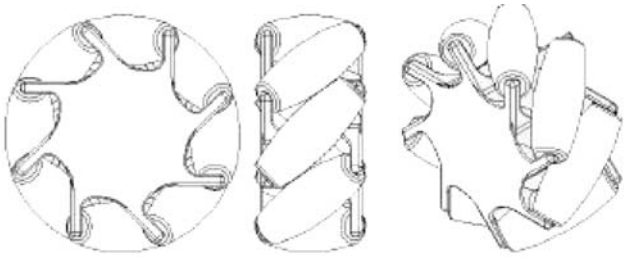

Figure 1-6. Mecanum wheel (Diegel et al., 2002)

Another special wheel design is the ball wheel mechanism. It uses an active ring driven by a motor and gearbox to transmit power through rollers and via friction to a ball that is capable of rotation in any direction instantaneously. An illustration of this type of wheel is shown in Figure 1-7. Each of these previously mentioned designs achieve

excellent maneuverability, but are limited to hard even surfaces due to the small roller diameters.

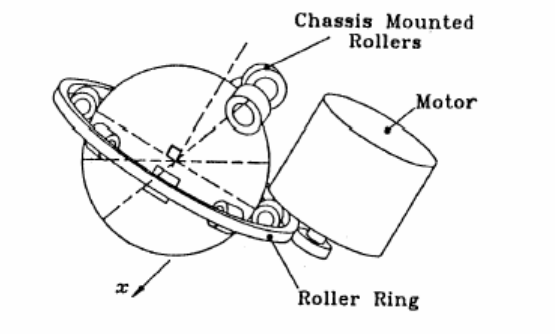

Figure 1-7. Ball wheel (Yu et al., 2000)

Conventional Wheel Designs

Conventional wheel designs have larger load capacities and a higher tolerance for ground irregularities compared to the special wheel configurations. However, due to their non-holonomic nature, they are not truly omni-directional wheels. These designs are not truly omni-directional because when a move with a non-continuous curve is encountered there is a finite amount of time before the steering motors can reorient the wheels to match the projected curve. The time constant of this process is assumed much faster than the gross vehicle dynamics for most applications. Therefore, it is assumed to be capable of zero-radius trajectories and retains the term omni-directional. Most platforms that contain conventional wheels and approximate omni-directional mobility incorporate at least two independently steered and independently driven wheels. Active castor wheels like the one shown in Figure 1-8 can be used to achieve this near omni-directional mobility. An example of a platform that uses this type of wheel arrangement is given in Figure 1-9. The platform shown in this figure was designed and built by Utah State University and is known as Technology II. It achieves omni-directional mobility via six independently steered and independently driven wheels.

Figure 1-8. Active castor wheel

Figure 1-9. Technology II (Utah State University)

Vehicle Criteria

Research in the area of highly mobile vehicle platforms that are capable of indoor and all-terrain activities is necessary to further develop control and path planning systems currently in use at the University of Florida. A conventional wheel arrangement with four independently driven and independently steered wheels would provide the necessary platform mobility to meet these research needs. The design of the drive system is critical for this research vehicle due to the size constraints given for indoor mobility and the power requirements needed for outdoor navigation. The focus of this paper is the design of a motorized wheel that can meet these needs.

Approach

The concept is to have four drive wheels, where the commonly unused space within the wheel hub of a wheel is used to mount a power train capable of propelling a 400 lb vehicle at a continuous speed of 7.33 ft/sec (5mph). An overview of the technology required to design and fabricate such a system is presented below. In the following chapters the specifics of the design and fabrication process will be addressed. This is concluded with a description of the method and apparatus used to test the drive unit and the performance specifications determined from these tests.

Background

Permanent-Magnet Motors

The most fundamental decision in the design of the drive wheel is the selection of the motor. The selection of the housings, bearings, gearing, cooling and motor control are all contingent upon the specifications of the motor. The two distinct types of motors that could be considered for this design are brushed and brushless permanent magnet DC motors. A brushed motor uses a pair of brushes and a commutator to switch the polarity of the windings in order to maintain a unidirectional torque. Some of the concerns with these motors include wear on the brushes and arcing due to the mechanical contact between the commutator and the brushes. This is dangerous in environments where fumes from flammable materials could be present. Brushed motors suffer small voltage losses due to the mechanical switching. They are also more difficult to cool in certain situations due to the generation of heat on the rotor.

Brushless motors use power transistors to perform the polarity switching necessary to produce a rotational motion. These switches excite the coils of the motor in

synchronism with rotor position. This type of motor is more costly but it is more efficient and maintenance free and, therefore, was selected for this research.

There are three physical configurations of permanent magnet DC brushless motors. The outer rotor configuration has a fixed armature winding on the stator with magnets mounted to an outer disk. These motors are generally used on applications where a constant rotational speed is desired. The large diameter rotor helps to increase the inertia which smoothes out speed variations. Outer rotor motors are more difficult to cool than other designs because there is very little conduction between the housing and heat-generating armature. Axial-gap disc motors are used in applications where there is a need for a thin low torque motor. The main advantage to this type of motor is their low cost, their flat shape and capability for very smooth rotation. Inner rotor motors consist of a rotating core spinning in the center of the stator. This configuration is common in servo systems due to the low inertia of the rotor thus allowing for quicker acceleration and deceleration. An iron core is used as a backing for the magnets. It is often enough to bond the magnets to the iron rotor, but in some high-speed situations the interior rotor may require a retaining can made out of stainless steel or some other high-resitivity alloy to prevent the magnets from flying apart. Figure 1-10 illustrates the three distinct types of brushless DC motors.

The DC brushless motor is basically a permanent magnet rotating past a series of current-carrying conductors known as phases. Brushless motors are available in two, three, and four phase configurations. The three phase motors are the most common and will be discussed further. Figure 1-11 illustrates the three types of three phase designs: delta bipolar, wye bipolar, and wye unipolar. It is shown from this figure how the

completion of the circuit through the transistor switches induces current flow in the phases.

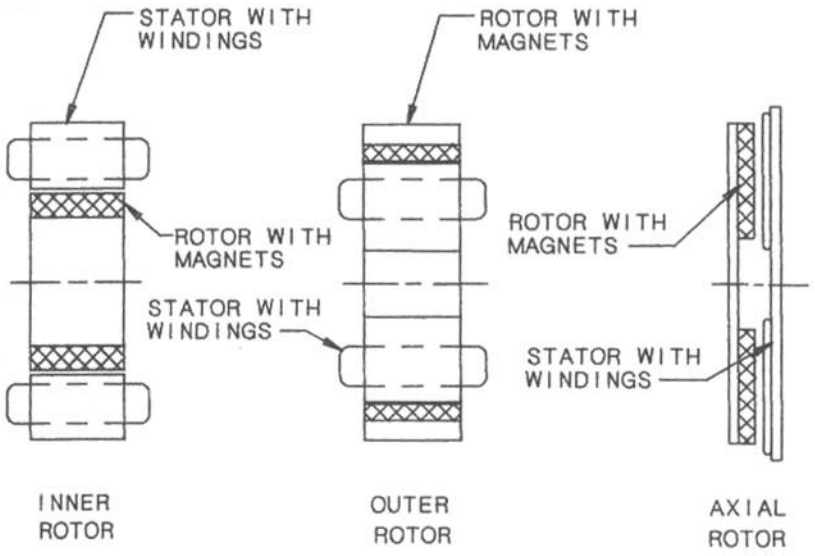

Figure 1-10. Brushless DC motor types (Hendershot and Miller, 1994)

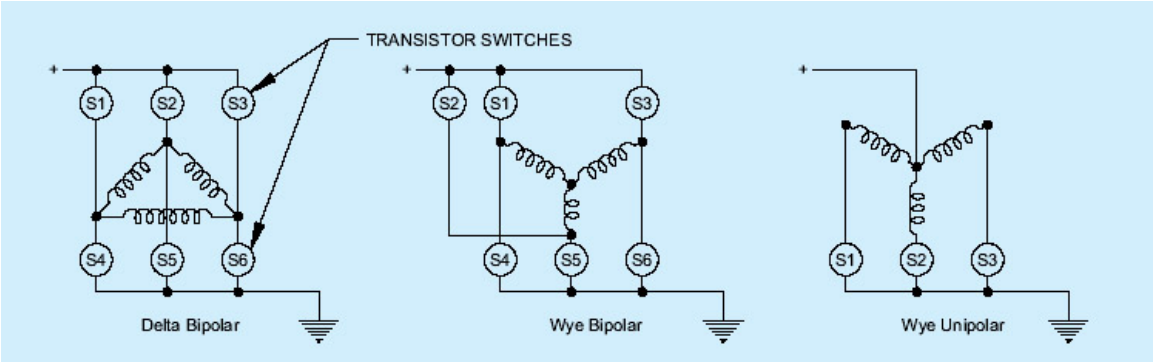

Figure 1-11. The three types of three phase designs (BEI)

When this energizing of the phases is completed sequentially a rotational motion is produced due to the desire of the permanent magnet to align itself with the zero torque position. The motor is said to operate with squarewave excitation because the DC current switches polarity in synchronism with the passage of alternate N and S magnet poles (Hendershot and Miller). The resultant output torque of a three phase bipolar configuration is shown in Figure 1-12.

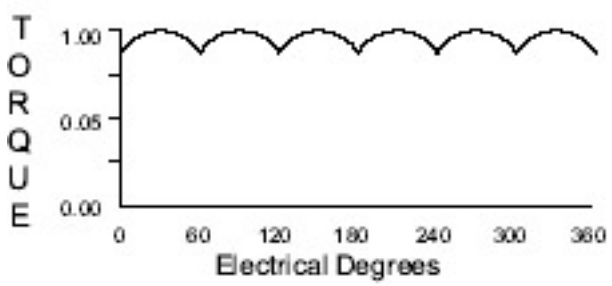

Figure 1-12. Effective torque ripple, three phase bipolar (BEI)

Performance characteristics

The speed-torque curve of a motor represents the steady-state capacity of the motor in driving various types of loads. The motor curve must be compatible with the speed torque curve of the load to ensure that the motor has enough torque to accelerate the load from standstill and maintain full speed without exceeding any thermal or electrical limits (Hendershot and Miller). The thermal and electrical limits are characterized by the boundary conditions on the curve.

When a motor rotates, a back electromotive force proportional to the speed of rotation is produced that directly opposes the applied voltage. Equation 1-1 relates the back-EMF (E) and speed (ω) with the back-EMF constant (k_E).

$$E = k_E \omega \qquad (1\text{-}1)$$

The applied voltage (V_S) in a DC motor is equal to the sum of the back-EMF and the resistive volt-drop in the motor windings as shown in Equation 1-2.

$$V_S = E + RI\,, \qquad (1\text{-}2)$$

where R is the resistance in the phases and I is the DC supply current. The maximum speed achievable for a motor with a constant supply voltage occurs at no load. Equation 1-3 gives the no load speed (ω_{NL}) by combining equations 1-1 and 1-2 and canceling out

the resistive voltage-drop due to the relationship between torque and current. The locked rotor torque (T_{LR}) is calculated from Equation 1-4. The two constants used in the following equations are given by the motor manufacture as the EMF constant (k_E) and the torque constant (k_T).

$$\omega_{NL} = \frac{V_S}{k_E} \tag{1-3}$$

$$T_{LR} = k_T I = k_T \frac{V_S}{R} \tag{1-4}$$

A motor speed-torque curve can be generated from the calculated values of the two previous equations due to their approximately linear relationship. Equation 1-3 shows that by adjusting the supply voltage to the motor the speed of the motor can be changed. As a load torque is applied, the current draw from the supply increases thereby increasing the resistive volt drop and decreasing the supply voltage available to the motor for maintaining its rotational speed. This explains the linear nature of the speed-torque curve. Figure 1-13 illustrates a sample speed-torque and power-torque curve where the maximum power output is defined by (P_{MAX}).

The ideal curve presented here cannot be obtained in a real motor but may be closely approached. Some of the losses that contribute to the non-linearity of the speed-torque curve include the core losses in the laminated iron, windage and bearing friction. The ideal curve provides the maximum theoretical performance characteristics of a motor at a constant supply voltage without taking into account any of the limiting factors such as the temperature and current limits of the materials. Typically only 30% of the locked-rotor torque may be obtained continuously due to these material limitations. Brief operation is permitted at slightly higher load levels for a short period of time provided the

accumulated heating effect does not cause the temperature to rise above the long term allowable temperature.

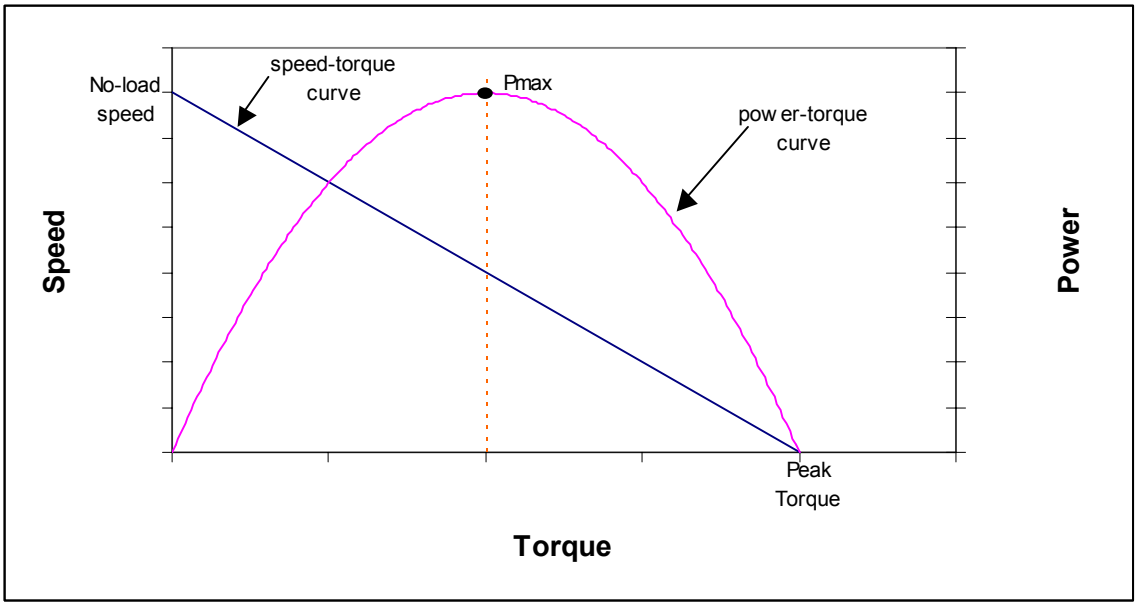

Figure 1-13. Permanent magnet dc motor characteristics

Cooling

Temperature limits the continuous load torque a motor is able to produce. If the temperature rises above the allowable value the winding insulation will begin to burn off and demagnetization of the permanent magnet will occur. Cooling increases the performance characteristics and the life of the motor. Most designs take advantage of the brushless motor's ability to conduct heat between the armature and the motor housing. Other modes of heat dissipation include natural convection and radiation. For high power density motors an oil mist, refrigerant or liquid coolant may be used to increase the power output without increasing the frame size. The life of the electrical insulation on the windings of the motor can be determined through statistical methods. The relationship between life and temperature is exponential and inversely related. For example, if the motor maintains a sustained $50°F$ increase in temperature the life of the motor windings

decreases by 50% (Hendershot and Miller). From this example, the importance proper cooling and rating of the motor is shown.

Position sensing

The brushless servo amplifier controls the excitation of the phases in the motor. In order for the amplifier to be in synchronization with the poles of the motor, the position of the rotor must be known. The most common position sensors include the resolver, encoder, and Hall-effect sensor. The resolver is an absolute position transducer that can give the rotor's position at any speed including zero. It provides a very fine resolution shaft position signal with a two-phase (sine/cosine) curve at the rotor frequency. Resolvers are very rugged and are similar in design to a brushless motor.

The second type of shaft position sensor is the optical encoder. Optical encoders also provide a very fine resolution shaft position signal through the use of phototransistors, photoemitters, and a code disk. Encoders can be purchased in both absolute and incremental configurations. Incremental encoders generate a quadrature output from the sensing of two out-of-phase tracks. They can only measure the relative position of the shaft, but are useful in the velocity control of brushless motors due to their high resolution. The absolute encoder is designed to produce a digital signal that distinguishes N distinct positions of the shaft. This type of encoder is much more expensive than the incremental encoder and is often unnecessary in servo applications where a homing sequence can be performed or only relative position is needed. The Hall-effect position sensor is the least expensive of the three sensors mentioned. This transducer is also the simplest shaft position sensor used in the generation of commutation pulses. A Hall switch is triggered by a magnetic field that is above a set threshold value. A three-phase motor will contain three Hall-effect sensors spaced at

60° or 120° electrical. Electrical degrees are simply mechanical degrees multiplied by the number of pole pairs in the motor. These sensors give adequate rotor position to excite the phases in the proper sequence.

Gearing

The use of gearing decreases the required motor size by converting the motor's high rotational speed and low torque to a torque and speed that match the load requirements. For this application this can be accomplished through the use of harmonic or epicyclic gearing. To simplify the drive wheel design a gearless system consisting of a high torque, low speed motor could be employed. However, to meet the power and size requirements it was decided to couple an epicyclic gear train to a high-speed motor.

Epicyclic gearing

Epicyclic gear trains (EGTs) are chosen for many applications due to their high power to weight ratio. Figure 1-14 illustrates a typical EGT. EGTs are often called planetary gear trains (PGTs) because of the orbiting motion the planet gears (elements 3,4,and 5 in Figure 1-14) have around the sun (element 1). The planets are connected by a carrier sometimes called an arm or spider (element 7), which rotates about an axis concentric to that of the sun and ring (element 6). Many applications make use of multiple planets to achieve a high power to weight ratio. Power branching allows the gears to share the tangential force evenly throughout the gear train. The advantage of this type of arrangement is that the radial forces produced during the transmission of torque across an involute gear pair are canceled out.

EGTs typically have a mobility of 2, which indicates that two inputs are needed to define a unique output. For the simple case one element is fixed giving the overall ratios

defined in Table 1-1. Epicyclic gear trains are designed to use spur, helical, or double helical gearing.

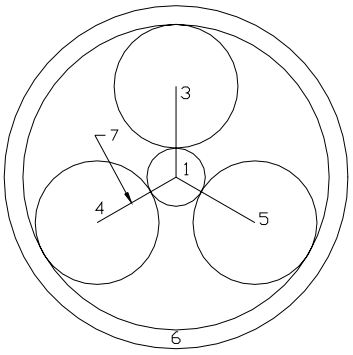

Figure 1-14: Epicyclic gear train spur gears

Table 1-1: Epicyclic gear arrangements (South and Mancuso, 1994)

Arrangement	Fixed Member	Input Member	Output Member	Overall ratio	Range of ratios normally used
Planetary	Ring	Sun	Carrier	Nr/Ns+1	3:1 - 12:1
Star	Carrier	Sun	Ring	Nr/Ns	2:1 - 11:1
Solar	Sun	Ring	Carrier	Ns/Nr+1	1.2:1 - 1.7:1

Ns = Number of sun teeth Np = Number of planet teeth Nr = Number of Ring Teeth

Spur gears

Spur gearing is used in the transmission of power between parallel shafts. Designers tend to use spur gears whenever application requirements permit due to their simplicity of manufacture. Spur gears are also very tolerant to machining errors. Their involute profile allows the center distance to change without altering the trueness of the gear action. Spur gears are typically used in applications with pitch line velocities below 66 feet per second due to the noise generated from the teeth coming in and out of mesh. The noise produced in gearing is a function of the speed of the gear pair. If noise were a concern helical gearing would be a possible solution.

Spur gear dimensions. Spur gears are measured in the English system by their diametral pitch, which is the number of teeth per inch of the gear pitch diameter. The diametral pitch of a gear cannot be measured though it can be used as reference dimension to calculate other size dimensions that are measurable. Some of these measurable dimensions are illustrated in Figure 1-15. Most gears produced today have a pressure angle of $20°$. Some designs incorporate $22.5°$ or $25°$ pressure angles but are not as smooth running as the $20°$ gears. In the past a $14.5°$ pressure angle was used but this often lead to problems with undercutting. Undercutting is a concern with any pressure angle. To reduce undercutting minimum tooth requirements must be maintained for each of the pressure angles.

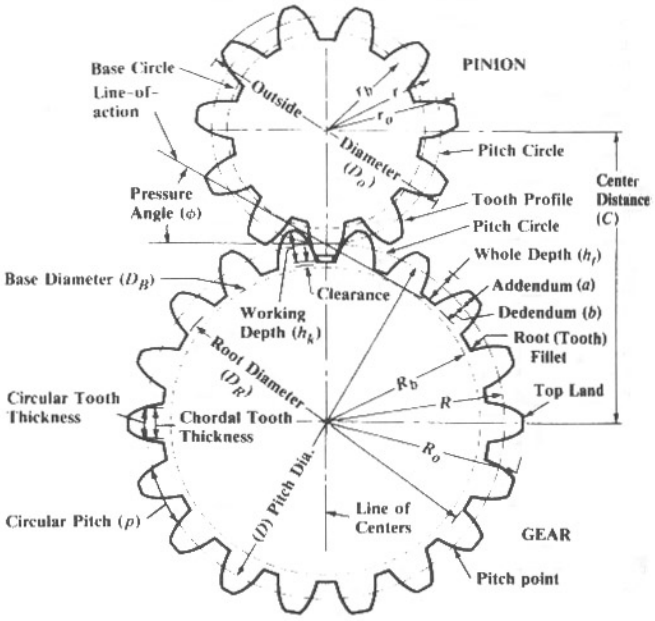

Figure 1-15. Spur gear terminology (Horton and Ryffel, 2000)

Table 1-2 provides an overview of involute spur gear dimensions. The equations in the table are used to determine the manufacturing and operating dimensions of a gear pair.

Table 1-2. Formulas for the dimensioning of spur gears (Horton and Ryffel, 2000)

Nomenclature:

ϕ = Pressure Angle		
a = Addendum	a_G = Addendum of Gear	a_P = Addendum of Pinion
b = Dedendum		
c = Clearance		
C = Center Distance		
D = Pitch Diameter	D_G = Pitch Diameter of Gear	D_P = Pitch Diameter of Pinion
D_B = Base Circle Diameter	D_O = Outside Diameter	D_R = Root Diameter
F = Face Width		
h_k = Working Depth of Tooth	h_t = Whole Depth of Tooth	
m_G = Gear Ratio		
N = Number of Teeth	N_G = Number of Teeth in Gear	N_P = Number of Teeth in Pinion
p = Circular Pitch	P = Diametral Pitch	

Table 1-2 cont. Formulas for the dimensioning of spur gears (Horton and Ryffel, 2000)

Formulas for Dimensions of Standard Spur Gears	
Circular Pitch	$p = \frac{\pi D}{N}$
Center Distance	$C = \frac{N_G + N_P}{2P}$
Diametral Pitch	$P = \frac{N}{D}$
Gear Ratio	$m_G = \frac{N_G}{N_P}$
Formulas for Tooth Parts, 20-and 25-degree Involute Full-depth Teeth ANISI Coarse Pitch Spure Gear Tooth Forms	
Addendum	a = 1.000 / P
Dedendum (Preferred)	b = 1.250 / P
(Shaved or Ground Teeth)	b = 1.350 / P
Working Depth	h_k = 2.000 / P
Whole Depth (Preferred)	h_t = 2.250 / P
(Shaved or Ground Teeth)	h_t = 2.350 / P
Clearance (Preferred)	c = 0.250 / P
(Shaved or Ground Teeth)	c = 0.350 / P
Pitch Diameter	D = N / P
Outside Diameter	D_O =(N+2) / P
Root Diameter (Preferred)	D_O = (N-2.5) / P
(Shaved or Ground Teeth)	D_O = (N-2.7) / P
Circular Thickness -- Basic	t = 1.5708

Gear strength. A primary difficulty in gear design is the calculation of the gear tooth stresses. The stresses calculated in gear design formulas are not necessarily true

stresses. For example, the load may be known but when this load is not uniformly distributed across the face width the calculations only serve as an estimate in determining the design parameters. Errors in tooth spacing also contribute to higher loads than expected. The accelerations and decelerations of a gear due to these errors cause dynamic overloads that cannot be accurately modeled in simple design formulas. Despite these problems, gear stress formulas can approximate the performance of a new gear design. A modified Lewis equation is defined in Equation 1-5. It assumes the load application at the tip of the tooth, even though this is an approximation because more than one tooth is in contact at any one time.

$$\sigma = \frac{F_t P}{k_d w Y}, \tag{1-5}$$

where σ = Stress, lb/in^2

F_t = Tangential force, lbs

P = Diametral pitch, $1/in$

w = Face width, in

Y = Lewis form factor (Horton and Ryffel, 2000)

k_d = Barth speed factor

The Barth speed factor is defined in the following equation. It partially accounts for the kinetic loading effects on the gear pair.

$$k_d = \frac{a}{a + v_r}, \tag{1-6}$$

where v_r = Pitch circle velocity, feet per minute (fpm)

a = 600 for ordinary industrial gears and 1200 for precision cut gears

Lubrication. Lubrication is required in order to limit metal-to-metal contact between two gear surfaces. Inadequate lubrication can lead to the scoring and pitting of gear teeth. When designing a gear train for the transmission of power through the analysis of gear, shaft, and bearing capacities it is also necessary to analyze the thermal limits of the gearbox. Most small gear drives are splashed lubricated by a quantity of oil in the gearbox. The surrounding air cools the gearbox and lubricant without the help of a pump and heat exchanger. A common practice is to calculate the maximum power a gearbox can carry for 3 hours without the oil temperature exceeding $200°F$ while having an ambient temperature of less than $100°F$.

CHAPTER 2
MOTOR AND GEAR TRAIN DESIGN

Load

Before completing the drive wheel design the load requirements must be determined. The torque output required for each of the four wheels on the omni-directional vehicle was found through empirical methods. The torque cannot be estimated by theoretical means due to the complexity of the tire ground contact and the corresponding rolling resistance. Because the rolling resistance is highly dependent on the tire dimensions, the tire inflation pressure and the ground characteristics, the load test was completed with similar values for each of these variables. Table 2-1 gives the values found for the load test.

Table 2-1. Thrust needed to translate a 400lb vehicle

Concrete	45 lb
Level grass	60 lb
Grass with 10 deg. Incline	130 lb
Grass with 20 deg. Incline	197 lb

Motor Selection

Motor selection for the drive wheel is based on the characteristics of the mechanical system coupled to the motor shaft. The combined selection of the motor and gear train is a highly iterative process. The final estimated values for the drive wheel are used to demonstrate the motor selection equations. The final design specifications are given in Table 2-2 along with the estimates for the physical properties of the mechanical system.

Table 2-2. Estimates for the physical properties of the wheel

Load			
Vehicle weight		400	lb
Rated speed of operation		5	mph
Equivalent Inertia*		0.166	in-oz-sec^2
Rated acceleration*		444.7	rad/sec^2
Tire size	4.10 - 3.50 - 6		
Outer diameter		12.1	inch
Inner diameter		6	inch
Width		3.5	inch
Gear Box			
Reduction		30.333	
Inertia estimate*		0.12	in-oz-sec^2
Efficiency		90	%
Frictional torque estimate*		27	in-oz
Motor	DIP37-19-005Z		
DC Resistance		0.25	Ohms
Torque sensitivity		10.6	oz-in/Amp
Back EMF constant		0.075	Volts/(rad/sec)
Peak torque		400	in-oz
Continuous stall torque		120	in-oz
Max Speed		8000	rpm
* Values taken at motor shaft			

Selecting the right motor for an application requires knowledge of the peak torque requirement, RMS torque requirement, and the speed of operation. The peak torque (T_P) is the sum of the torque used to accelerate the inertia of the system (T_J), the torque to move the load (T_L), and the torque to overcome friction (T_F). This relationship is given in Equation 2-1.

$$T_P = T_J + T_L + T_F \tag{2-1}$$

The torque required to accelerate the vehicle is a product of the inertia of the load (J_{L+M}) and the load acceleration (α) as given in Equation 2-2. The inertia in the system is the sum of the inertia of the rotating bodies in the wheel and the equivalent inertia of the vehicle relative to its mass and wheel diameter. From these calculations the peak

motor torque required to accelerate the vehicle at a rate of $7.33\,ft/\sec^2$ is 258 in-oz. The load and motor inertia are given in Table 2-2.

$$T_J = J_{L+M} \cdot \alpha \qquad (2\text{-}2)$$

The Root-Mean-Square (RMS) torque is a value used to approximate the average continuous torque requirement. It is a statistical approximation defined by Equation 2-3. The traction type loading of the vehicle requires a constant torque over a prescribed speed range, so for this application the vehicle is assumed to operate at a constant speed. Therefore, the RMS torque is assumed to be equal to the sum of the torque needed to move the load and the torque required to overcome friction. The RMS torque is calculated to be 130 in-oz.

$$T_{RMS} = \sqrt{\frac{T_P{}^2 t_1 + (T_L + T_F)^2 t_2 + (T_J - T_L - T_F)^2 t_3}{t_1 + t_2 + t_3 + t_4}} \qquad (2\text{-}3)$$

where $t_1 =$ Acceleration time, sec.

$t_2 =$ Dwell time, sec.

$t_3 =$ Deceleration time, sec.

$t_4 =$ Off time, sec.

A motor candidate was selected according to the previous calculations and the known size constraints. The motor specifications required to complete the analysis are given in Table 2-2 and an extended list of these specifications is given in Appendix A with the motor drawing. The next step in the verification of the motor for the drive wheel was to analyze the motor winding parameters. The supply voltage available on the vehicle is rated at 48 volts. The voltage drop due to the speed of the motor and the corresponding back EMF is defined in Equation 2-4. The voltage found from Equation 2-

4 is used to determine the available current to produce torque. The current is equal to the voltage divided by the motor winding resistance.

$$V = V_{SOURCE} - k_E \omega \qquad (2\text{-}4)$$

where $k_E =$ Back EMF constant, $in - oz / Amp$

$\omega =$ Rotational speed of the motor shaft, rad/sec

From these calculations the voltage available to produce torque during 7.33 ft /sec (5 mph) operation of the vehicle is 15 V. The available current to produce torque is then found to be 60 Amps. The current required by the load is defined by Equation 2-5 where K_t is the torque sensitivity constant. From these calculations, the current required for the RMS torque is 12.26 amps and the current required for the peak torque is 24.34 amps thus making this motor winding a good match for the drive wheel.

$$I_S = \frac{T}{K_t} \qquad (2\text{-}5)$$

Controller Selection

A brushless DC servo amplifier is used to drive the brushless motor at a high switching frequency. The amplifier excites the coils of the motor in synchronism with rotor position. The rotor position is commutated to the amplifier through the Hall-effect sensors built into the motor and a 1000 count encoder housed within the drive wheel. The drive wheel needs the encoder for velocity control and to decrease the torque ripple (cogging) at low speeds. These requirements along with the motor current and voltage requirements are used to select an amplifier for the system. The amplifier selected for the control of the drive wheel is model number BE40A8 that is produced by Advance Motion Controls. The amplifier has an operating voltage range of 20 – 80 Volts, a continuous

supply current of 20 amps and a peak supply current of 40 amps. The current available to the motor can be adjusted on the amplifier to prevent motor damage. From this performance criterion it is shown that the amplifier meets the needs of the system.

Gear Train Design

Incorporated within the iterative motor selection process is the design of the gear train. An exhaustive search methodology was used to optimize the gear train to meet the size constraints and load capacities. Figure 2-1 depicts the schematic of the double stage epicyclic gear train designed for the drive wheels.

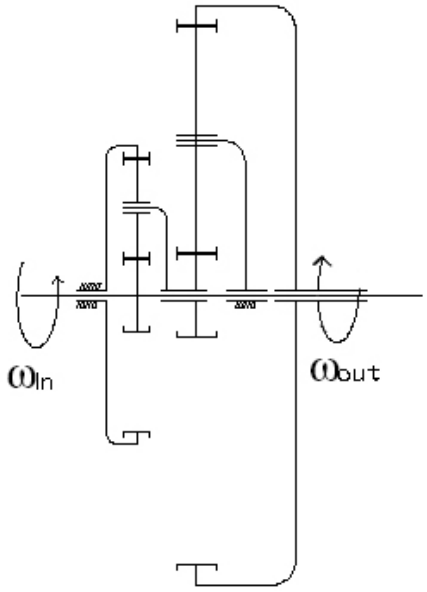

Figure 2-1. Gear train torque path schematic

The first gearing stage is a planetary arrangement where the ring gear is fixed to ground and the sun and carrier are the input and output respectively. The ratio for the first stage is 4.67:1. The carrier from the first stage drives the sun gear for the second stage. This is a one-piece unit allowing for a reliable transfer of power between the two stages of gearing. The second stage is of the star configuration with a ratio of 6.50:1. The final

ratio of the dual epicyclic gear train is 30.3:1 allowing for 5 mph operation of the vehicle with a motor speed of 4250 rev/min. Table 2-3 and Table 2-4 give the manufacturing data for the two stages of gearing. The complete table of gear specifications is given in Appendix B and dimensioned drawings for the gears can be found in Appendix A. This data was acquired from the equations presented in Chapter 1.

Table 2-3. Manufacturing data for the 1st stage planetary arrangement

1st Stage Planetary Arrangement						
		Mesh 1		Mesh 2		
	Sun		Planets		Ring	
Manufacturing Data	EXT3627		EXT3636		INT3699	
Diametral Pitch	36		36		36	
Number of Teeth	27		36		99	
Pressure Angle	20		20		20	
Pitch Diameter	0.75		1		2.75	
Tooth Form	Stand. Aden.		Stand. Aden.		Stand. Aden.	
Outer / Inner diameter	0.8056	0.8006	1.0556	1.0506	2.6944	2.6994
Root Diameter	0.6793		0.9293		2.8207	
Pin Diameter	0.0480		0.0480		0.0400	
Dimension over pins	0.8105	0.8085	1.0622	1.0602	2.7176	2.7196
Arc tooth thickness (norm)	0.0436		0.0436		0.0436	

Due to constraints, the first stage epicyclic gearing has a non-standard diametral pitch of 36 teeth/in. The second stage of the gear train has a diametral pitch of 24 teeth/in. The selection of the pitch and the pitch diameter of each gear are critical. To assemble each gear set Equation 2-6 has to hold true.

$$N_r = N_S + 2N_P \qquad (2\text{-}6)$$

where $N_S =$ Number of teeth on the sun gear

$N_P =$ Number of teeth on the planet gear

$N_r =$ Number of teeth on the ring gear

Table 2-4. Manufacturing data for the 2nd stage planetary arrangement

2nd Stage planetary arrangement						
		Mesh 1		Mesh 2		
	Sun		Planets		Ring	
Manufacturing Data	EXT2420		EXT2455		INT24130	
Diametral Pitch	24		24		24	
Number of Teeth	20		55		130	
Pressure Angle	20		20		20	
Pitch Diameter	0.8333		2.2917		5.4167	
Tooth Form	Stand. Aden.		Stand. Aden.		Stand. Aden.	
Outer / Inner diameter	0.9167	0.9117	2.3750	2.3700	5.3333	5.3383
Root Diameter	0.7293		2.1877		5.5207	
Pin Diameter	0.0720		0.0720		0.0600	
Dimension over pins	0.9269	0.9249	2.3861	2.3841	5.3618	5.3620
Arc tooth thickness (norm)	0.0655		0.0655		0.0655	

To evenly distribute multiple planet gears around the periphery of the sun gear, the selection of the number of teeth on the ring, sun, and planet gears is not arbitrary (Dooner and Seireg). Equation 2-7 is used to evenly space the planets around sun gear where n is the number of planets in the epicyclic gear train.

$$\frac{N_r + N_S}{n} = Integer \tag{2-7}$$

The modified Lewis equations presented in Chapter 1 were used to find the maximum allowable tooth load for each the gears. A factor of safety of 3 was used in the computation of the gear dimensions to account for the machining inaccuracies and dynamic overloading present in the system.

Gear Backlash

Backlash is designed into the gear train to compensate for machining inaccuracies and thermal expansion. Backlash is the play between mating teeth and is measured as the amount of excess space between the tooth and the width of the tooth space of the engaging gear on the pitch circle. Backlash prevents the jamming of gear teeth and provides space for lubrication, which prevents overloading, overheating, and excessive

wear. The calculation of the center distance tolerance for the two epicyclic gear trains was very important in the design of the drive wheel. The inaccuracies due to shaft, bearing, and gear tolerances and their machining allowances were taken into account for each gear mesh. The gear profile inaccuracies and the thermal expansion of the gears were also taken into account to determine the amount of desired backlash. The breakdown of the inaccuracies accounted for in the backlash calculations is given in Appendix B.

Bearing Life

The planet bearings for the first and second stages of gearing are analyzed throughout the design iteration to determine their expected operating life. The L_{10} life of a bearing refers to the life associated with 90% reliability and is defined in Equation 2-8.

$$L_{10} = \left(\frac{C}{P}\right)^3, \qquad (2\text{-}8)$$

where L_{10} = Life of the bearing in millions of revolutions

C = Basic load rating, lb. (provided by bearing manufacture)

P = Equivalent radial load, lb

From Equation 2-8 it was found that all of the bearings within the gear train of the drive wheel would exceed 50,000 hours of operation. The life of these bearings is high due to the low radial loads produced by the planetary gearing. The planet bearings are used for the calculations due to the load they carry for the transmission of torque.

Motor Cooling

Increasing the power density of the motor can be accomplished through the use of forced cooling. Due to the sealed nature of the drive wheel the motor is unable to be

cooled by forced air. The motor housing contains 18 passages that circulate an ethylene glycol and water mixture around the outer diameter of the stator. These passages yield about 25 square inches of cooling area allowing for continuous duty operation at higher torque levels than previously calculated. The coolant flows through each of the individual drive hubs using a central pump and heat exchanger. The temperature of the motor windings is continually monitored with a thermistor that is epoxied to the motor windings with a thermally conductive epoxy.

The motor housing drawings depicting the coolant paths are given in Appendix A. From the dimensions of the coolant path the maximum flow rate for laminar flow, the pressure loss and the power dissipated are estimated.

Gearing Features

Throughout the gear train there are many unique features that allow the drive train to fit within the hub of a wheel. Some of the features are illustrated below. Figure 2-2 illustrates the first stage sun gear and the motor shaft integrated as one unit. The slots in the shaft act as an internal collet for joining the motor rotor and shaft. As the expanding pin is threaded into the end of the shaft, the shaft expands creating an interference fit with the rotor. Figure 2-3 illustrates the first stage carrier and the second stage sun gear integrated as one unit to provide a reliable transfer of power between the two stages. Figure 2-4 shows the first stage ring gear integrated as a part of the gear housing. Notice the tooth relief groove separating the inner face of the housing and the ring gear teeth. On the reverse side of this gear is a seal surface to keep the gear oil within the confines of the gear train.

Figure 2-2. Main shaft and its expanding collet

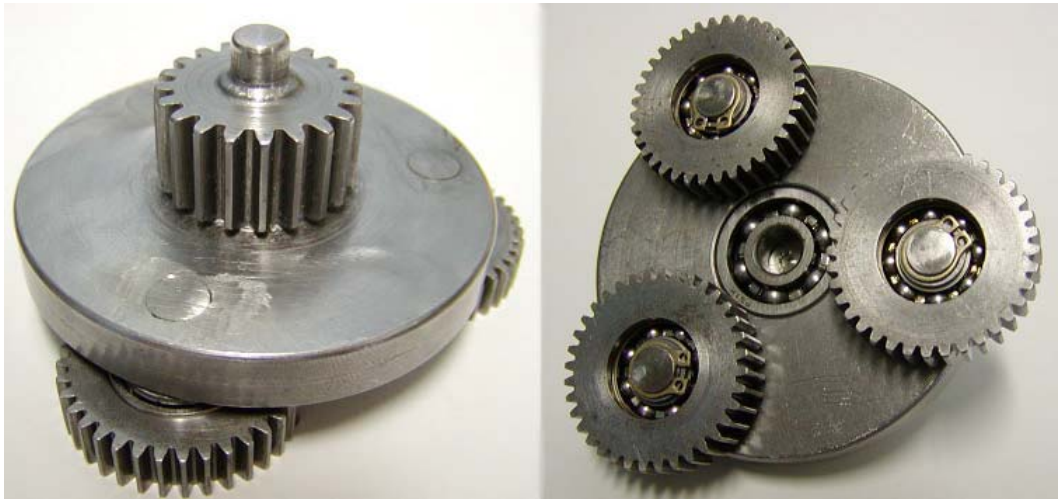

Figure 2-3. First stage planets and second stage sun gear

Figure 2-4. First stage ring gear

Figure 2-5 depicts the second stage sun and planet gears. The planets are supported by a fixed carrier, which is attached to the first stage ring gear.

Figure 2-5. Second stage gearing

CHAPTER 3
DRIVE WHEEL HOUSING AND JOINT DESIGN

Load Considerations

The tire is subjected to external forces due to the relative motion of the vehicle and its weight. To determine if these loads cause failure within the design of the drive wheel the maximum forces must be found. The forces the tire resists and their respective directions are shown in Figure 3-1. The forces are assumed to load the tire at the center of the tire contact area with the ground. The moment M_{zG} in Figure 3-1 is given as the maximum turning moment needed to overcome the force distribution restricting the wheel's rotation about the z-axis. The reaction forces from the wheel clamp are also shown in the figure and all are assumed positive.

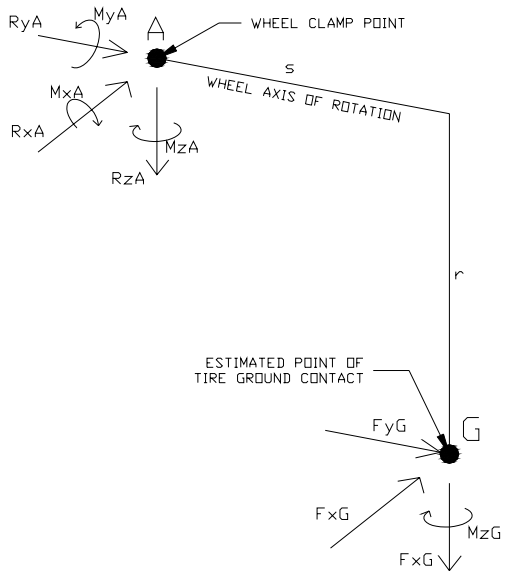

Figure 3-1. Drive wheel ground contact forces

The vehicle is assumed to be a maximum of 400 lbs of equally distributed weight as given by the design criteria. The maximum weight (W) each wheel is assumed to support is 150 lbs to account for the pitch and roll of the vehicle on inclines and in turns. A maximum coefficient of friction (μ) value of 0.8 is also assumed, therefore $(\mu \cdot W)$ is the maximum force attainable in the XY plane. The loading on point G in Figure 3-1 is used to obtain the 3 reaction forces and 3 reaction moments resulting from the wheel clamp at point A. These reaction forces are then used to determine the forces placed on the main bearings supporting the external wheel hub. The free body diagram in Figure 3-2 was used to derive Equations 3-1 through 3-4. These equations describe the loading on points B and C in the figure.

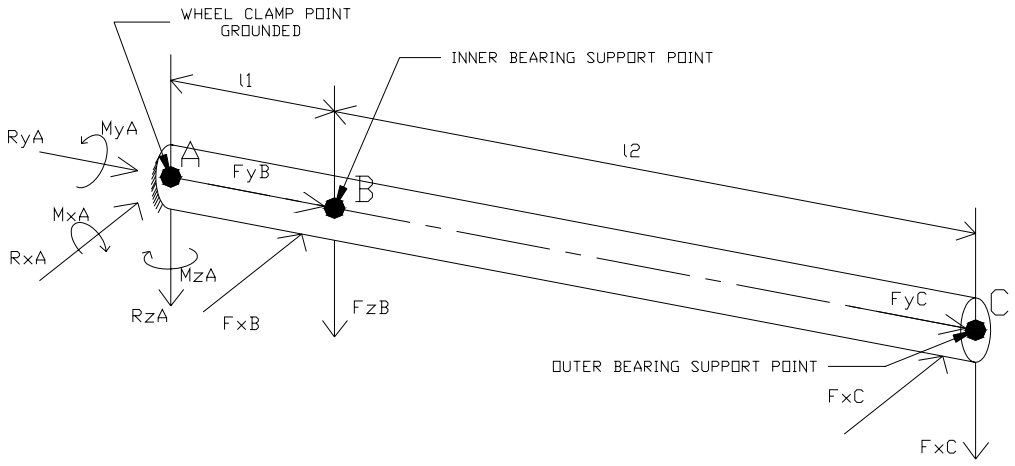

Figure 3-2. Free body diagram of the drive train

$$F_{xB} = -R_{xA} + \frac{M_{zA} - l_1 \cdot R_{xA}}{l_2} \tag{3-1}$$

$$F_{zB} = -\frac{M_{xA} + R_{zA} \cdot l_1 + R_{xA} \cdot l_2}{l_2} \tag{3-2}$$

$$F_{xC} = \frac{M_{zA} - l_1 \cdot R_{xA}}{l_2} \tag{3-3}$$

$$F_{zC} = -R_{xA} + \frac{M_{xA} + R_{zA} \cdot l_1 + R_{zA} \cdot l_2}{l_2} \tag{3-4}$$

Due to the design of the housings and shaft that support bearings B and C, only one bearing at a time can carry the force on the Y-axis. Bearing C carries the full load in the Y direction if $R_{yA} > 0$ and the opposite is true when the reaction force $R_{yA} < 0$.

In order to estimate the life of the main bearings and predict their failure the maximum forces they experience must be calculated. The drive hub is designed to use Reali-Slim bearings manufactured by Kaydon. The technical drawing of the bearings can be found in Appendix A. The load capacity in the radial direction is lower than that of the capacity in the axial direction of the selected bearings so, a function is created to maximize the magnitude of the force exerted in the radial direction on bearing B. It was found that the loading on bearing B would be greater than on C. The constraint was given that the magnitude of the forces in the XY plane must not exceed $(\mu \cdot W)$. The magnitude of the forces in the X and Z direction and the force in the Y direction could then be used to estimate the dynamic life of the bearings. Values obtained from the search function are shown in Table 3-1. Knowledge of the exerted loads on the main bearings allows the support housings that enclose the gears and motor to be analyzed for failure.

Figure 3-3 shows the complete assembly of the support housings and its related components. The assembly in the figure is analyzed as a rigidly supported beam with two load points. The internal shear and moment loads are determined for each point along the Y-axis where a possibility of failure could occur.

Table 3-1. Maximum forces attainable for the wheel main bearings

Fxg =	-28.4609	lbs
Fyg =	-101.069	lbs
Fzg =	150	lbs
Rxa =	28.46095	lbs
Rya =	101.0692	lbs
Rza =	-150	lbs
Mxa =	-172.915	in-lbs
Mya =	170.7657	in-lbs
Mza =	-397.748	in-lbs
Fxb =	-106.155	lbs
Fyb =	0	lbs
Fzb =	202.3055	lbs
Fxc =	77.69397	lbs
Fyc =	101.0692	lbs
Fzc =	-52.3055	lbs

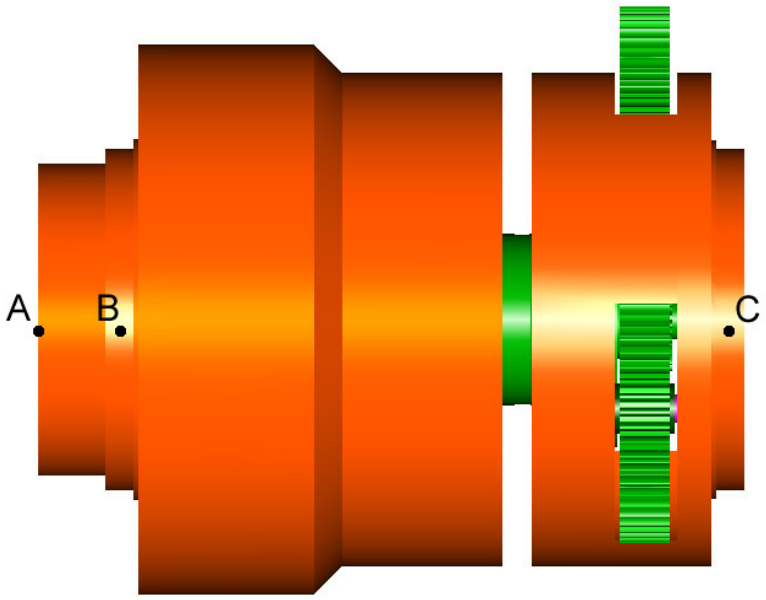

Figure 3-3. Internal drive train housings

Joints

The drive wheel joints are designed to carry the shear forces without placing a significant amount of shear stress on the threaded fasteners. Each part contains features to

locate the mating part within the correct tolerances. This is critical in the design process due to the integration of the motor, gear train and related housings. These features are toleranced to allow for acceptable clearances throughout the operating temperature range and to have the ability to be produced by conventional machining practices.

The threaded fasteners in the joints are assumed to only carry a tensile force due to the moments about the X and Z-axes. The internal forces within the joint are treated like those of a prismatic beam in bending. This approximation is assumed due to the significant preload that is applied to the screws. Figure 3-4 illustrates the second stage carrier cover and the forces internal to the joint. Only the reactions due to the moment produced by the positive force in the Z-axis direction are shown in this figure.

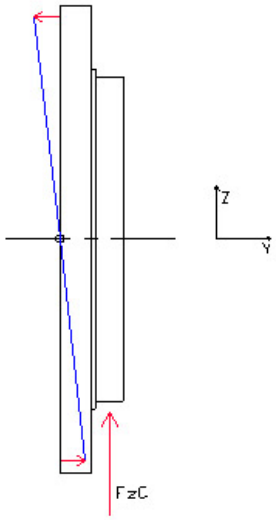

Figure 3-4. Carrier cover joint loading

The center of gravity of the fastener group determines the neutral axis. Tension due to the load state plus preload is seen in the bottom bolts while fastener preload is the only force present in the top bolts. Equation 3-5 is used to determine the forces imposed upon the bolts with the knowledge of the moments.

$$P_i = \frac{M_z \cdot r_{xi}}{\sum_{i=1}^{n} (r_{xi})^2} + \frac{M_x \cdot r_{zi}}{\sum_{i=1}^{n} (r_{zi})^2}, \quad (3\text{-}5)$$

where r_{xi} and r_{zi} are the distances from the centerline of the plate to the center of the threaded fastener parallel to their respective axes, P_i is the force that the $(i)th$ threaded fastener supports, and M_x and M_z are the moments about the X and Z-axes. Equation 3-5 was optimized for each joint resulting in the maximum attainable load for each screw.

Socket head bolts were used in the design of this drive wheel due to the ability to counter bore the head of the fastener in the housing with minimal material removal. To determine the ideal bolts for each of the joints, the suggested preload for the fastener size is calculated. Equation 3-6 can be used to calculate these values for reusable connections.

$$F_i = 0.75 \cdot A_t \cdot S_p \text{ (Horton and Ryffel, 2000)} \quad (3\text{-}6)$$

In the previous formula, F_i is the bolt preload, A_t is the tensile stress area of the bolt, and S_p is the proof strength of the bolt. The variable A_t is determined through the use of screw thread tables located in most design handbooks. Proof strength for commonly used fasteners can also be obtained from this reference, but for the socket head bolts in use throughout this design, an approximation had to be made with Equation 3-7 where S_y is the yield strength of the material.

$$S_p = 0.85 \cdot S_y \text{ (Horton and Ryffel, 2000)} \quad (3\text{-}7)$$

Bolt preloads are desired in loaded joints due to their ability to keep the bolts tight, increase joint strength, to create friction between parts to resist shear, and to improve the fatigue resistance of the bolted connection. Equation 3-8 is used to estimate the torque for tightening the fasteners to achieve this recommended preload.

$$T = K \cdot P_i \cdot d \tag{3-8}$$

In this equation T is the wrench torque, K is the constant that depends on bolt material and size, P_i is the bolt preload and d is the nominal bolt diameter. A value of 0.2 is used for K (Horton and Ryffel, 2000).

Many of the joints use internal threads. Therefore knowledge of the strength of these internal threads is of importance. It is more desirable to have an externally threaded member fail than an internally threaded member. To prevent stripping of the internal threads, the minimum length of engagement of the fastener must be calculated. These calculations are not presented here, but when carrying them out dissimilar thread materials must be accounted for to achieve an accurate value.

The joint between the first stage ring gear and motor housing contains a fiber gasket to prevent oil from seeping beyond the seal plate. This joint is analyzed for bolt strength as well but extended calculations are performed to analyze the failure modes of the gasket. The gasket stiffness and the relative stiffness of the housings and threaded fasteners are used to analyze the joint to prevent joint separation. The effective gasket pressures are also determined to prevent gasket crushing and leaking.

CHAPTER 4
PERFORMANCE TESTING

The drive wheel was tested to gain further understanding of the concepts presented in the previous chapters and to verify the design for the use of vehicle propulsion in an omni-directional vehicle. At the time of this writing, only one drive wheel has been fabricated, thus the wheel cannot be tested on the vehicle platform. Instead testing took place on a bench dynamometer in a controlled environment. This chapter describes the test equipment that was built to evaluate the performance characteristics of the drive wheel.

The wheel was load tested similarly to the way it would be used on a vehicle platform. A brake that allows the wheel to continue to rotate while applying a variable resistive torque is used to simulate varying terrain conditions. This resistive torque is logged along with the current draw on the motor, the speed of the motor, and the motor winding temperature. To gain an understanding of the effect of forced cooling on the motor, temperature sensors are located in the coolant inlet and coolant discharge lines. This data is logged with the motor conditions and the room temperature to provide performance statistics on the drive wheel. In the following sections the equipment used to test the drive wheel will be described in further detail.

Dynamometer

In order to simulate the vehicle on the test bench, an arm that constrains the motion of the wheel to a rotation about its axis and a linear motion that is approximately vertical is used. The arm is sprung to force the tire into contact with the dynamometer roller. The

roller used for the testing is a solid steel mass 4.9 inches in diameter and 10 inches in length. The large inertia of this roller effectively smoothes out torque variations in the wheel. The roller then transmits the power from the wheel through a flexible coupling and then to the variable braking system. The braking system for this dynamometer uses an Ingersoll-Rand 7808-B pneumatic motor that was originally designed for industrial manufacturing processes. This type of braking system is not common in dynamometers but was used for this application because of its availability and cost. Dynamometers typically use some type of hydrodynamic brake, friction brake or induction motor to provide the resistive torque needed to load the test motor. These brakes dissipate power by dissipating energy in the form of heat. Hydrodynamic systems get rid of this heat by circulating the fluid through a reservoir and heat exchanger circuit. Heat removal for the pneumatic motor is not quite as simple. The pneumatic motor used for the testing of the wheel is back driven against the air pressure to provide a braking torque. An increase in the air supply pressure proportionally increases the torque required to back drive the motor. This type of braking system, however, does not remove the generated heat as well as the fluid systems due to the differences in specific heats of the fluids. A set of fins was attached to the air motor to help dissipate the heat generated within the motor housing. The fins also act as a reservoir for bathing the motor in ice during load testing. A pan with a drain was placed under the air motor to catch the water runoff.

Recording the amount of braking torque applied to the test motor can be accomplished in different ways. The most common way is to support the brake by two bearings, allowing it to freely rotate about its axis. A load-measuring device is then placed between the brake support and ground to resist the rotation of the brake. This

device can be a torsion load cell or a linear load cell coupled to a moment arm off of the brake support. For the dynamometer built to test the drive wheel, a linear tension spring was attached between a torque reaction arm and a ground support. A potentiometer was then used to measure the angular displacement of the brake. Calibration was necessary for this type of load sensing system. The dynamometer was calibrated using a ratcheting moment arm and a series of weights to develop a polynomial expression to relate the voltage output of the potentiometer and the resistive torque placed on the wheel. The conditions remained the same throughout the three calibration sequences except for the order of the applied weights. Figure 4-1 illustrates the three calibration curves describing the voltage torque relationship. The bench dynamometer is illustrated in Figure 4-2.

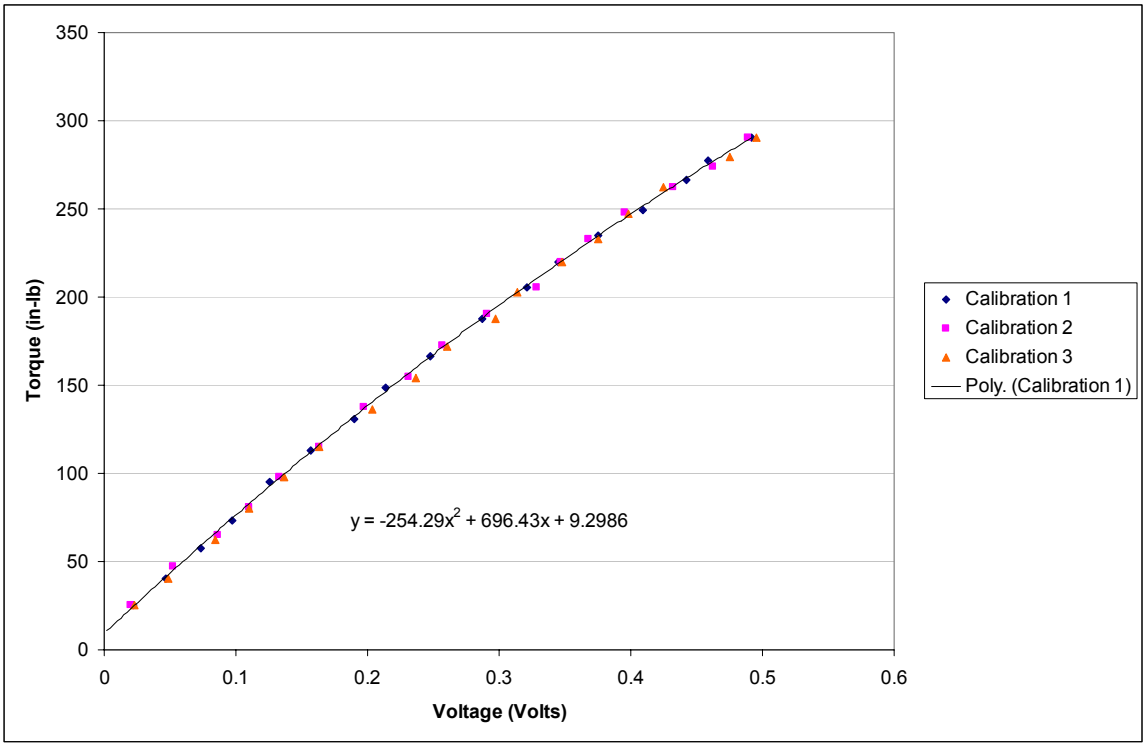

Figure 4-1. Dynamometer calibration curves

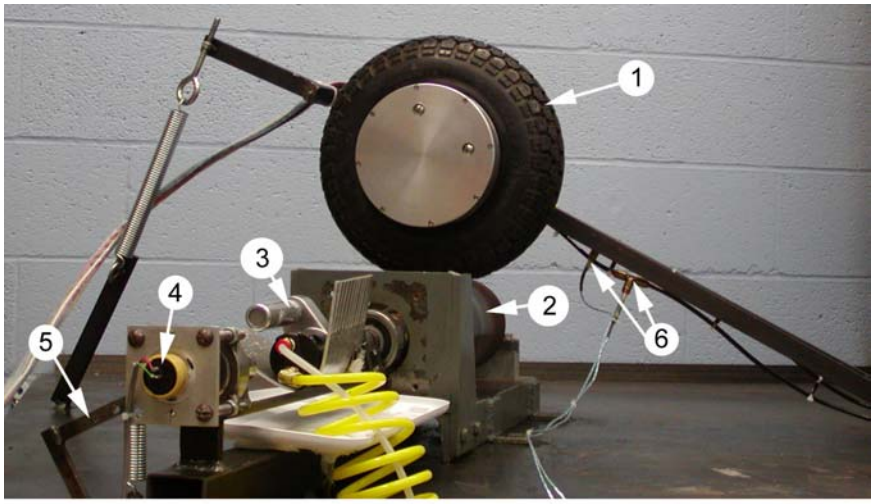

1. Drive wheel
2. Dynamometer roller
3. Air brake
4. Potentiometer
5. Torque reaction arm and linear spring
6. Coolant inlet and discharge thermistors

Figure 4-2. Bench dynamometer

Cooling

A cooling unit was built to circulate an ethylene glycol and water mixture through the drive wheel and heat exchanger. The cooling panel, shown in Figure 4-3, consists of a pump, heat exchanger, cooling fan, flow meter, pressure gauge, and valve for flow control. The components used in the cooling unit are not necessarily the optimum for the application. They simply provided the necessary cooling for the benchmarking of the drive wheel and were used due to their availability. To determine the heat dissipated through the liquid cooling system the inlet and discharge coolant lines of the wheel were fitted with thermistors. These temperatures were logged along with the temperature of the room and motor windings to see the effects of varying the torque, speed, and coolant flow rate.

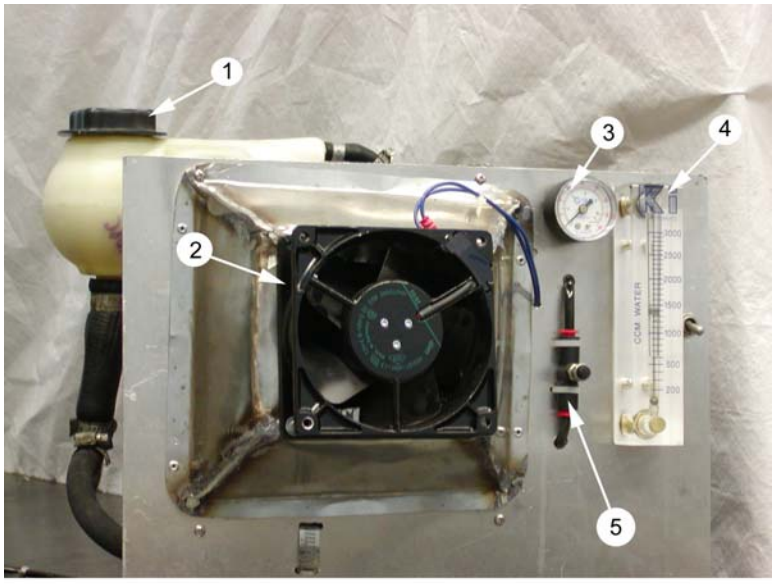

1. Coolant reservoir
2. Cooling fan
3. Pressure gauge
4. Flow meter
5. Coolant flow control valve

Figure 4-3. Coolant panel

Data Acquisition

Voltages from the health sensors on the motor were acquired through digital data acquisition equipment and converted into the units for each of the sensors. LabView was used to convert and display the data from each of the sensors and append it to a spreadsheet file specific to the test run. It was set up to acquire data at a rate of 10 Hz or 120 Hz depending on the type of test.

The brushless servo amplifier has signal output pins to monitor the speed of the motor, the supply current sent to the motor, and the fault state of the system. These voltages were run directly into the data acquisition board without any prior conditioning. The velocity output from the amplifier is internally isolated, however the current output is not isolated and requires data averaging to achieve a clean value. The thermistors are wired with a shielded twisted pair and conditioned with a capacitor prior to acquisition to

cancel out the interference from the mechanical and electrical systems they monitor. The potentiometer used for torque measurement was powered by a constant 5 Volt supply and is wired as a voltage divider. Figure 4-4 illustrates the brushless servo amplifier, thermistor power and conditioning board and the breakout box for the data acquisition. The complete test system schematic is illustrated below in Figure 4-5.

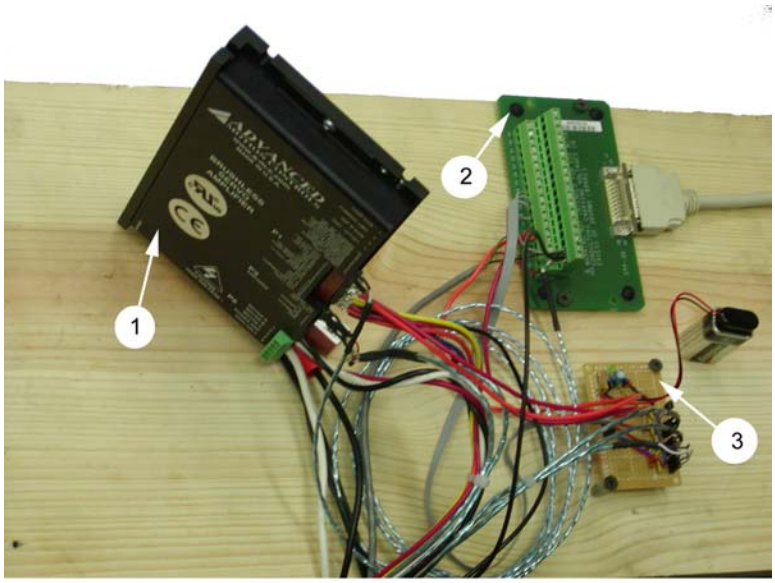

1. Brushless servo amplifier
2. Breakout board for digital data acquisition
3. Thermistor signal conditioning board

Figure 4-4. Amplifier and signal conditioning board

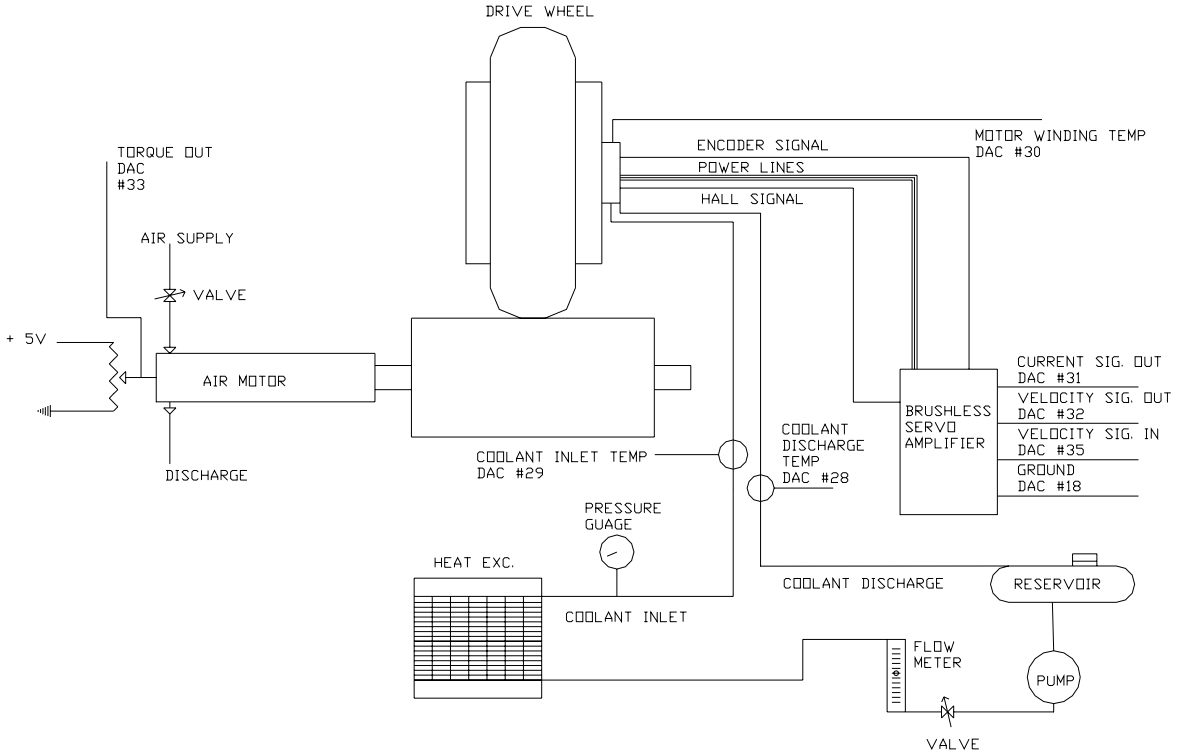

Figure 4-5. Testing schematic

CHAPTER 5
RESULTS

Many performance issues have been detailed in the previous chapters to provide justification for the drive wheel design. The performance of the fabricated wheel will be presented in this chapter to evaluate the design decisions. In these performance tests the continuous torque, acceleration, efficiency, and general temperature constants of the wheel will be determined. Finally the wheel constants will be summarized to give the relevant specifications required to control and apply the wheel to any vehicle platform.

Speed/Torque Curves and Load Testing

Studying the speed/torque curves is the best way to gain an understanding of a brushless DC motor. The motor's capabilities for various loading conditions are acquired from this curve. As mentioned previously, it is necessary to match the speed/torque curve of a motor to that of the load to obtain optimum performance in the system. The speed/torque curve ensures that the motor is capable of accelerating a load from zero speed to full speed without exceeding any thermal, mechanical, or electrical limits (Hendershot and Miller, 1994). These limits are characterized by the boundary of regions on the speed/torque curve.

It was mentioned in Chapter 2 that a traction type loading, like that of the drive wheel, requires a constant torque over a prescribed speed range. The drive wheel was load tested on a dynamometer in order to obtain the speed/torque curve needed to compare to the load requirements but due to the design of the air braking system on the dynamometer a constant torque test over the full speed range was impossible. At low

speeds, the braking force of the air motor pulses in succession with the vanes loading and unloading. In a typical application for the drive wheel the controller operates in closed loop mode to maintain a constant commanded velocity. This system was used to achieve a speed/torque curve for a constant velocity that could be compared to the constant torque curve of the load. Figure 5-1 illustrates the speed vs. torque curve for the drive wheel and the estimated criteria to maneuver a 400lb vehicle over a series of terrain conditions. These plots were overlaid to show the compatibility of the drive wheel and the given load criteria. The continuous load criterion is met throughout the various load conditions. It is only when an incline in excess of 15° is encountered that the speed drops below the designed speed. The supply voltage to the system for this test is 48 Volts. The drop in speed at 230 in-lbs of torque could be overcome by increasing the supply voltage. The motor winding temperature was closely monitored throughout this test to ensure that the thermal limits of the motor were not exceeded.

For completeness the drive wheel was also tested with a constant voltage supply to show the speed/torque linearity commonly provided in most suppliers' catalogs. The test was performed at 50% of the rated voltage for the wheel as proof of the equations defined in Chapter 1. This curve and the related current-torque curve are given in Figure 5-2.

Maximum Continuous Torque Testing

A load test was completed for an extended amount of time to determine the maximum continuous torque the wheel is capable of producing. Data was gathered for a period of 70 minutes from the various health sensors on the motor and controller as the wheel was loaded. The loading was performed in a stepping method during the search for the maximum continuous torque. The motor winding temperature was allowed to reach a near steady state value before the next load step was performed. This is because, for this

application, the maximum allowable winding temperature given by the motor manufacture limits the continuous torque. The data points from the test are plotted in Figure 5-3.

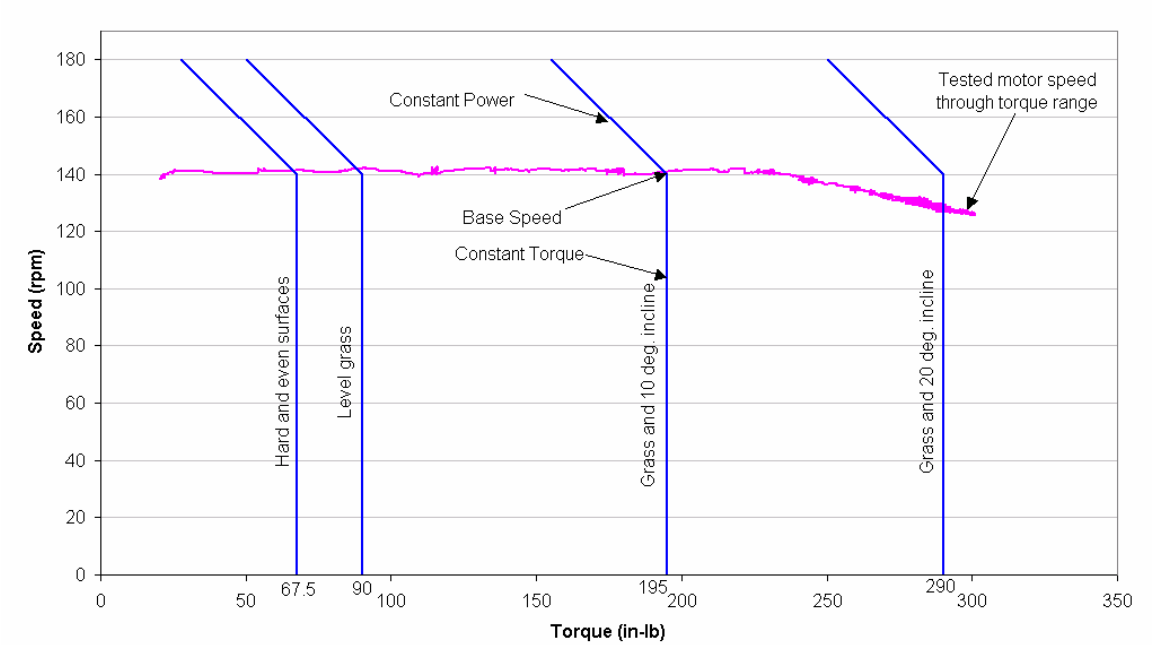

Figure 5-1. Speed/Torque curves for drive motor and load

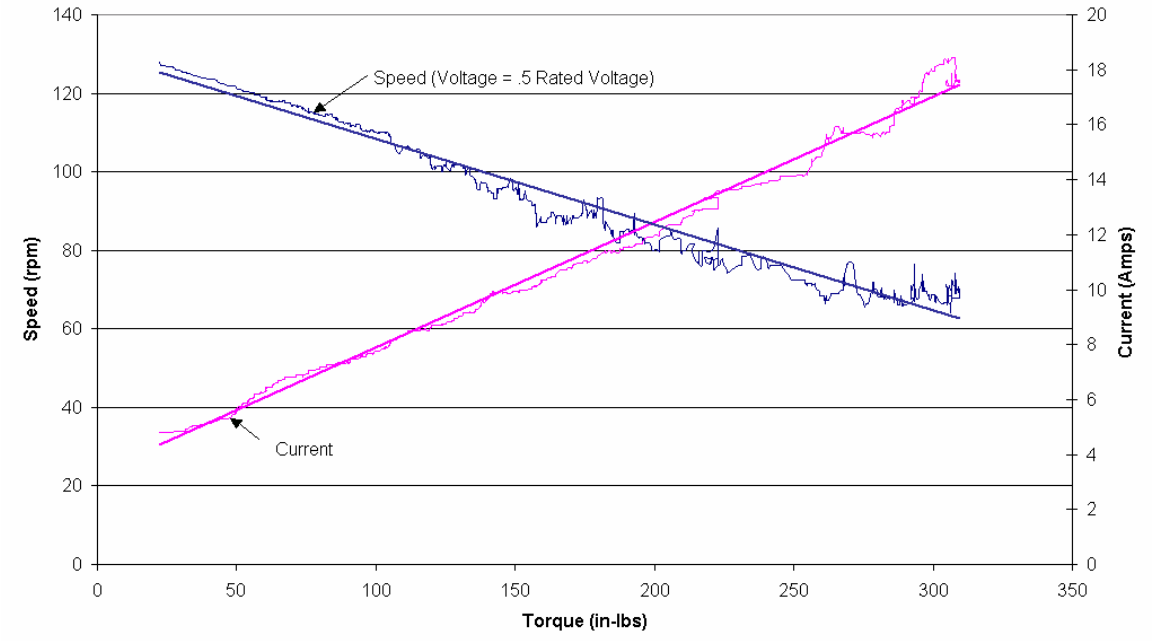

Figure 5-2. Speed/Torque with a constant voltage supply 50% of the rated voltage

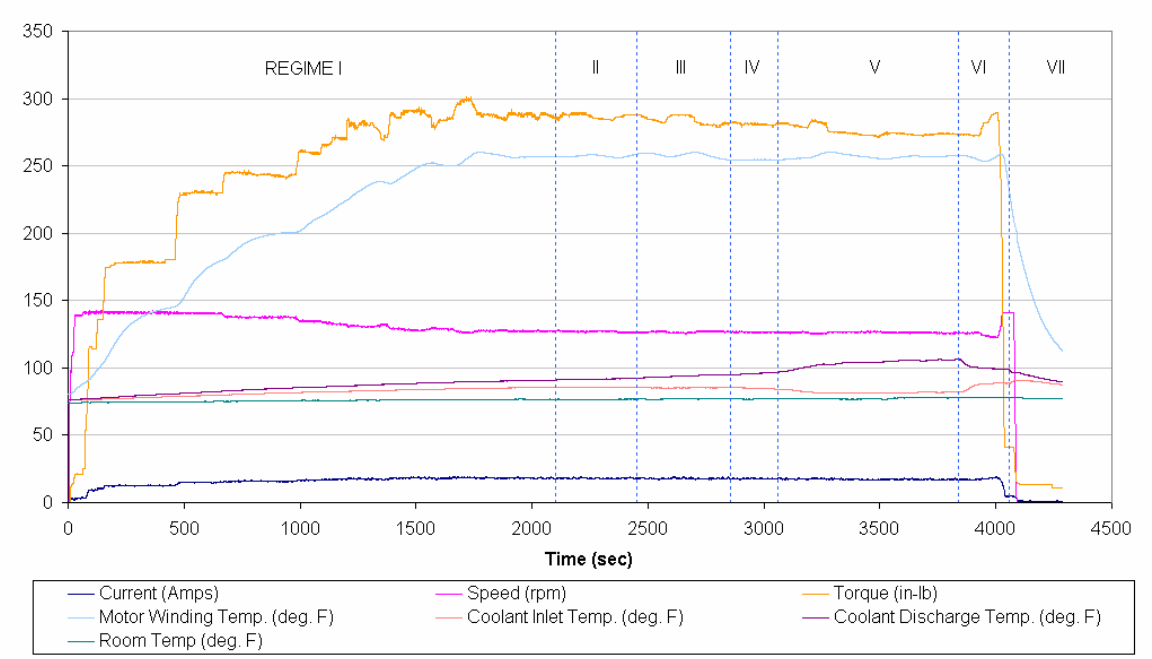

Figure 5-3. Maximum continuous torque test

Figure 5-3 is divided into seven regions corresponding to seven different coolant flow rates. Each region's relevant data is given in Table 5-1 for comparison. This data shows how decreasing the coolant flow rate increases the change in temperature between the coolant inlet and discharge. As this difference becomes larger, the motor housing temperature increases thus lowering the maximum continuous torque. A value of 1200 cubic centimeters per minute (CCM) was chosen as the maximum tested coolant flow rate because it efficiently yielded the desired change in temperature of $5°F$. After this test was completed the gear lubricant temperature was measured to be $109°F$.

To test the effectiveness of the external cooling system for the wheel the maximum continuous torque was found for no coolant flow. Figure 5-4 plots the data points gathered during the test run. The continuous allowable torque generation by the wheel without forced cooling is limited to 170 $in \cdot lb$. The liquid cooling increases the allowable output torque by 60% thus making this design an effective way of increasing the power

density of the drive system. The gear train lubricant temperature was measured after this test as well and was found to be $150°F$. The difference of $41°F$ between the two tests shows the effectiveness of liquid cooling the motor to decrease the gear train temperature.

Table 5-1. Steady state averages for continuous torque test.

Average Steady State Values	I	II	III	IV	V	VI	VII
Flow Rate (CCM)	1200	900	700	400	200	500	1200
Current (Amps)	18.21	18.08	17.92	***	17.17	***	***
Speed (rpm)	127.52	127.15	126.72	***	126.51	***	***
Torque (in-lb)	287.54	286.71	284.21	***	273.27	***	***
Motor Winding Temp. (deg. F)	257.58	257.27	258.36	***	256.57	***	***
Coolant Inlet Temp. (deg. F)	85.29	85.50	85.26	***	81.66	***	***
Coolant Discharge Temp. (deg. F)	90.44	91.60	93.94	***	104.85	***	***
Delta Coolant Temp. (deg. F)	5.14	6.10	8.69	***	23.18	***	***
Room Temp. (deg. F)	76.60	76.58	76.90	***	77.40	***	***
*** Did Not Reach Steady State							

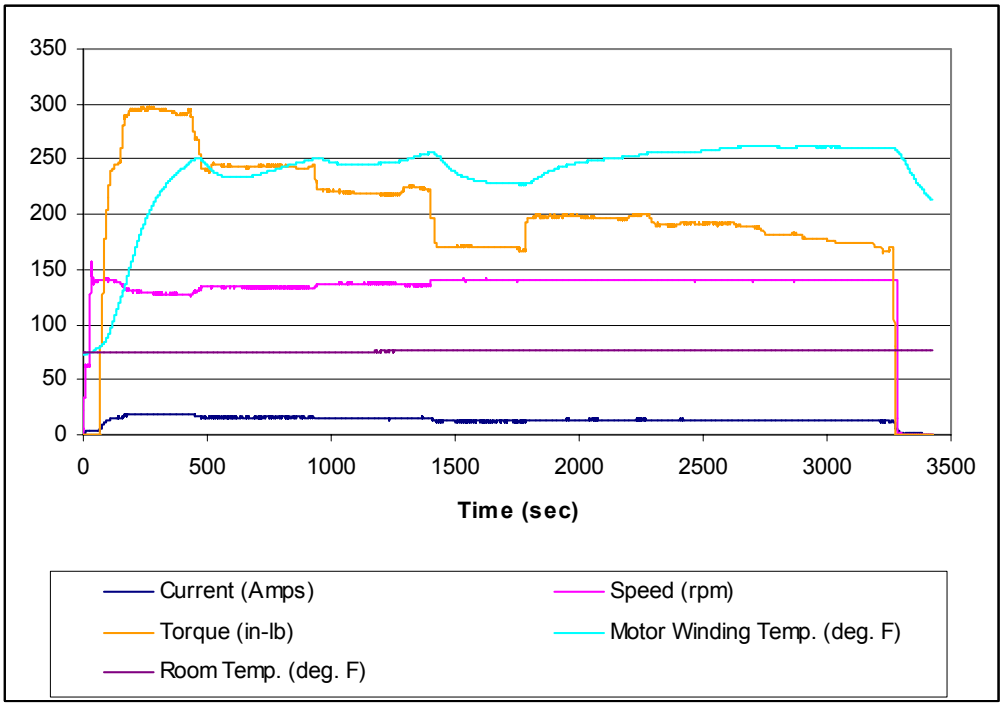

Figure 5-4. Continuous torque without forced cooling

Acceleration

The mass and inertia of the vehicle and drive components dictate the rate at which the platform can accelerate and decelerate. To determine the theoretical acceleration of the vehicle, the inertia of the wheel and the torque required to overcome friction must be computed. A series of acceleration tests were conducted to acquire these values from the physical system. The tests measured the acceleration of the wheel for ten different output torques. The current available for the motor to accelerate the wheel was limited through the use of the current limit potentiometer on the brushless servo amplifier. Varying the supply current to the motor proportionally changed the torque the motor produced. Three step functions were sent to the controller for each of the ten different potentiometer values. This data was then analyzed to determine the average acceleration, deceleration and corresponding torque for each step. The first five of these acceleration tests are plotted in Figures 5-5 – 5-9. The relevant torque and acceleration data is also given in each figure. The figures are listed in the order of minimum to maximum tested acceleration.

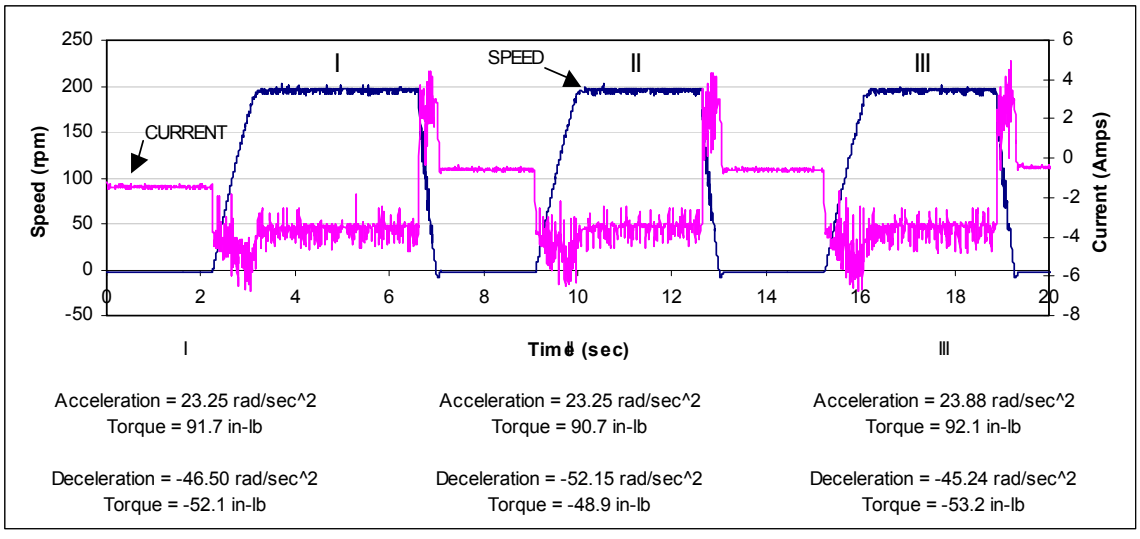

Figure 5-5. Speed-time, current-time plot #1

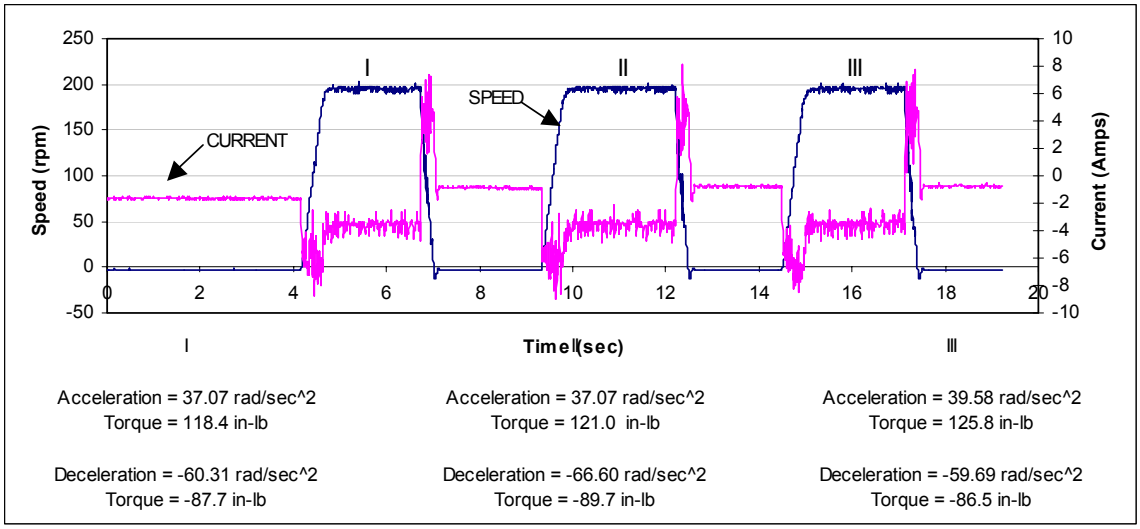

Figure 5-6. Speed-time, current-time plot #2

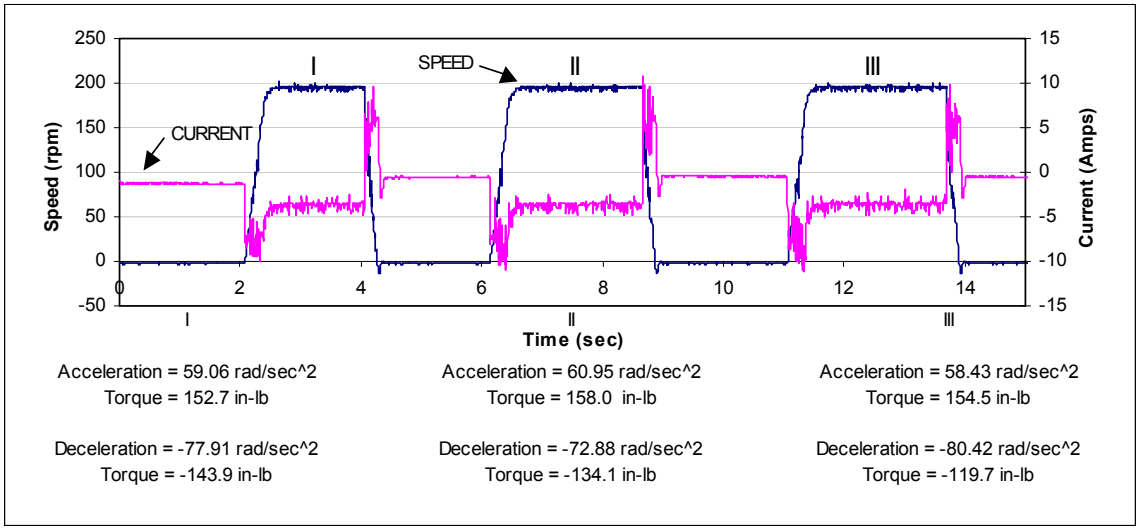

Figure 5-7. Speed-time, current-time plot #3

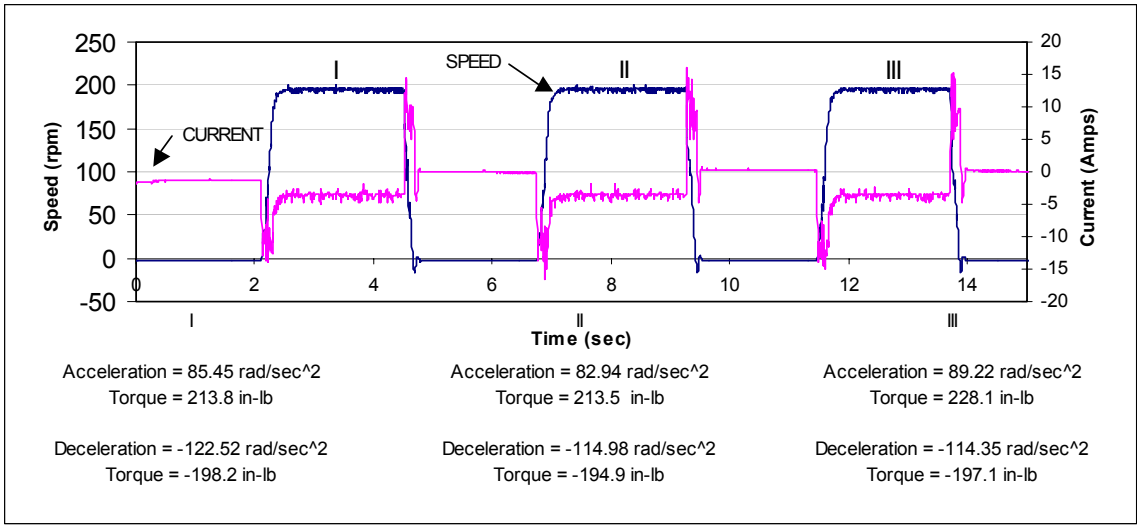

Figure 5-8. Speed-time, current-time plot #4

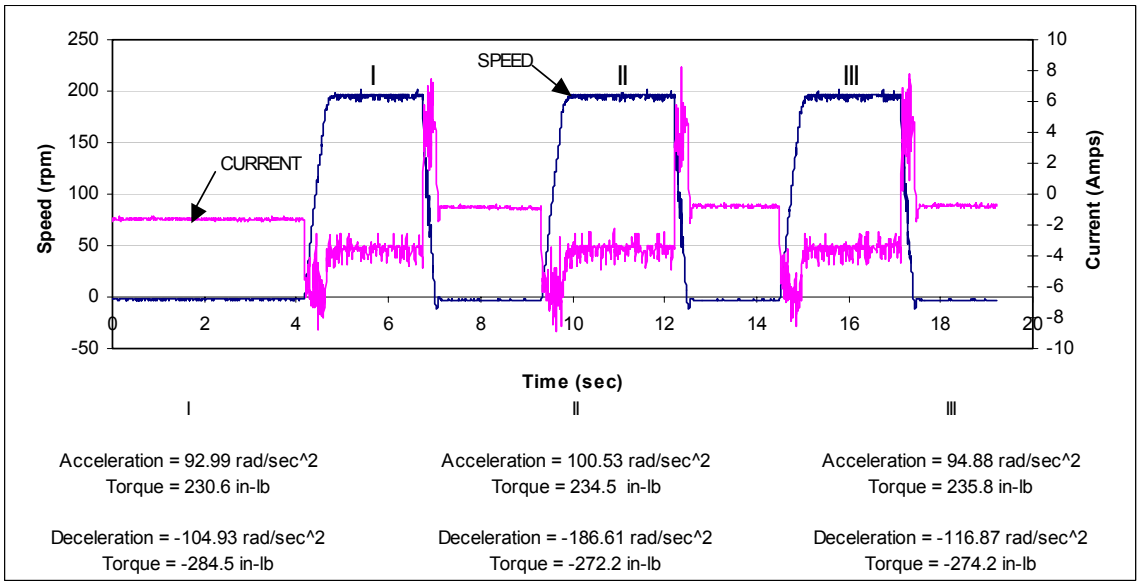

Figure 5-9. Speed-time, current-time plot #5

The average acceleration and torque for each step was then plotted in Figure 5-10 to show their correlation. Linear regression was used to determine the slope and Y-intercept of these points. The rotational inertia of the drive system is defined as torque divided by acceleration, which is the slope of this linear trend of points. The frictional torque can also be found from this plot because as the acceleration goes to zero the torque intercepts the Y-axis at some value above zero, equivalent to the torque needed to

overcome friction. The inertia of the drive system and the torque required to overcome friction were found to be 1.975 $in \cdot lb \cdot \sec^2$ and 44.48 $in \cdot lb$ respectively. The torque lost due to friction was used to compute an efficiency of 86% for the gear train, which is close to the 90% norm for planetary gear heads. The acceleration of a 400 lb vehicle can now be computed to determine the move profile available to the controller when the vehicle is on level grass. The acceleration was found to be 27.58 $ft/\sec^2$ thus allowing for a move beginning at rest to the rated speed of $7.33\,ft/\sec$ (5mph) in less than 0.27 seconds. These values assume zero slippage between the tire and ground, which is impossible, especially at this acceleration.

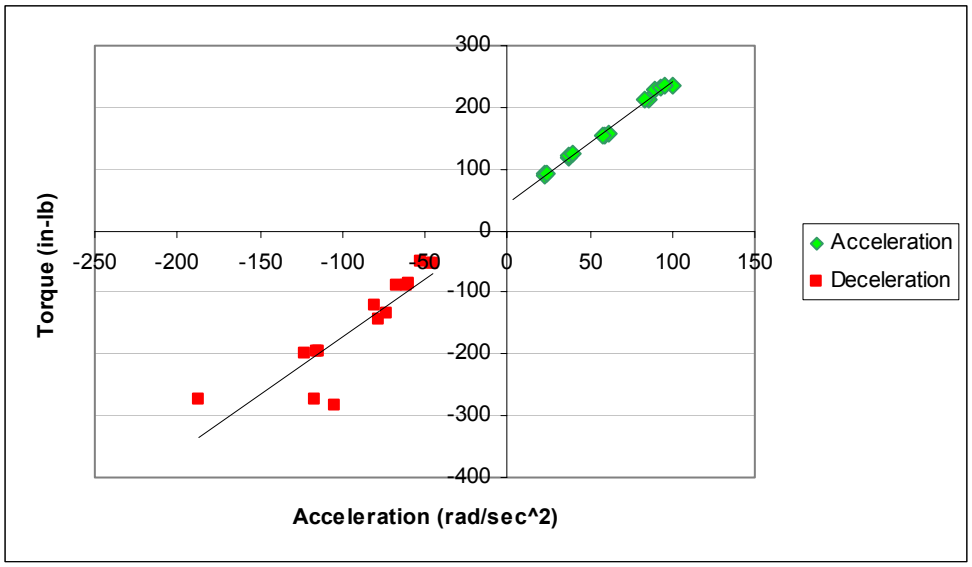

Figure 5-10. Torque-acceleration plot to determine inertia and frictional torque

Energy Balance

An energy balance was completed for the system to quantify the losses at the wheel's maximum continuous torque. Figure 5-11 illustrates the input and output power for the system. The power in and the power out values are used to calculate the efficiency for the mechanical system, which is found to be 59%. This efficiency is a combination of the

amplifier, motor and gearbox efficiencies. The power dissipated to the environment through natural convection and other means is calculated to be 57 Watts as shown in the following calculations. A portion of the heat generated from the losses present in the motor, gear train, and tire-ground contact account for this value.

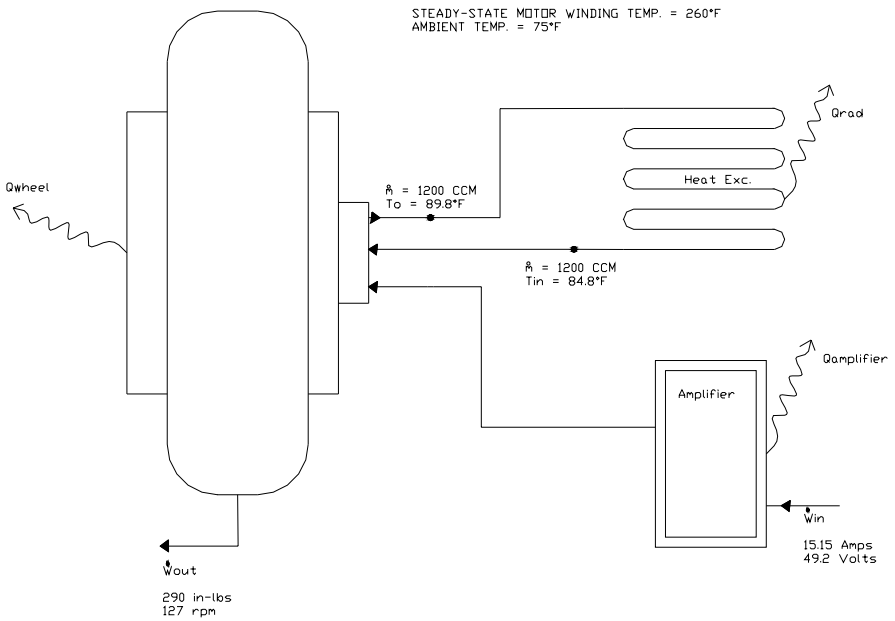

Figure 5-11. Energy balance schematic

The energy balance is completed below.

$$\dot{W}_{IN} - \dot{W}_{OUT} - Q_{RADIATOR} - Q_{AMPLIFIER} - Q_{WHEEL}$$

$$\left(I(Amps)\cdot V(Volts)\right) - \left(\frac{T(in-lb)\cdot\omega(rpm)}{84.45\left(\frac{in-lb}{\min - Watt}\right)}\right)$$

$$-\left(\dot{m}(kg/\sec)\cdot c_p(J/kg)\cdot\left(T_{OUT}(°C) - T_{IN}(°C)\right)\right) - Q_{AMPLIFIER}(W) - Q_{WHEEL}(W) = 0$$

$$\left(745(W)\right) - \left(436(W)\right) - \left(189(W)\right) - \left(60(W)\right) - Q_{WHEEL} = 0$$

$Q_{WHEEL} = 57 \cdot Watts$,

where $\dot{W}_{IN} =$ Work input, Watts

$\dot{W}_{OUT} =$ Work output, Watts

Thermal Resistance and Capacitance

Knowledge of the rate at which the wheel generates and stores heat is useful in determining acceptable move profiles for the vehicle. The thermal resistance and thermal capacity values combined provide the ability to determine the temperature rise during intermittent loading. Thermal resistance is the temperature rise of the wheel during steady state operation for the amount of work lost due to inefficiency. These losses can be calculated from the power input to the amplifier and the given wheel system efficiency. The thermal resistance value is defined by Equation 5-1 and is found to be $0.332°C / Watt$. Thermal capacity, as stated in Equation 5-2, is the amount of work necessary to raise the temperature of the system by $1°C$. The system time value τ is found by loading the wheel to the maximum continuous torque while initially at room temperature. The time value is the amount of time the system takes to reach the maximum allowable temperature. From the test shown in Figure 5-12, the time value was determined to be 920 seconds and the thermal capacity was then calculated to be $2770 J / °C$.

$$R_{THERM} = \frac{T_S - T_\infty}{\dot{W}_{IN} - \dot{W}_{OUT}} \qquad (5\text{-}1)$$

$$C_{THERM} = \frac{\tau}{R_{THERM}} \qquad (5\text{-}2)$$

where $T_S =$ Steady state stator temperature, $°C$

$T_\infty =$ Ambient temperature, $°C$

$\tau =$ Thermal time value, sec

$R_{THERM} =$ Thermal resistance, $°C/Watt$

$C_{THERM} =$ Thermal Capacity, $J/°C$

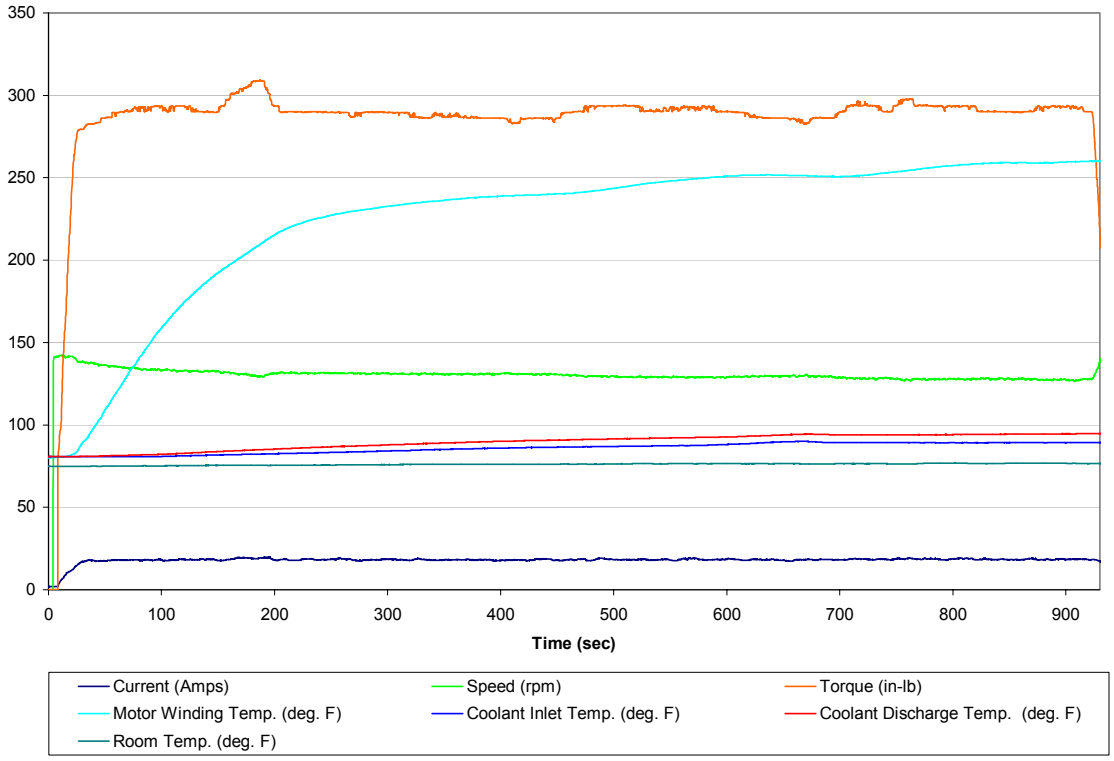

Figure 5-12. Thermal capacity test with 1200 CCM coolant flow

Motor Parameters and Constants

Table 5-2 lists the winding constants and the motor parameters for the fabricated drive wheel. These parameters were obtained from a combination of the motor manufacture's specifications and the load testing described previously.

Table 5-2. Drive wheel parameters

WINDING CONSTANTS	UNITS	TOLERANCE	SYMBOL	WDGZ
DC Resistance	Ohms	± 12 .5%	R	0.25
Voltage @ Tp	Volts	Nominal	Vp	9.43
Current @ Tp	Amperes	Nominal	Ip	37.8
Torque Sensitivity	in-lb/Amp	±10%	Kt	19.2
Back EMF Constant	Volts/(Rev/Min)	±10%	Kb	0.238
Inductance	Millihenry	± 30 %	L	0.45
WHEEL PARAMETERS	UNITS	SYMBOL	VALUE	
Peak Torque *	in-lb	Tp	758	
Continuous Stall Torque	in-lb	Tcs	290	
Wheel inertia	in-lb-sec^2	Jw	12.41	
Acceleration no load	rev/sec^2	Anl	32.8	
Max Allowable Speed	RPM	Sm	263	
Max Allowable Winding Temp.	$^\circ C$	Mtemp	125	
Thermal Resistance	$^\circ C/Watt$	Rt	0.438	
Thermal Capacity	$J/^\circ C$	Ct	2100	
Frictional Torque	in-lb	Tf		
Phases / Winding Type			3/Y	
Poles			8	
Lubrication				
Type of oil			5W30	
Fill amount	ml		150	
Tire				
Tubeless type			4.10-3.50-6	
Pressure	psi		30	
System Efficiency***	%		59	
Weight	lb	Wt	18	

* 10 sec @ 25°*C* Ambient Temp.

** 25°*C* Ambient, 125°*C* Winding Temp, 1200 CCM Coolant Flow @ 29°*C*

*** Including the amplifier and tire ground interface

CHAPTER 6
SUMMARY AND CONCLUSIONS

A compact high power drive unit was developed for use on autonomous vehicle systems, specifically high mobility omni-directional vehicle platforms. A unique approach was taken to the design of the drive system due to the many constraints placed on the vehicle. The design was focused on an optimal drive system that would reside in the commonly unused space in the rim of a wheel. Many different gearbox and motor configurations were considered, but the final design was to integrate a double stage epicyclic gear train, a liquid cooled frameless motor and the hub of a wheel to produce a powerful compact solution for the mobility of omni-directional vehicles.

The drive wheels were designed to allow for navigation in highly populated obstacle environments and varying terrain conditions including those with inclines as steep as $20°$. The wheels were also designed to allow for a continuous 5 mph operation throughout these terrain conditions. The drive wheels were designed for an omni-directional platform that incorporates four independently driven and independently steered wheels similar to the active castor wheels presented in Chapter 1. The hub propulsion units are independent of steering and suspension systems and have the ability to be adapted to other vehicle designs.

The only process performed off campus throughout the fabrication of the drive wheel was the shaping of the gear tooth profiles. The fabricated drive wheel was load tested for the ability to meet the given criteria and to determine the characteristics of the drive system. The drive wheel was found to provide $290\,in-lb$ of torque continuously at

a speed of 4.5 mph for a supply voltage of 48 volts. These values require a coolant flow rate of 1200 cubic centimeters per minute at an inlet temperature of $85°F$. These characteristics can be used to further the research in intelligent vehicle control systems.

The drive wheel has proven that it offers the power needed for an omni-directional vehicle to perform various tasks in indoor and outdoor environments. The completion of three more units will allow for the implementation of this unique drive system on a vehicle platform. The four drive units will be completed with a modified cooling system designed to improve heat transfer and machinability of the motor housing. The vehicle control unit (VCU) also needs to be completed for this vehicle. Some work has been done in the area of transforming the wrench commands into wheel velocities and steering angles but the testing and evaluation of the algorithms has yet to be performed. The Primitive Driver Component will have the ability to monitor the state of each wheel and, because the thermal characteristics of the wheels are known, it will have the capability to modify the move profile sent to the wheels. For example when the vehicle is at or near its maximum allowable winding temperature due to the previously commanded moves the vehicle control unit could begin to react to the current terrain conditions and commanded moves by allowing only a percentage of the commanded velocity and torque to be transferred to the drive wheels.

APPENDIX A
DIMENSIONAL DRAWINGS

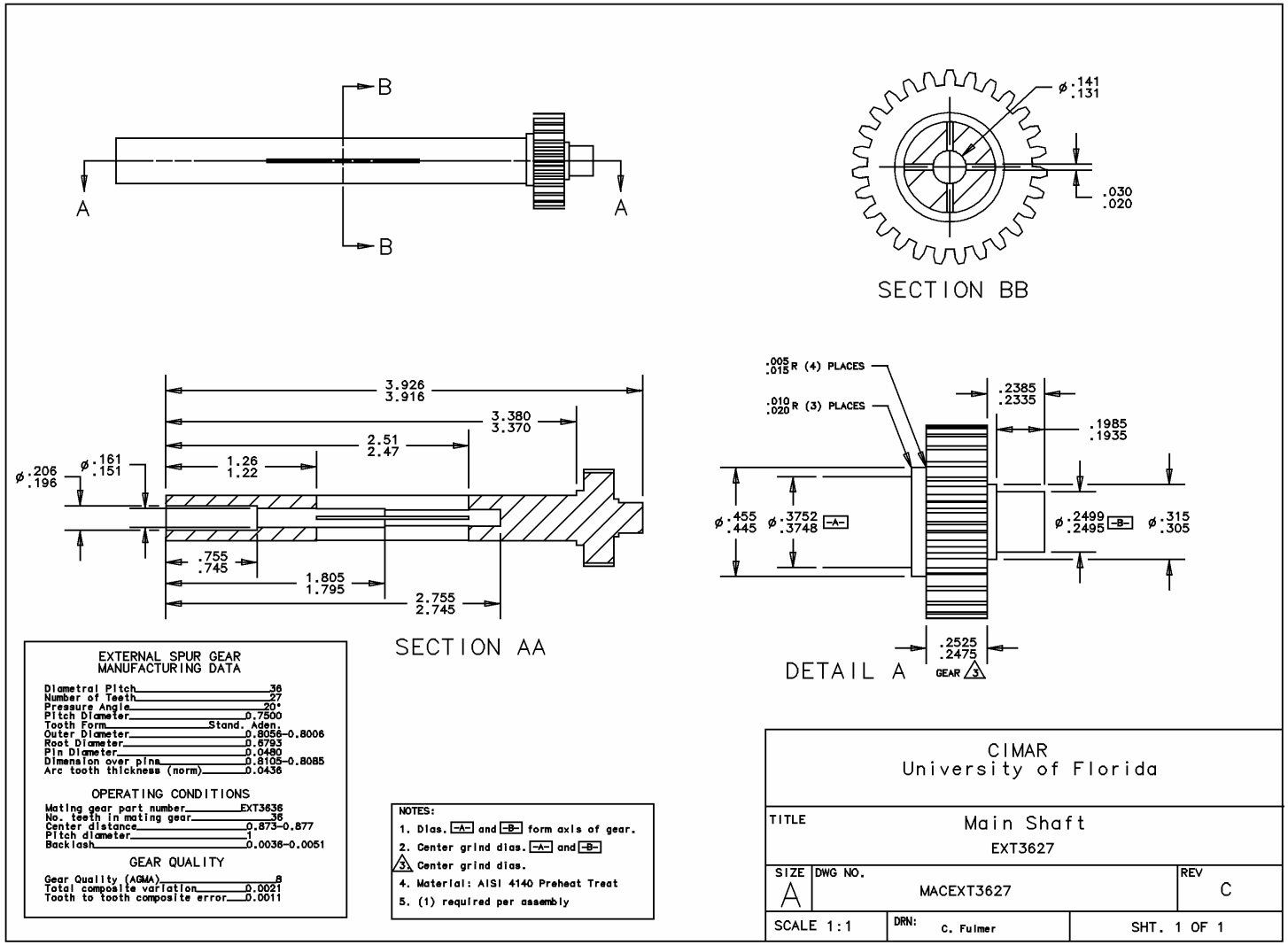

Figure A-1. Main shaft

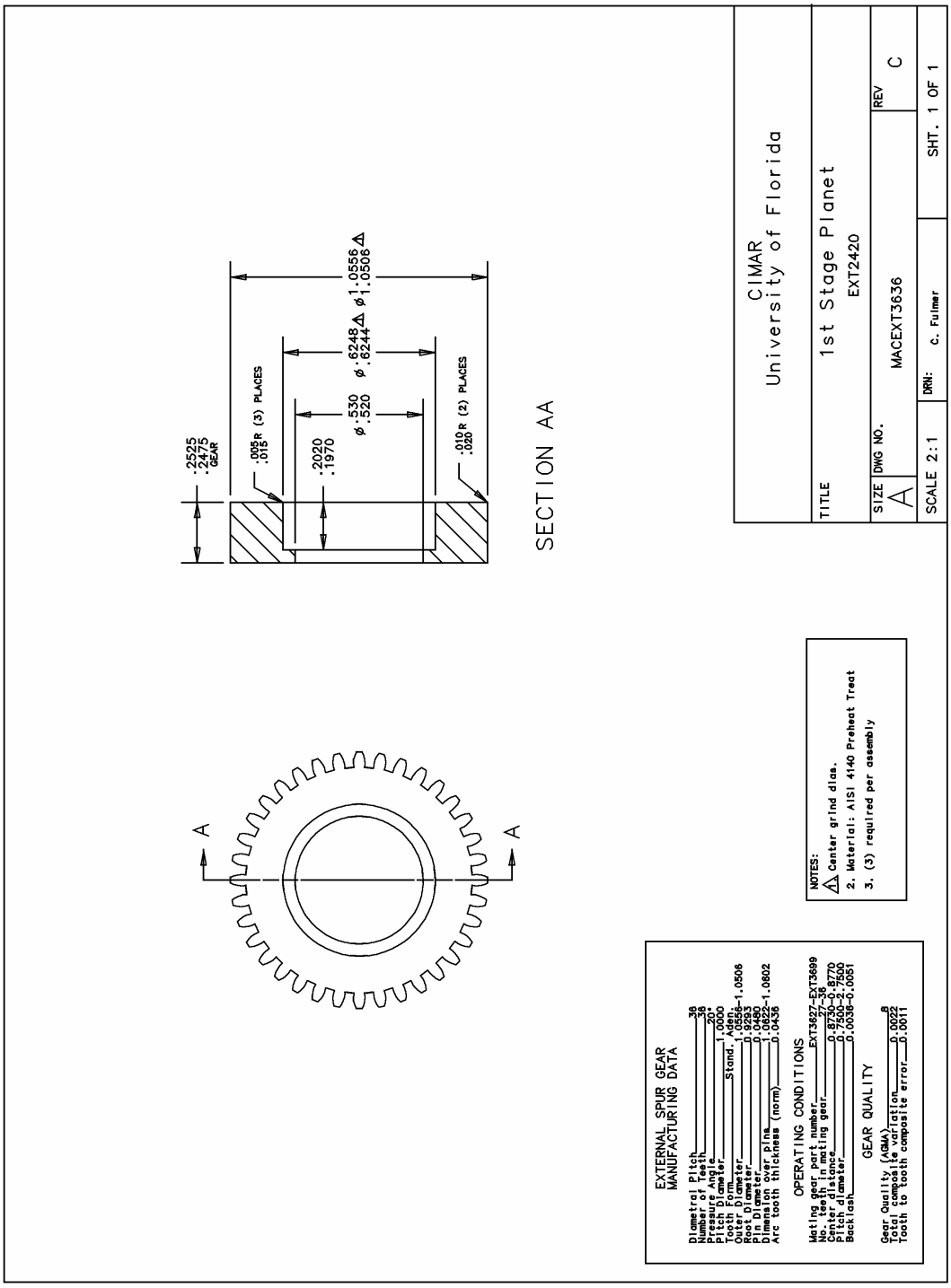

Figure A-2. 1st stage planet gear

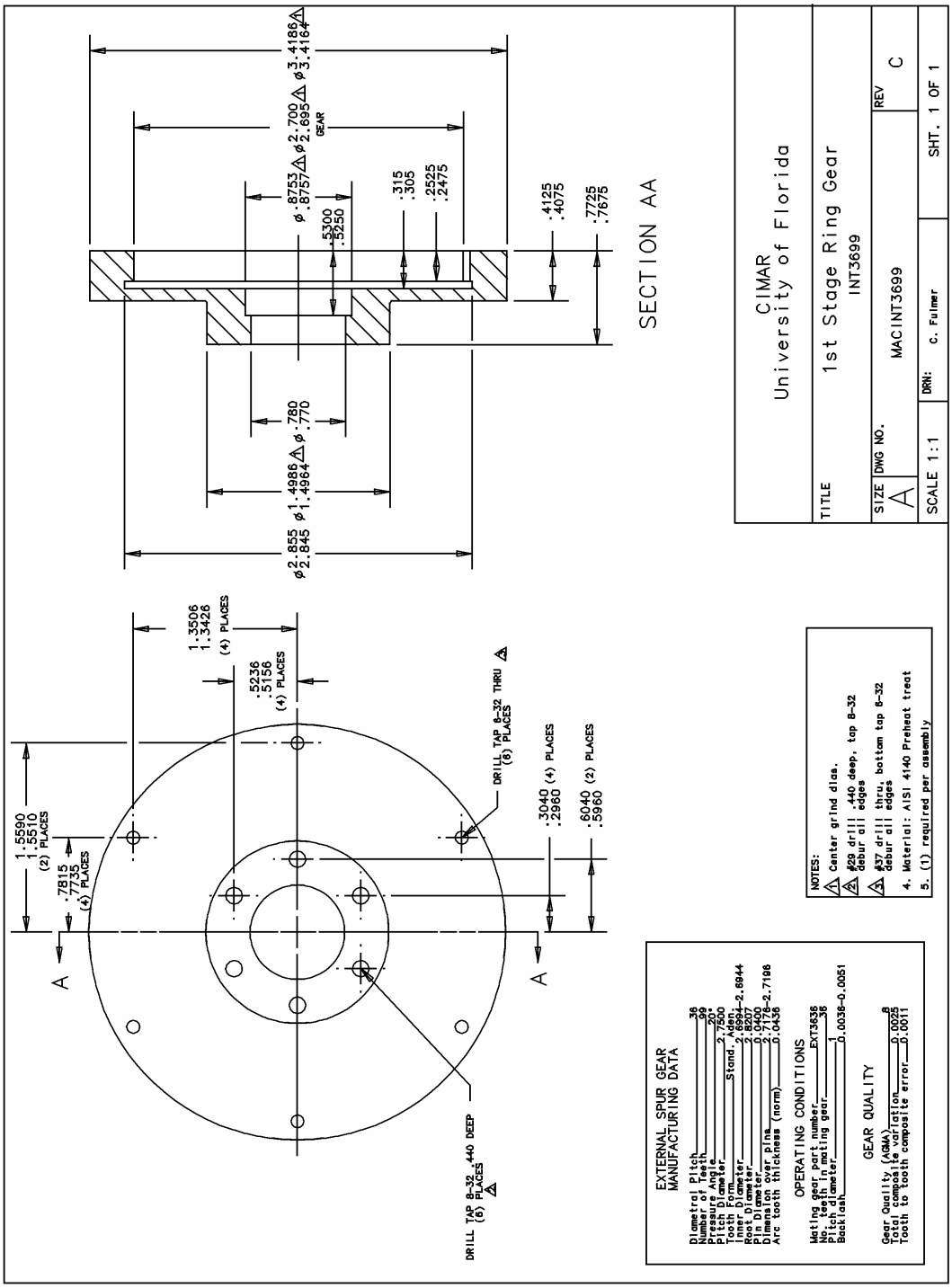

Figure A-3. 1st stage ring gear

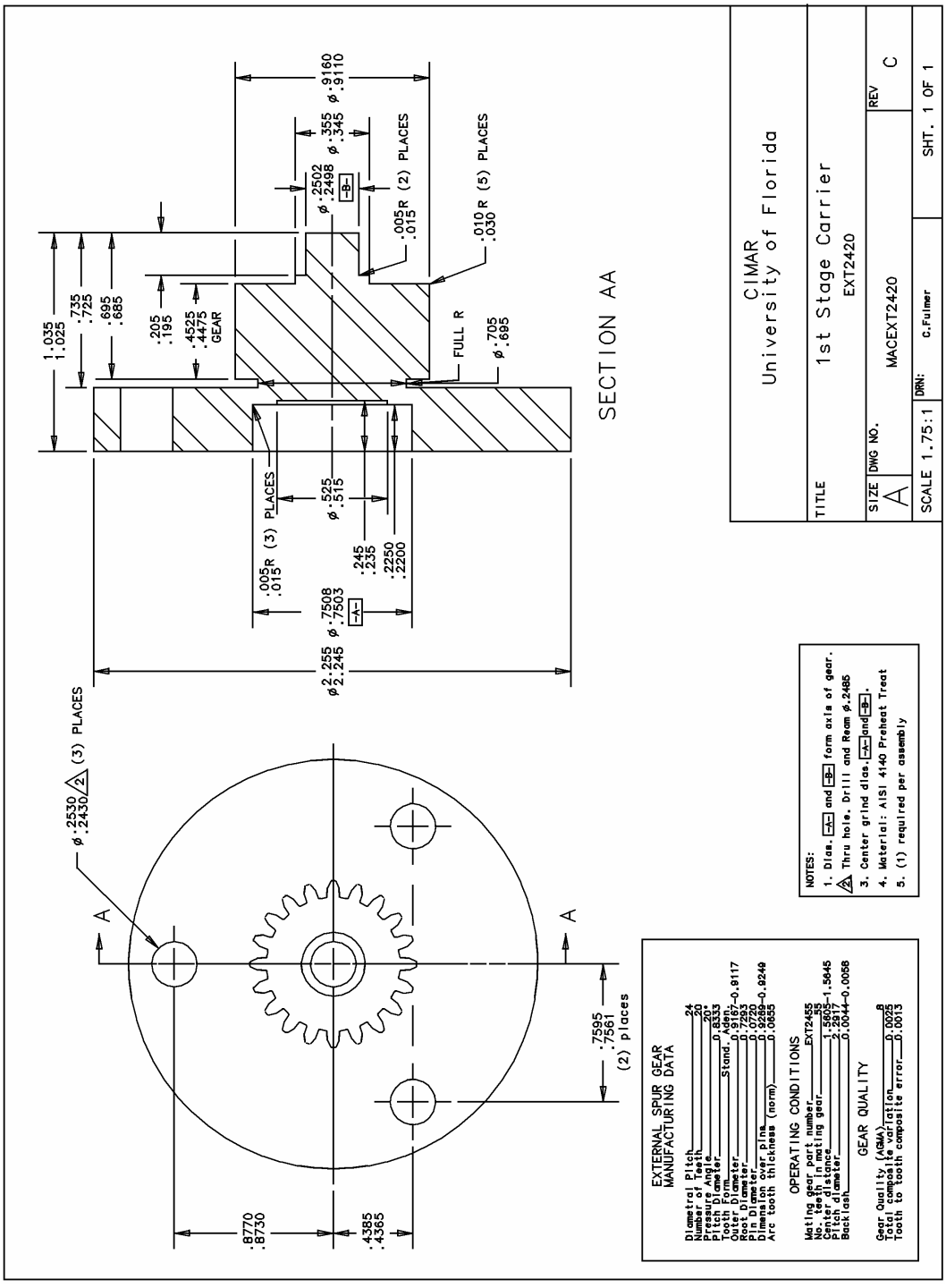

Figure A-4. 1st stage carrier

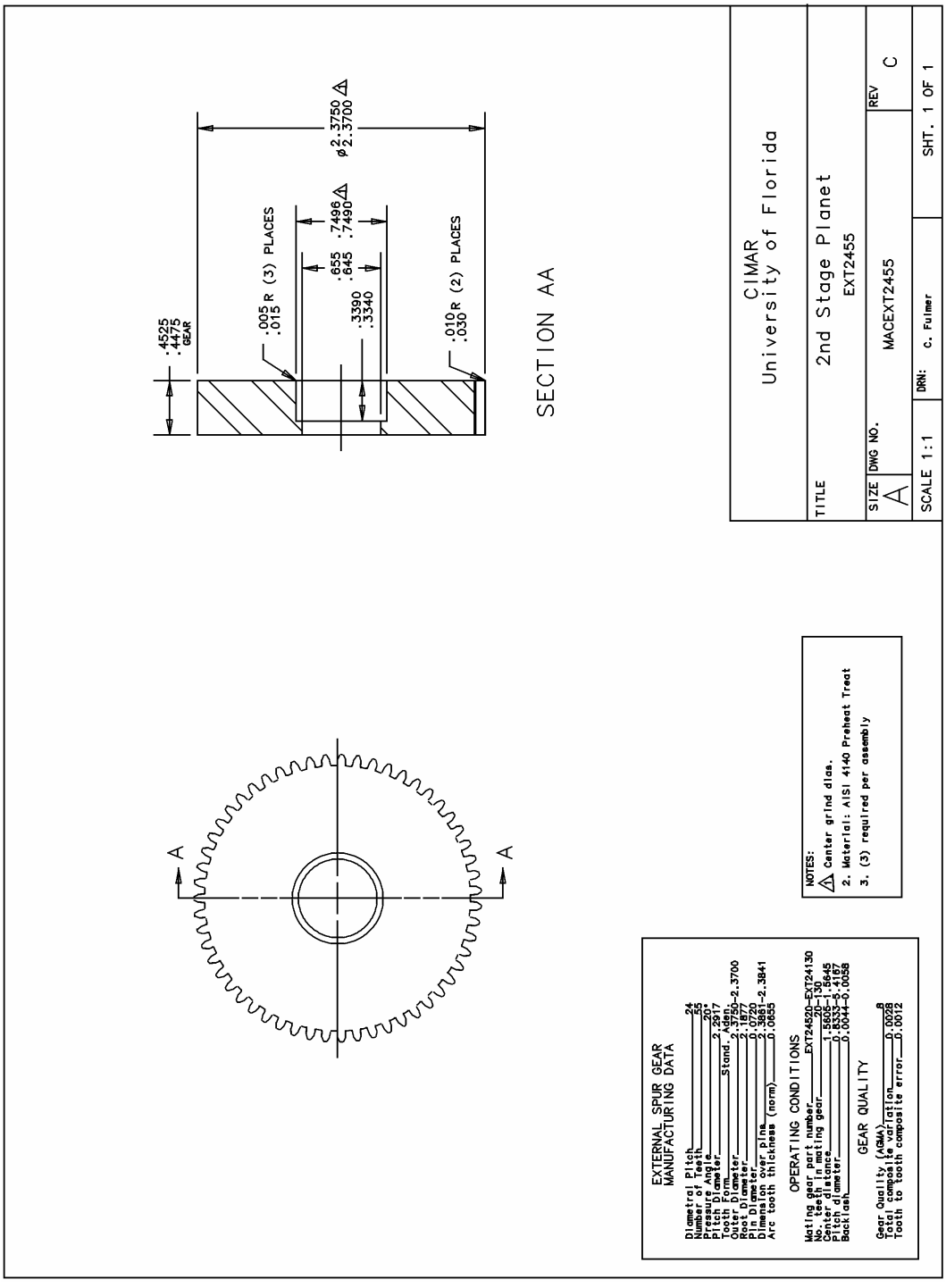

Figure A-5. 2nd stage planet gear

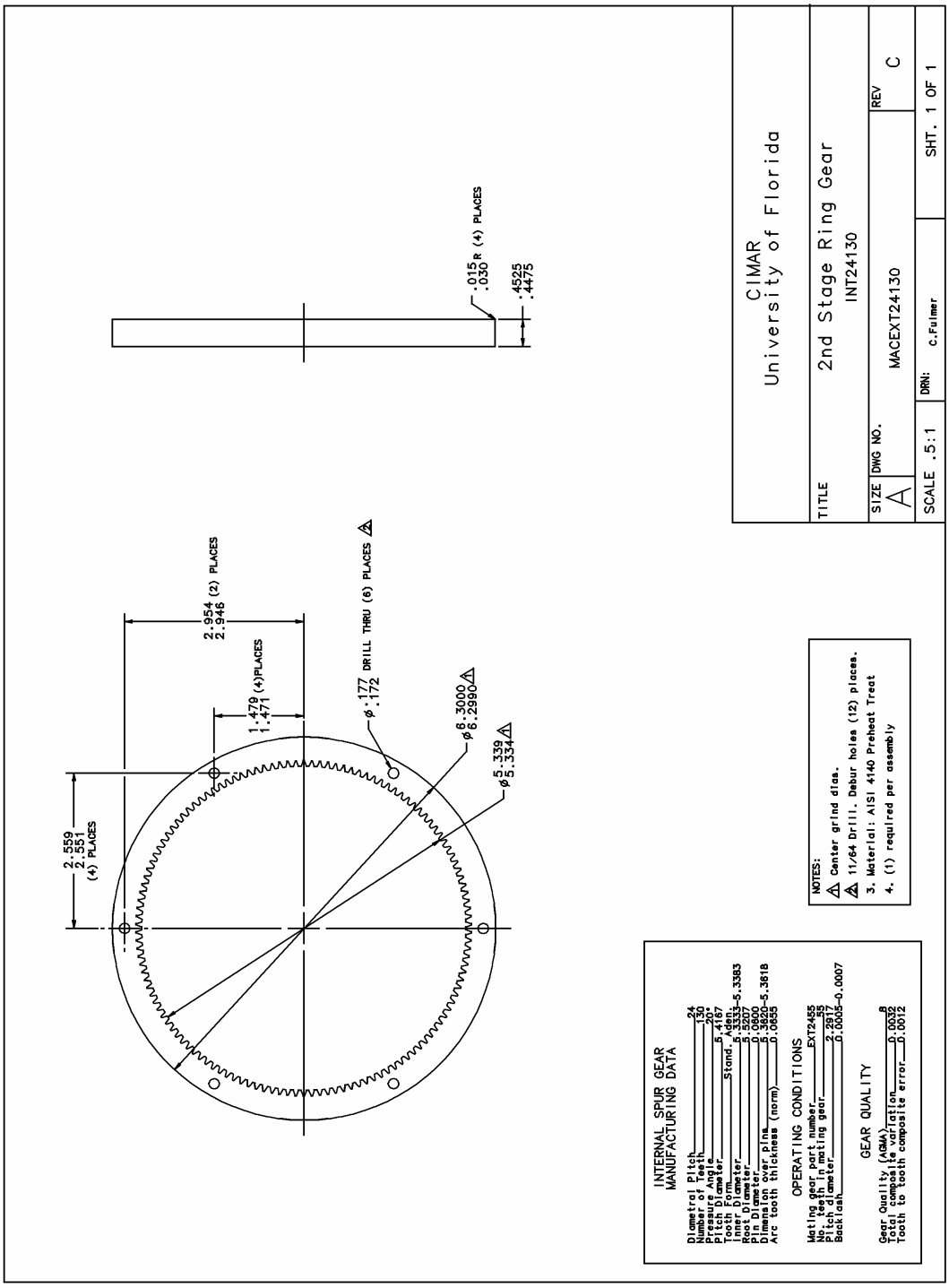

Figure A-6. 2nd stage ring gear

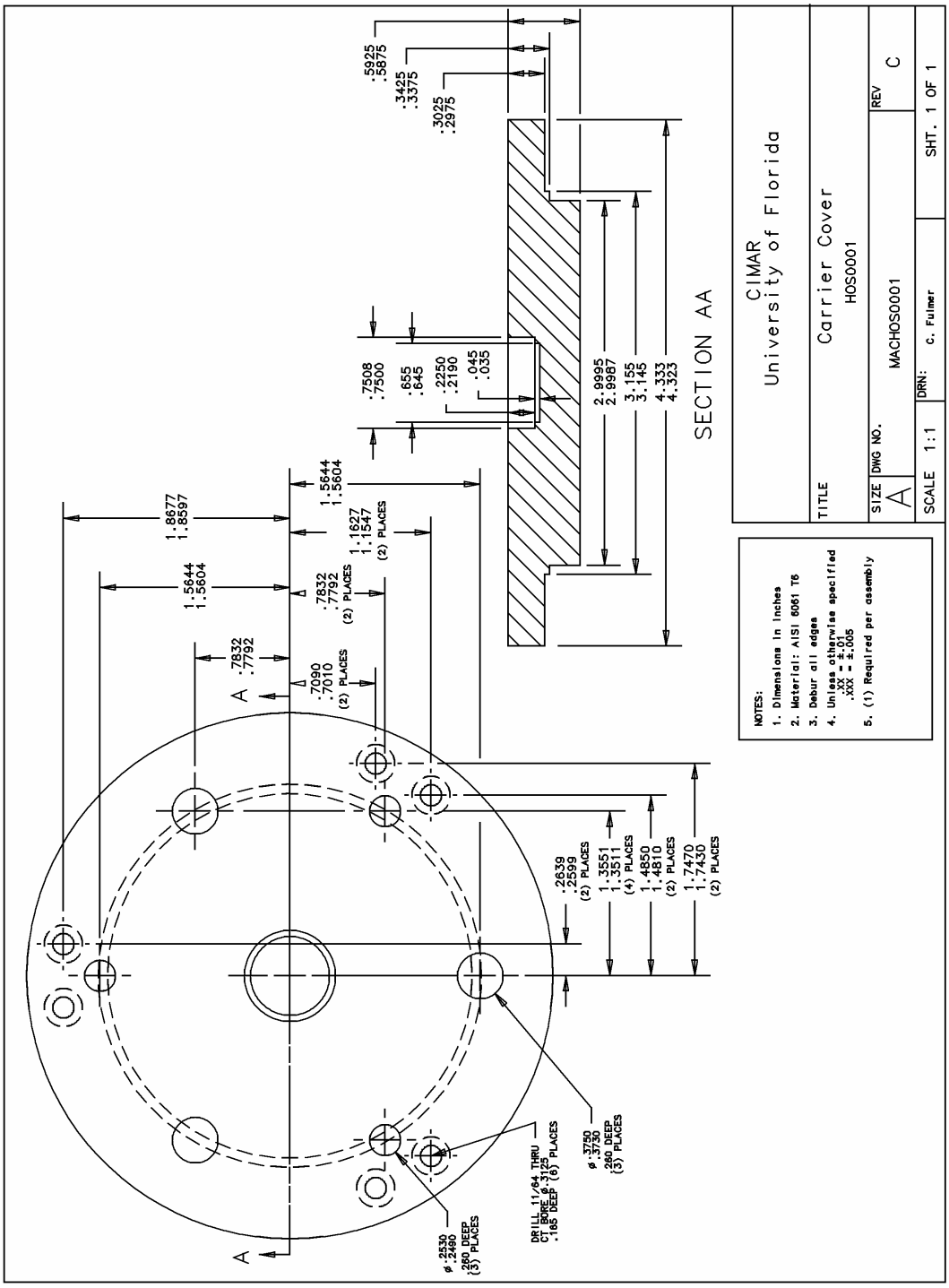

Figure A-7. Carrier cover

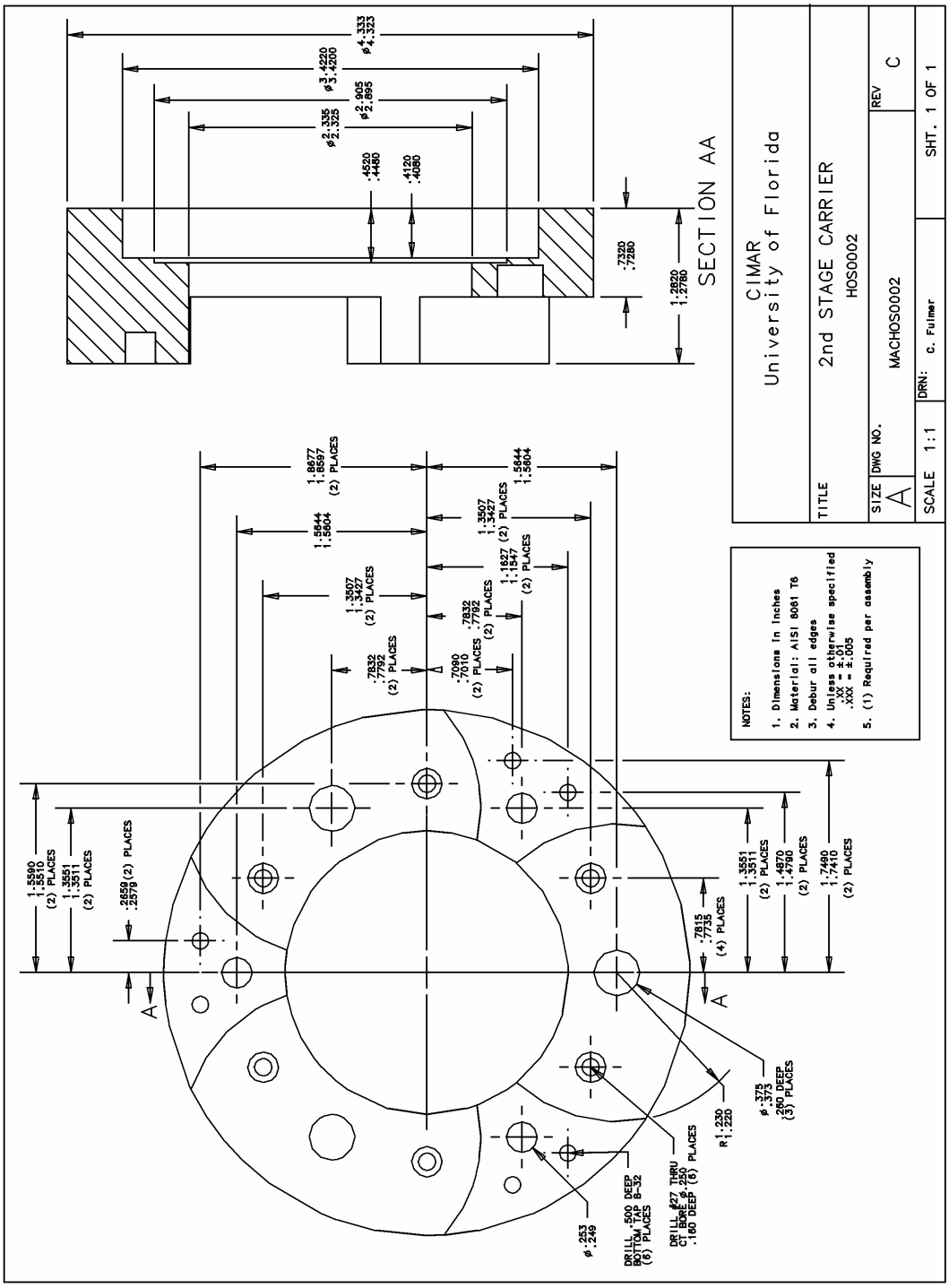

Figure A-8. 2nd stage carrier

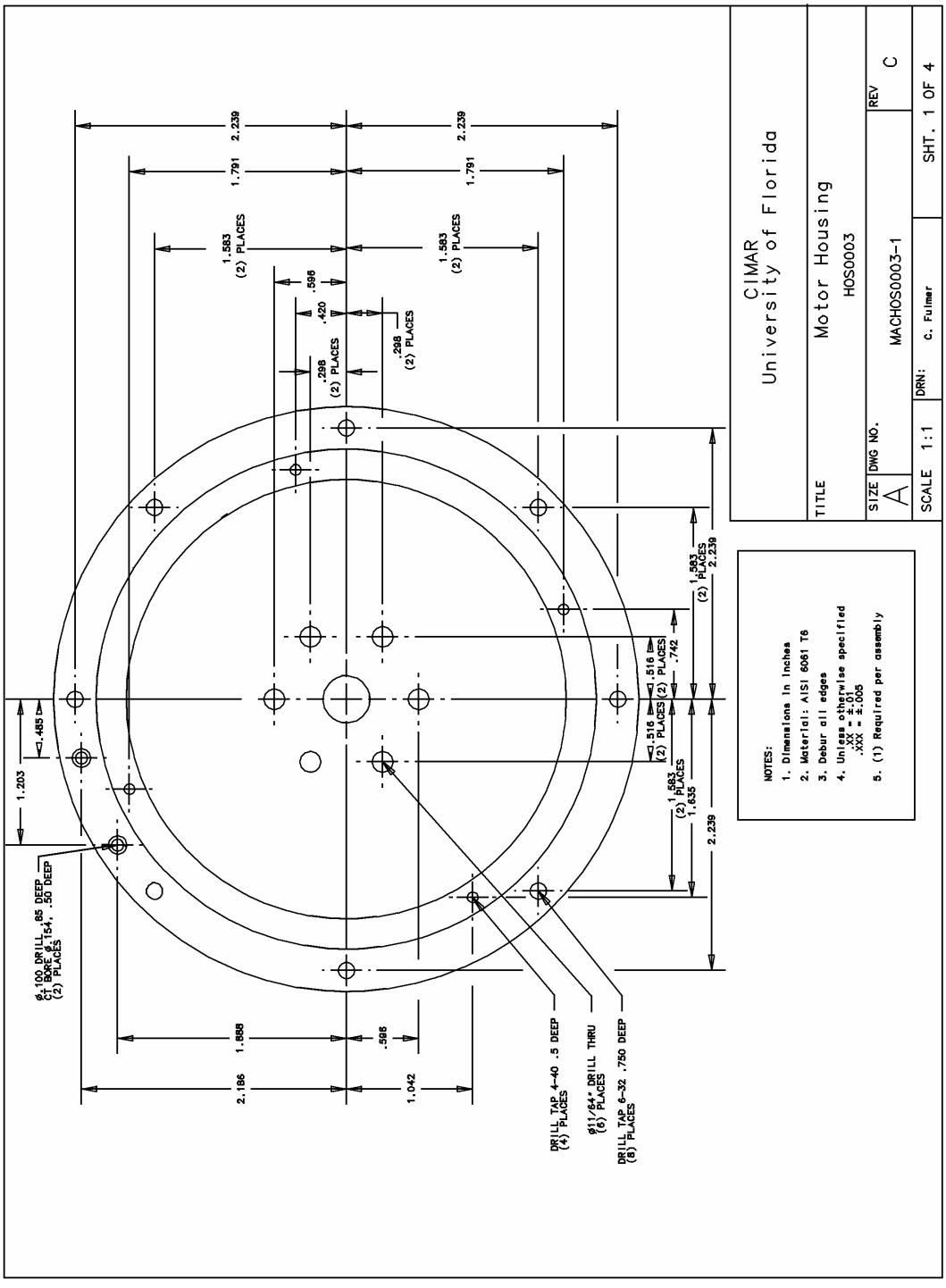

Figure A-9. Motor housing 1

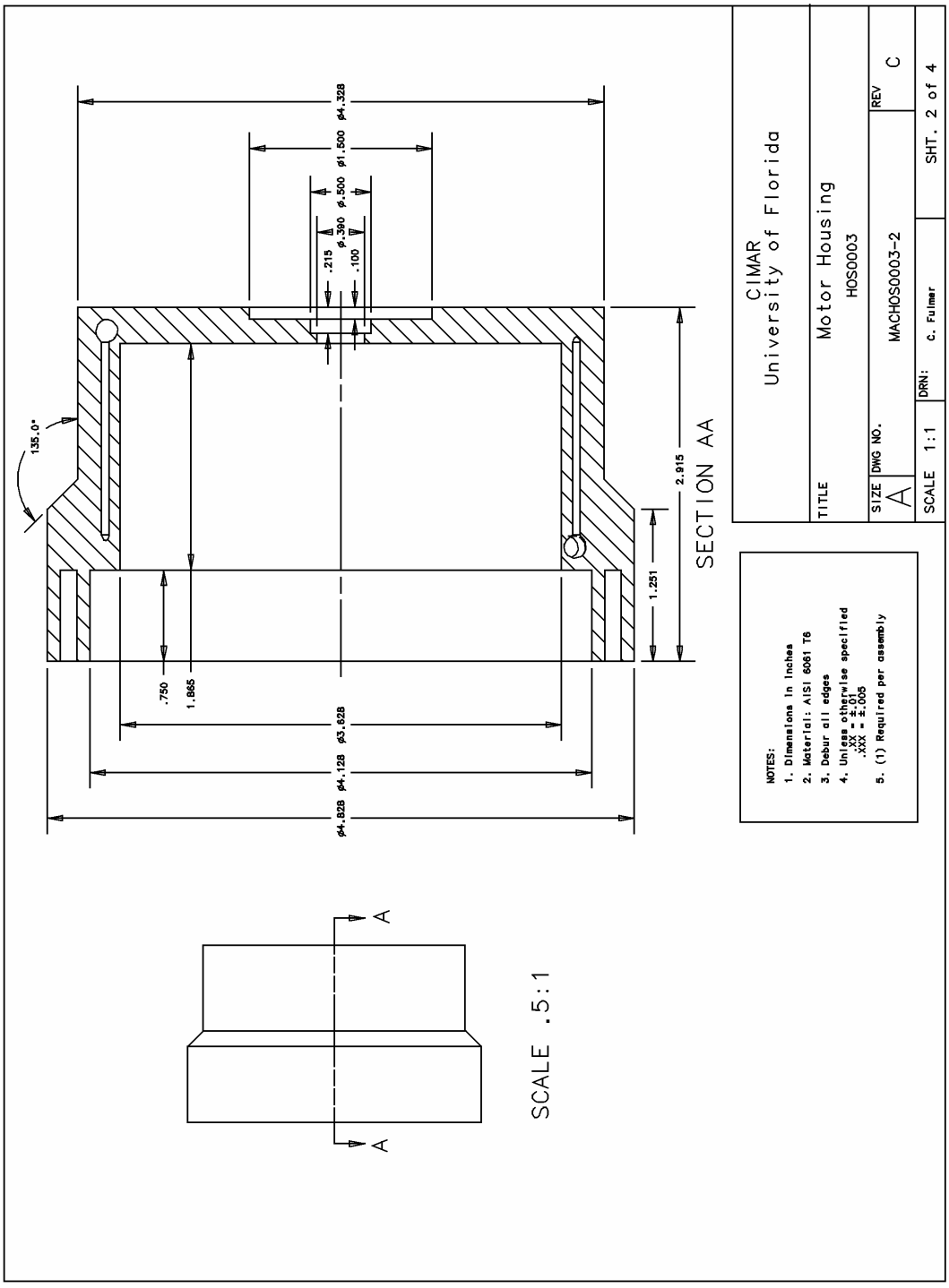

Figure A-10. Motor housing 2

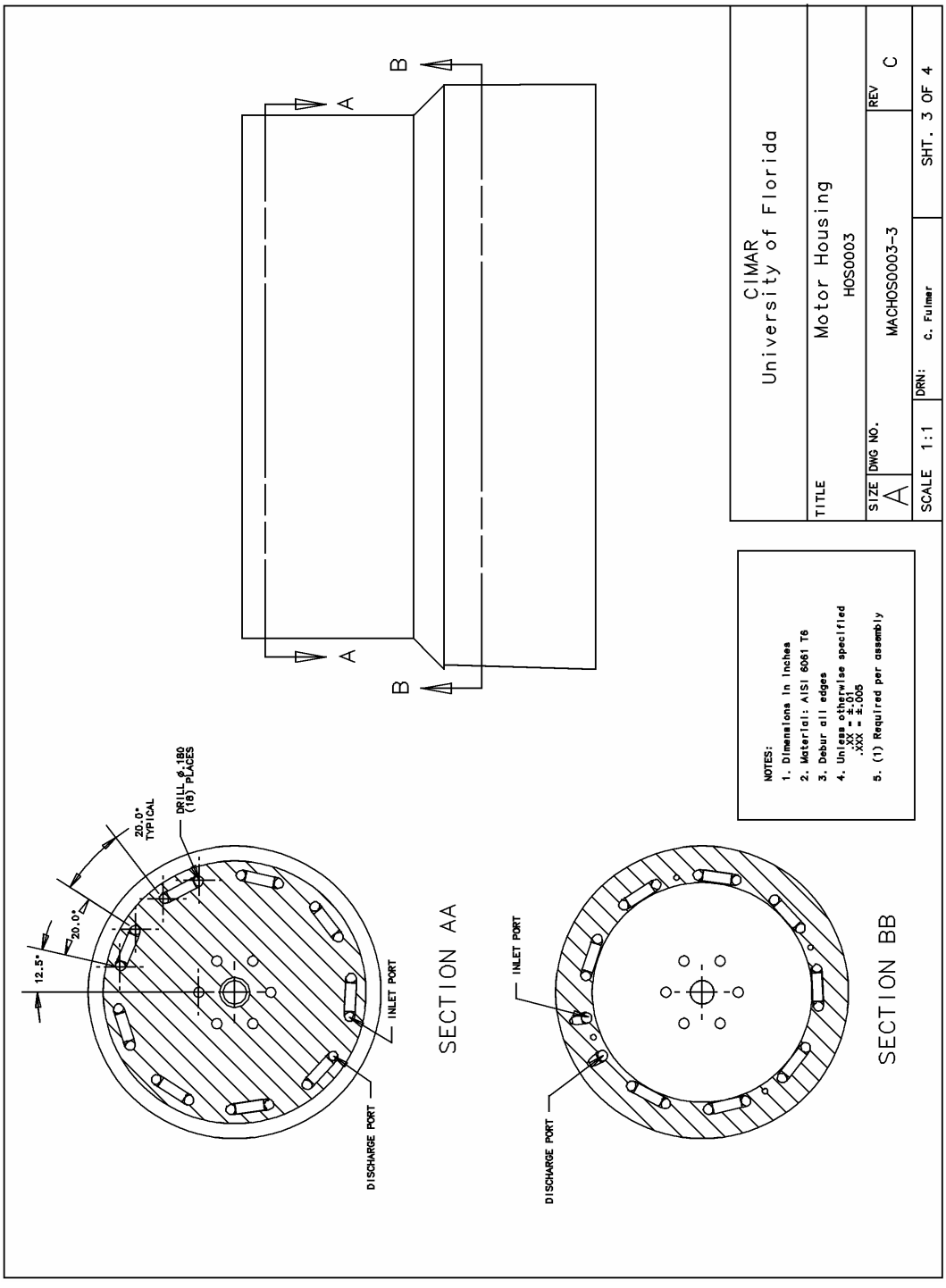

Figure A-11. Motor housing 3

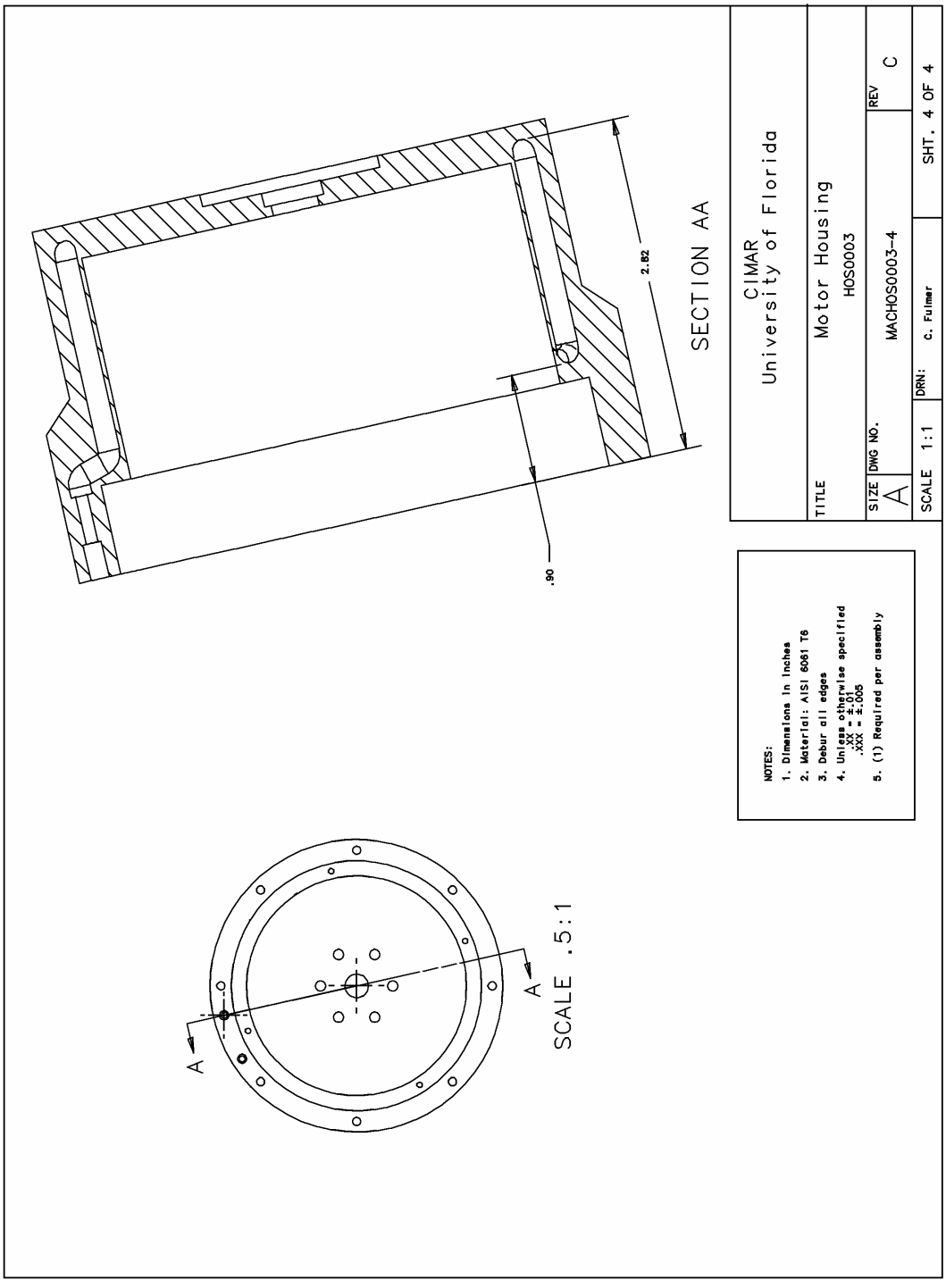

Figure A-12. Motor housing 4

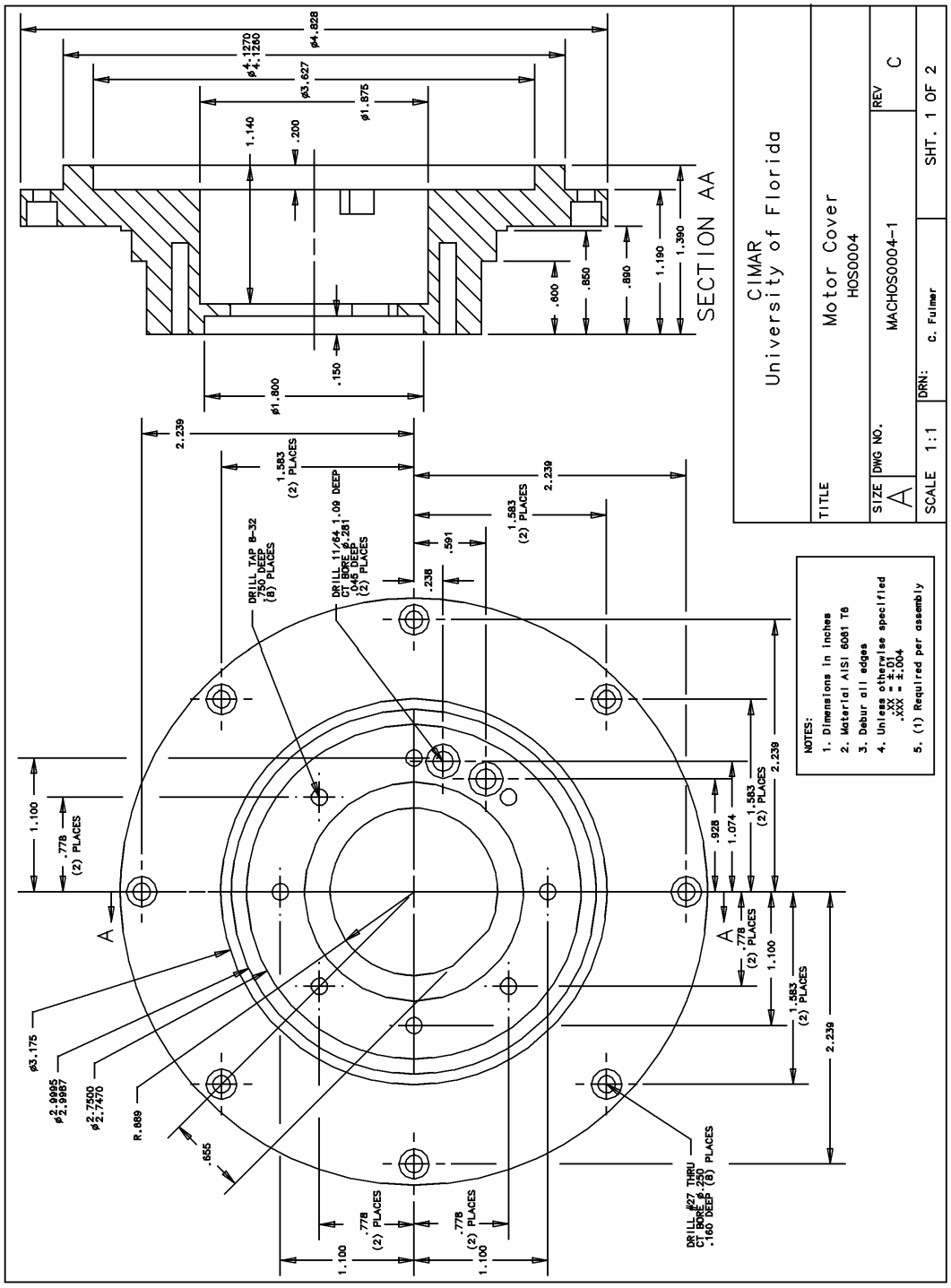

Figure A-13. Motor cover 1

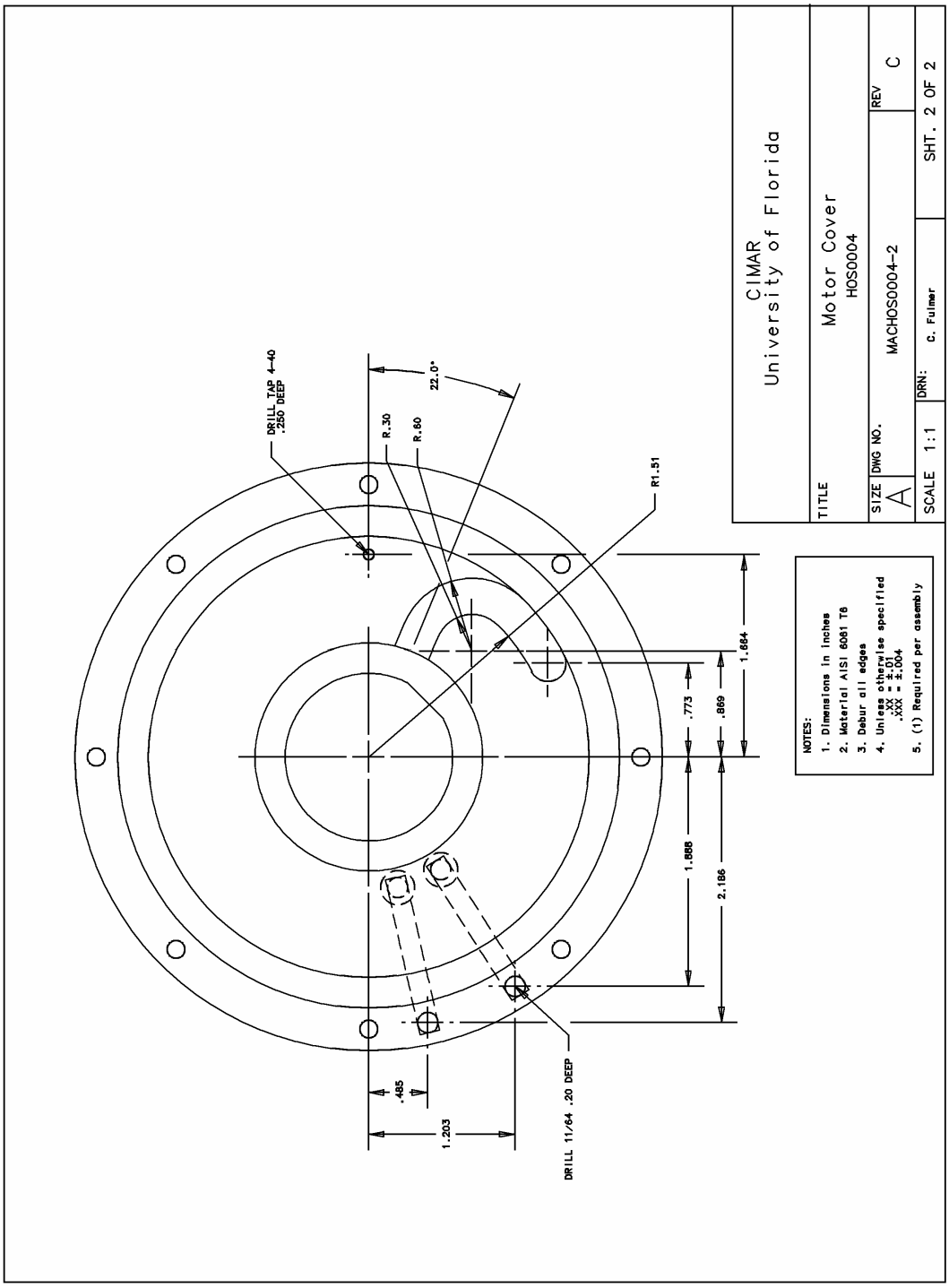

Figure A-14. Motor cover 2

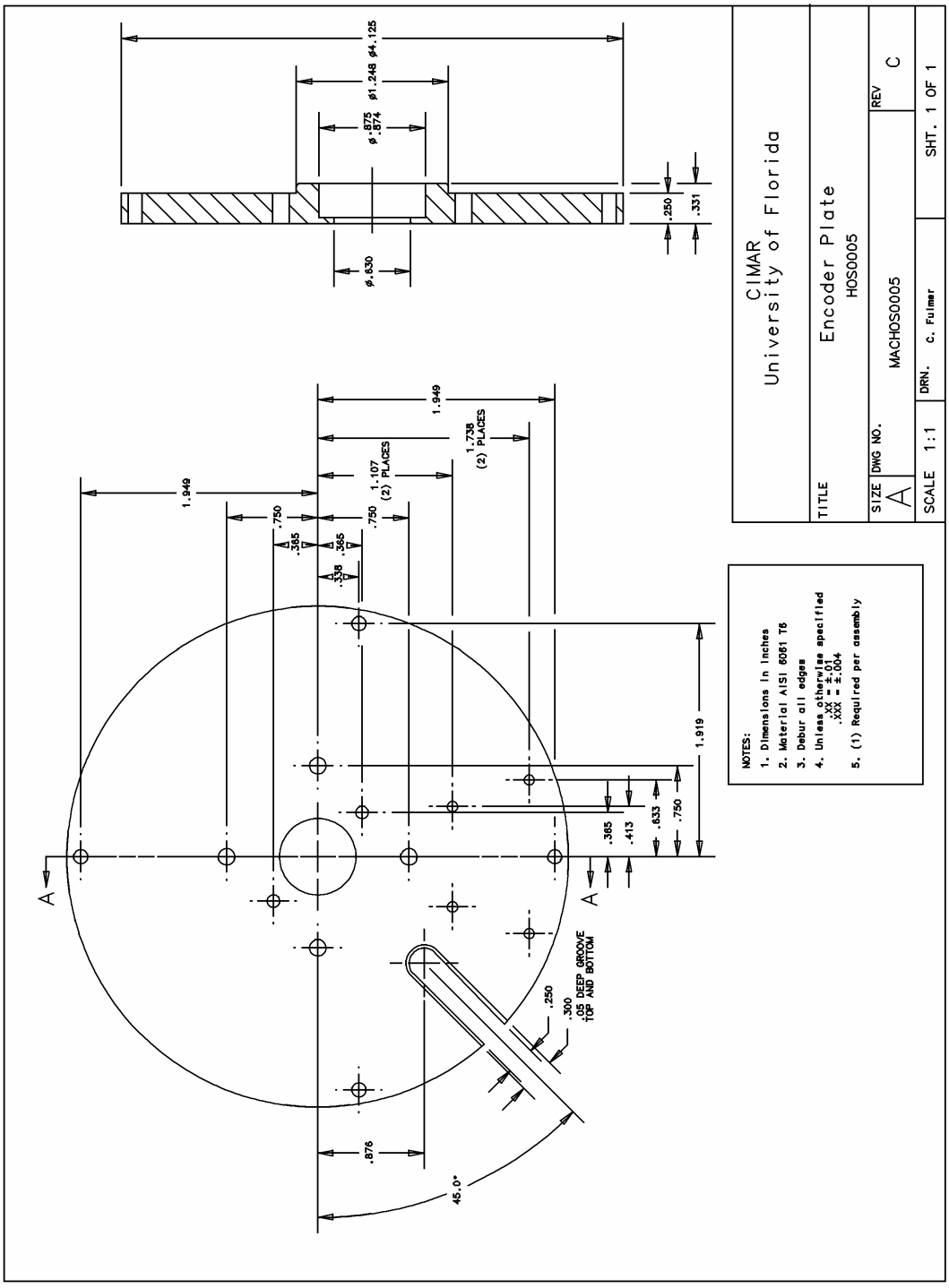

Figure A-15. Encoder plate

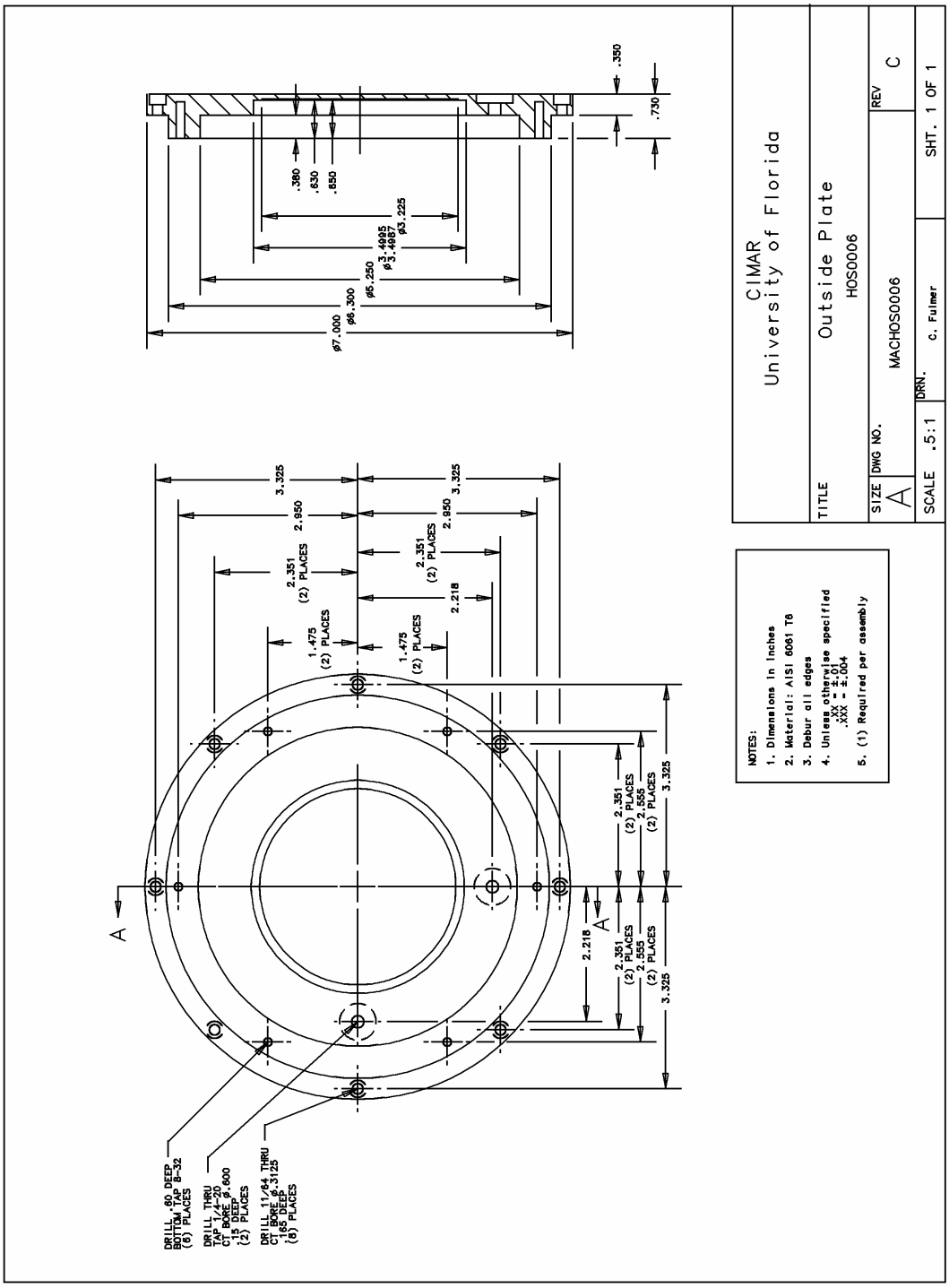

Figure A-16. Outside plate

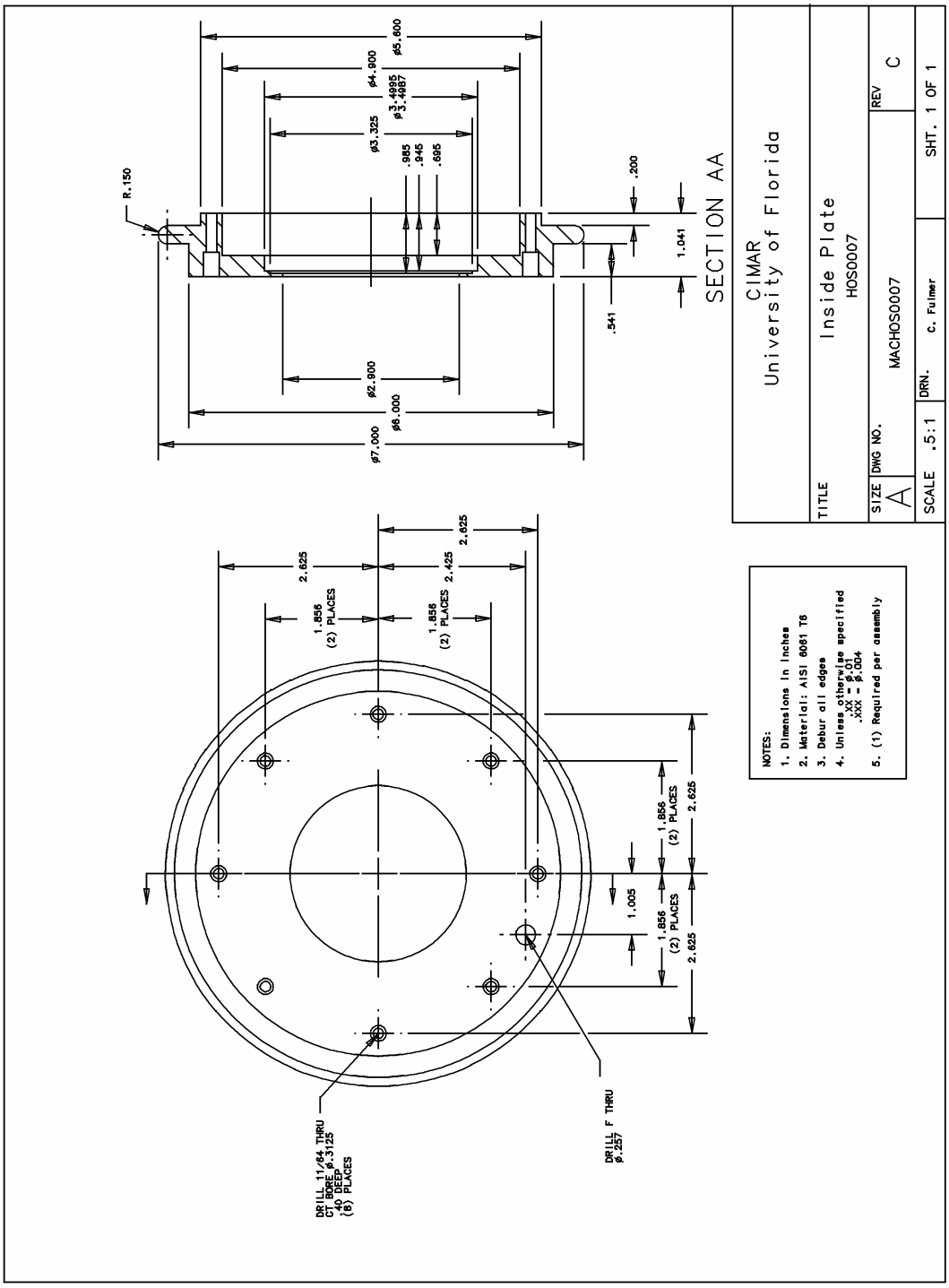

Figure A-17. Inside plate

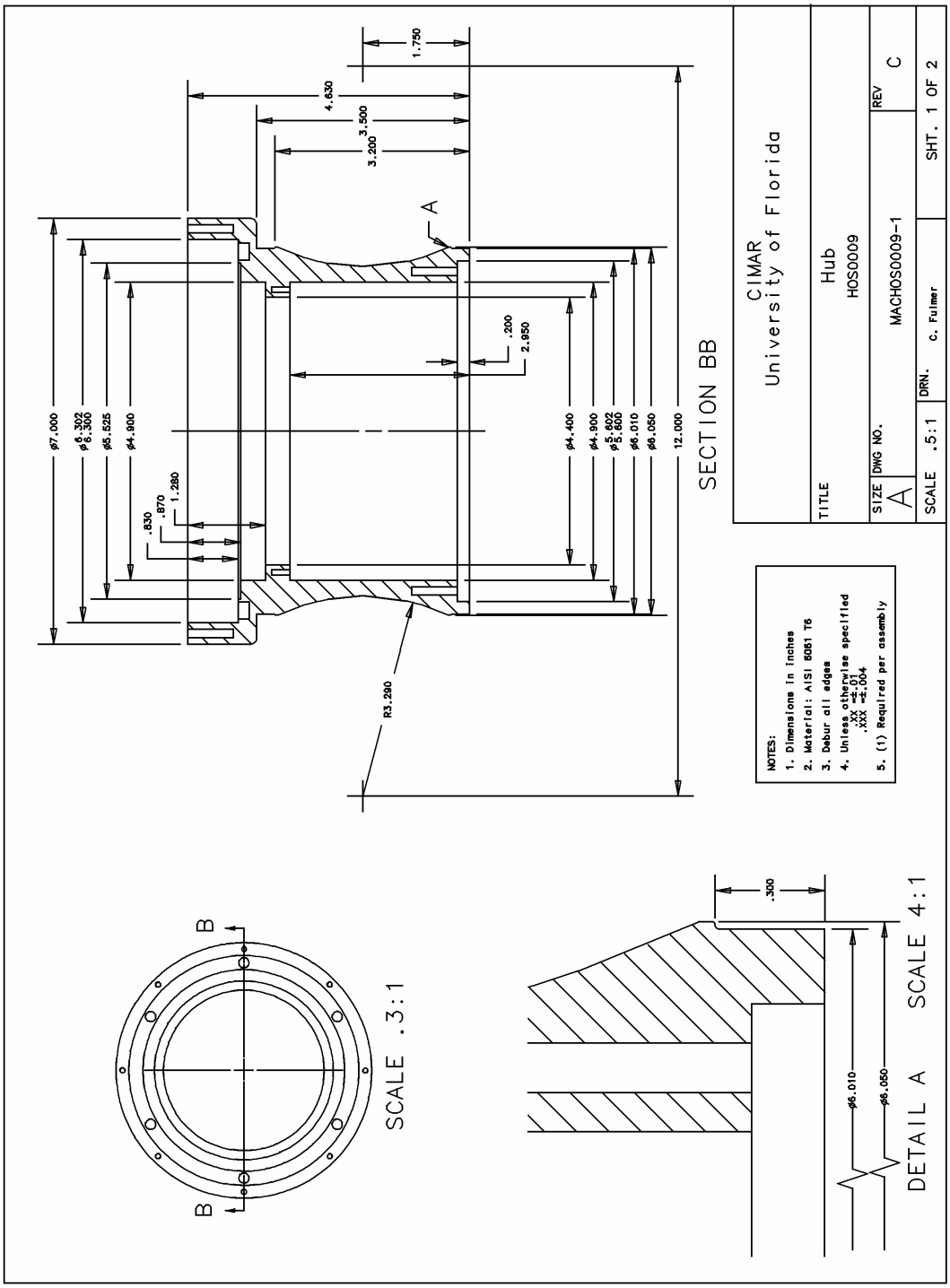

Figure A-18. Hub 1

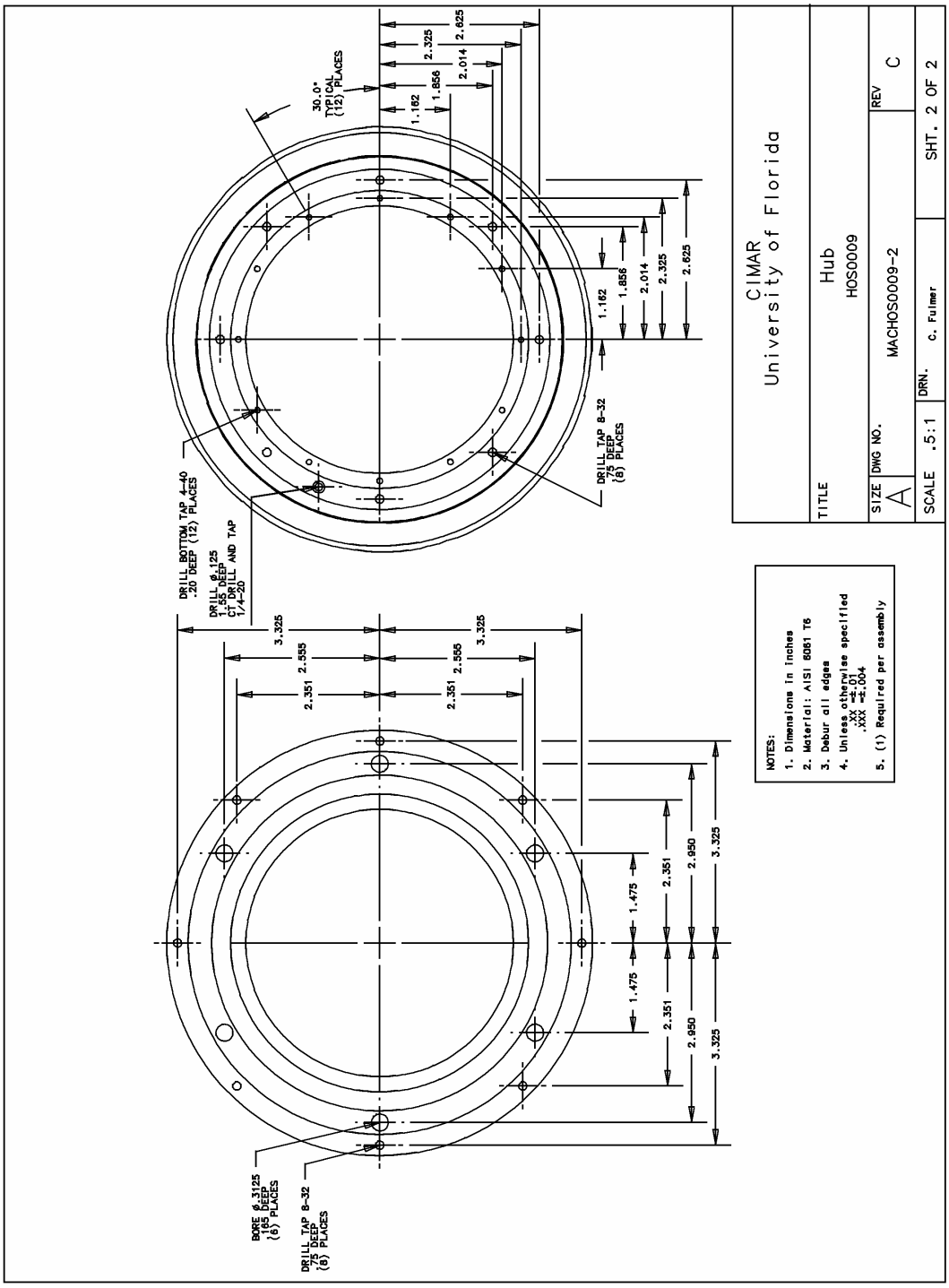

Figure A-19. Hub 2

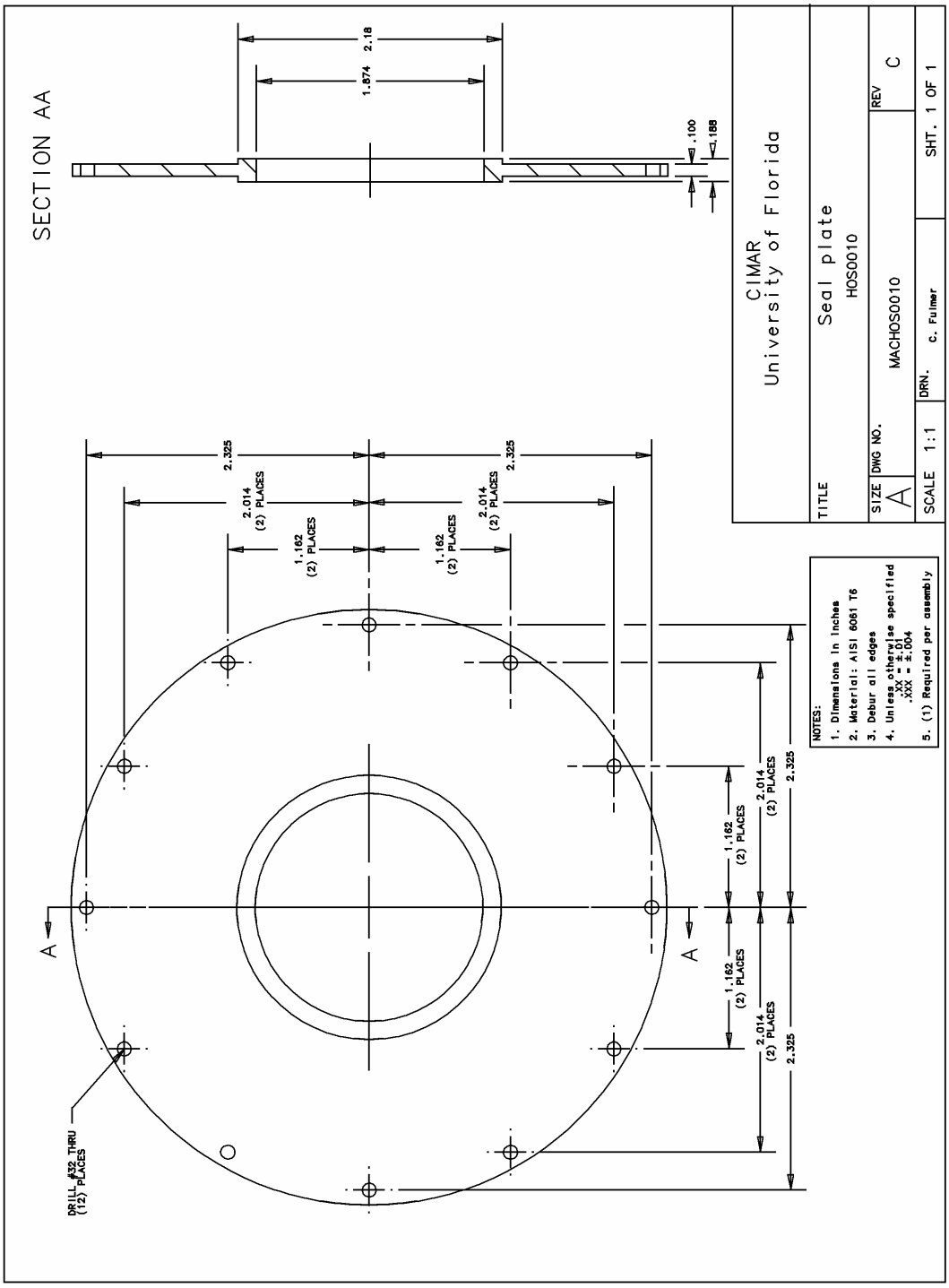

Figure A-20. Seal plate

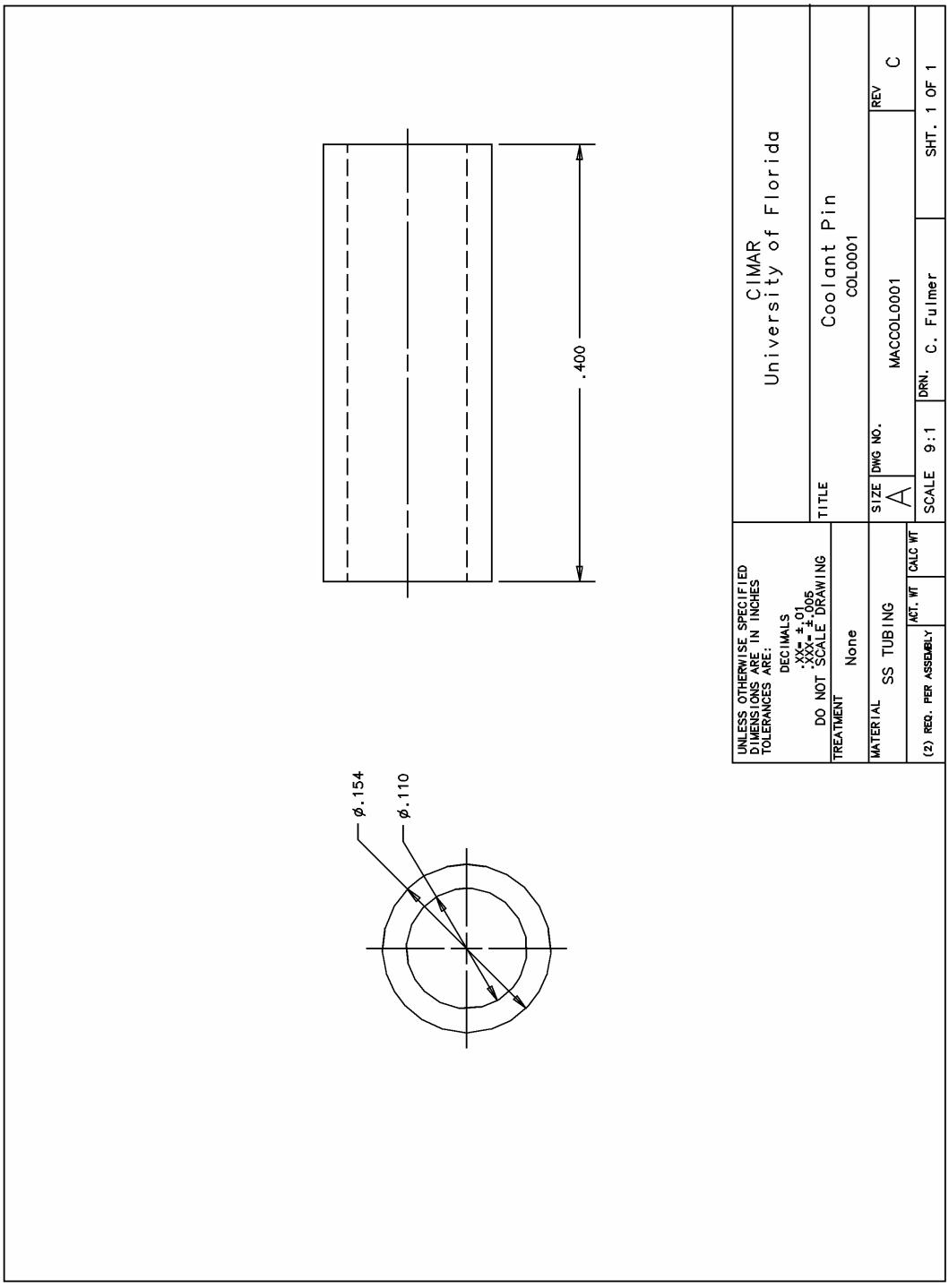

Figure A-21. Coolant pin

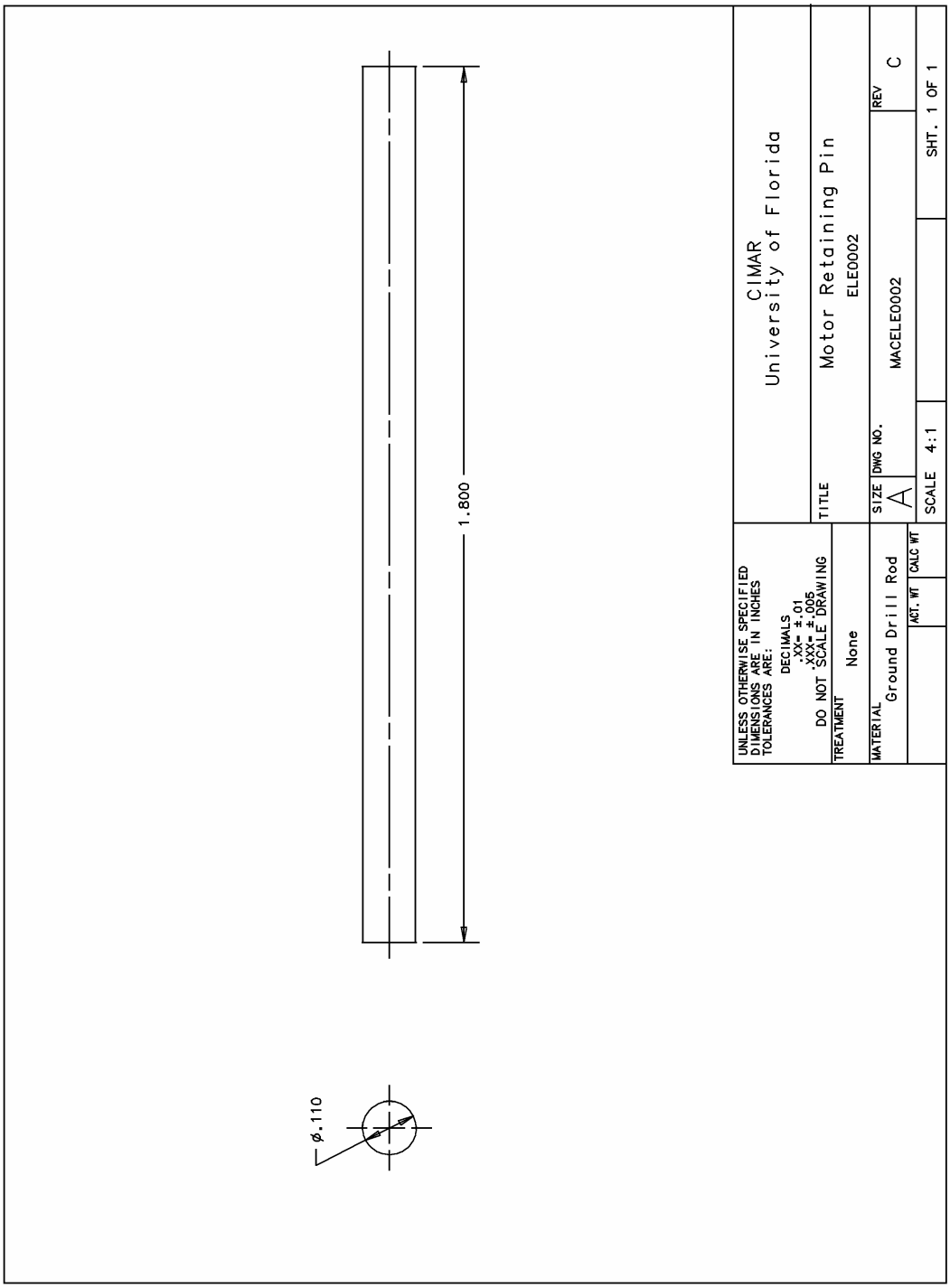

Figure A-22. Motor retaining pin

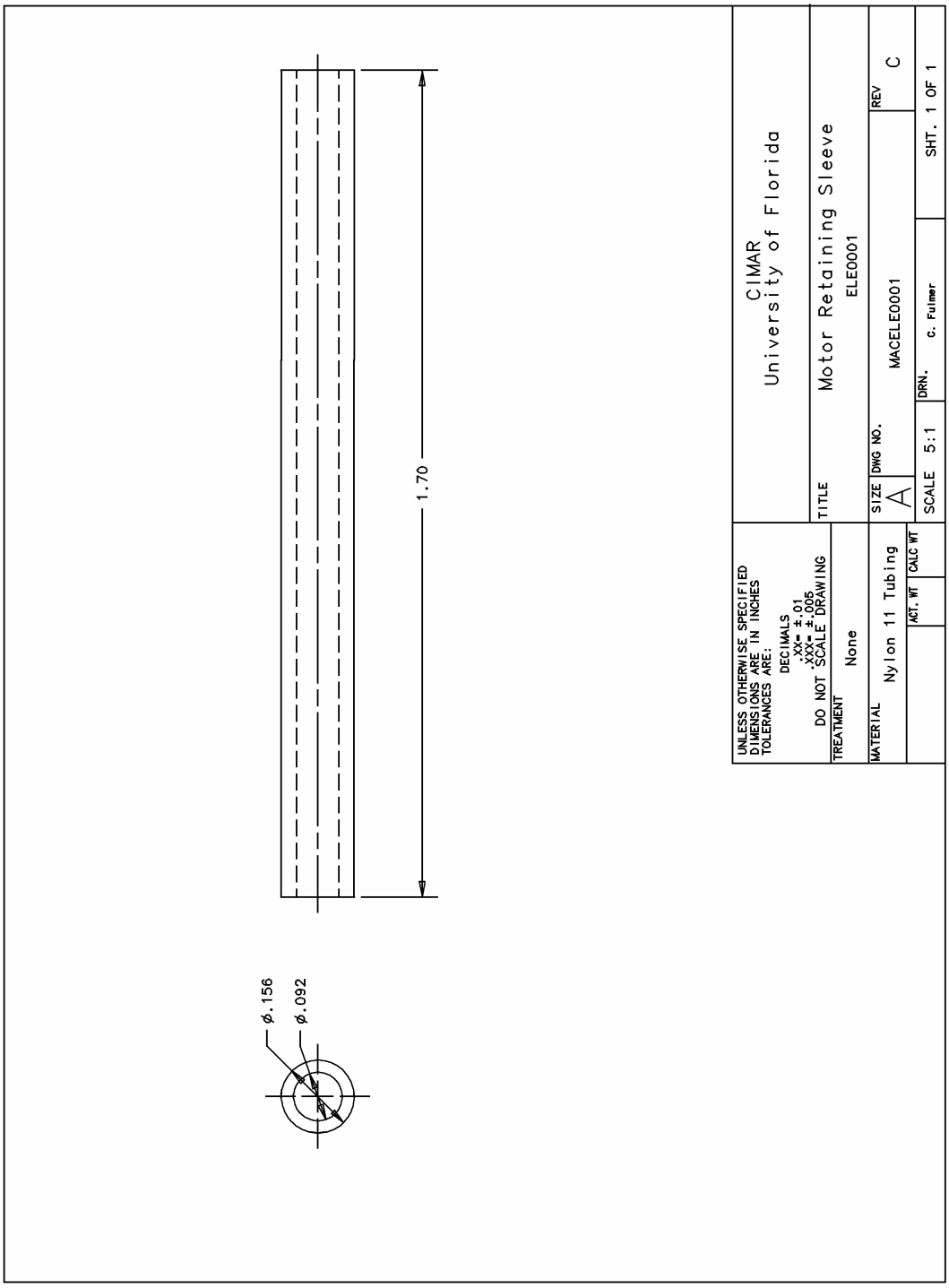

Figure A-23. Motor retaining sleeve

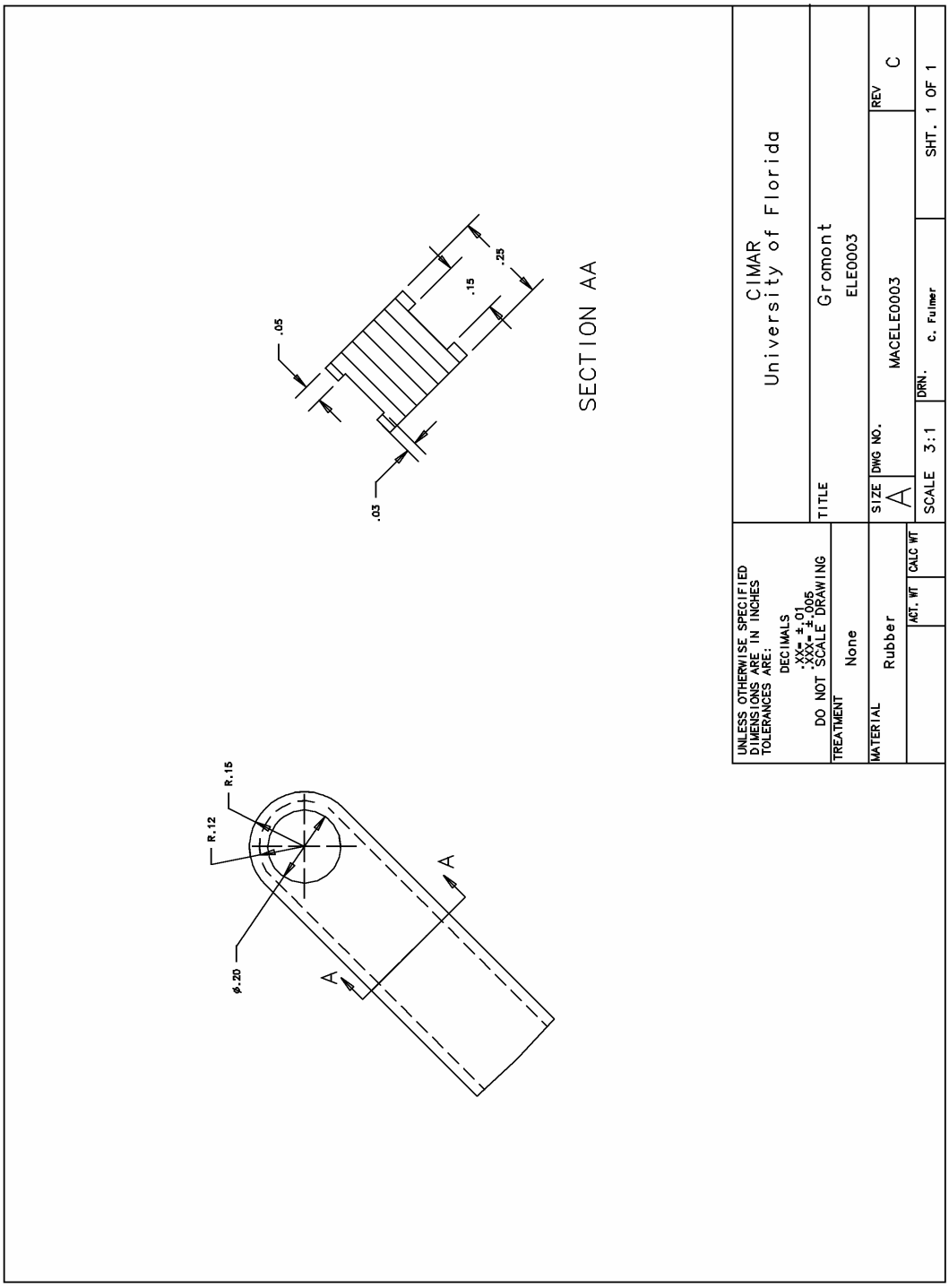

Figure A-24. Grommet

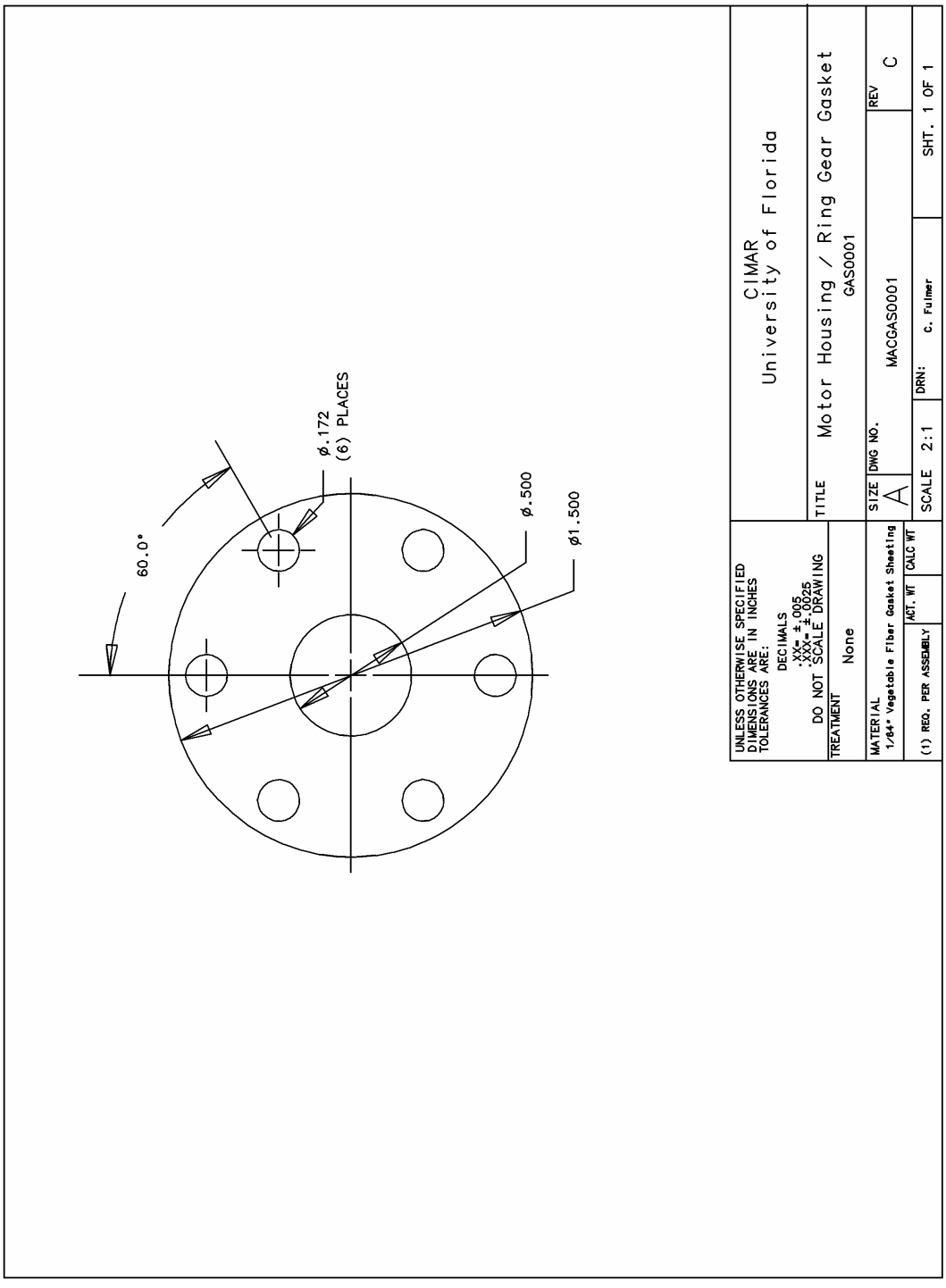

Figure A-25. Motor housing/ring gear gasket

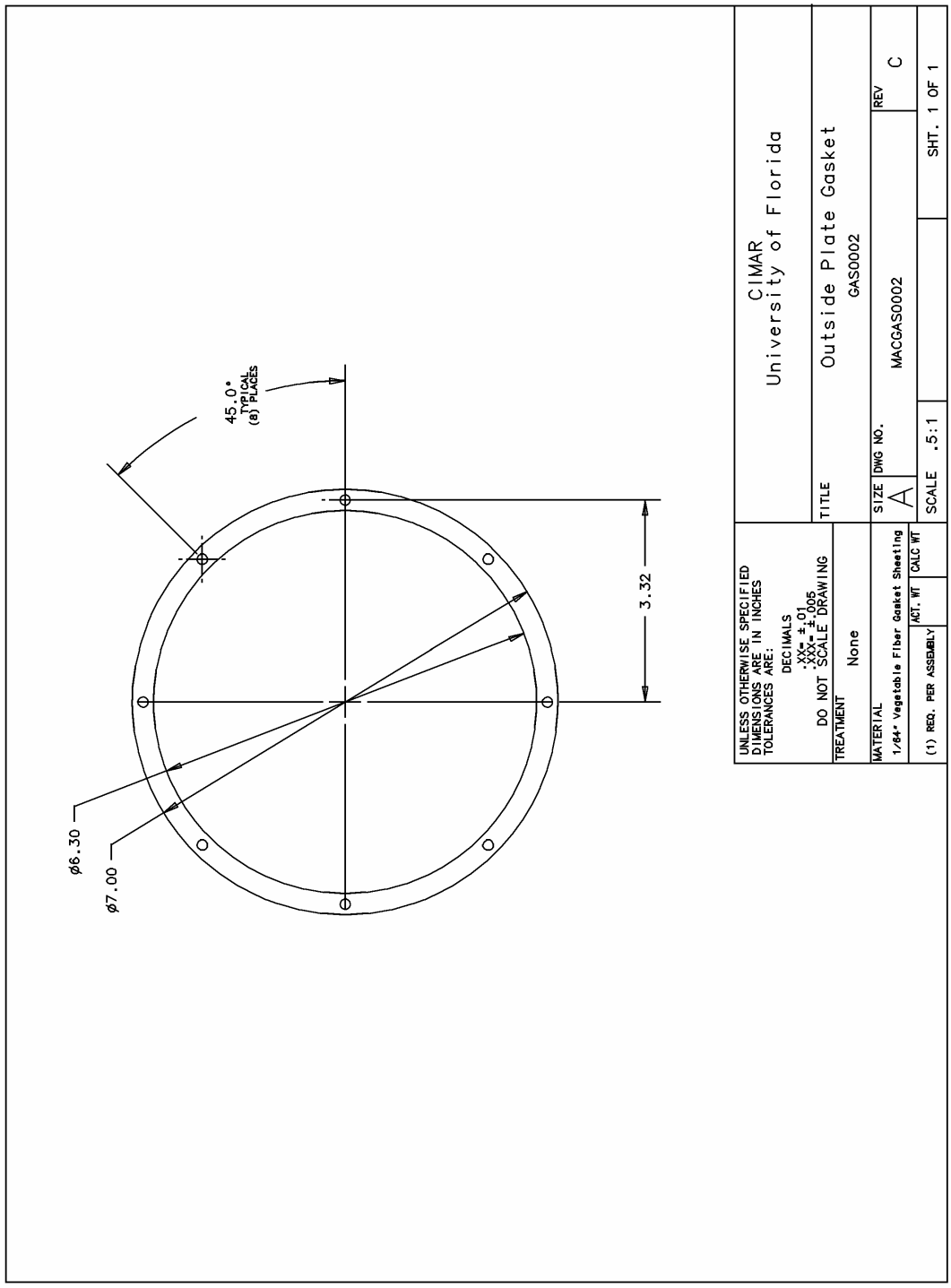

Figure A-26. Outside plate gasket

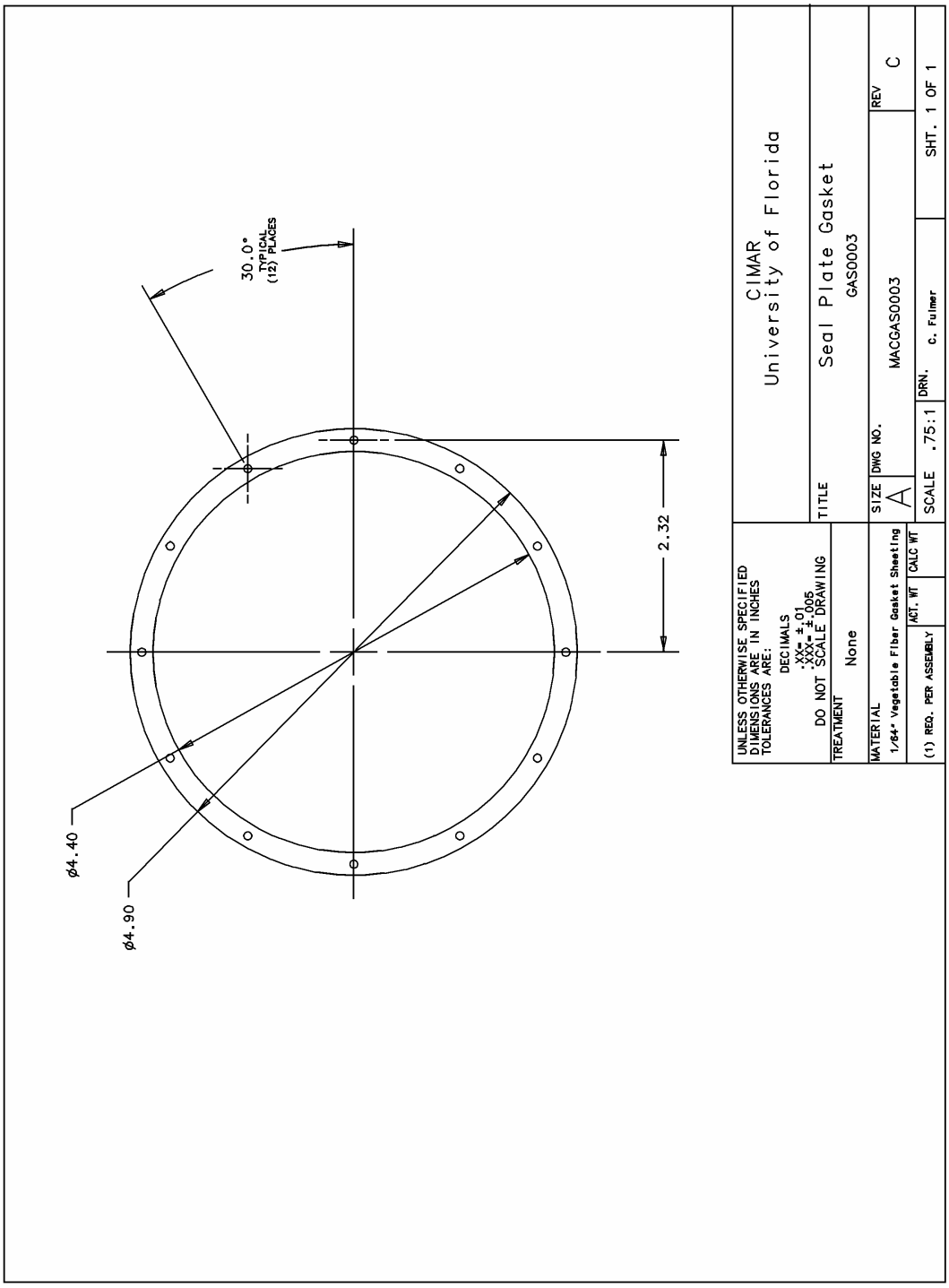

Figure A-27. Seal plate gasket

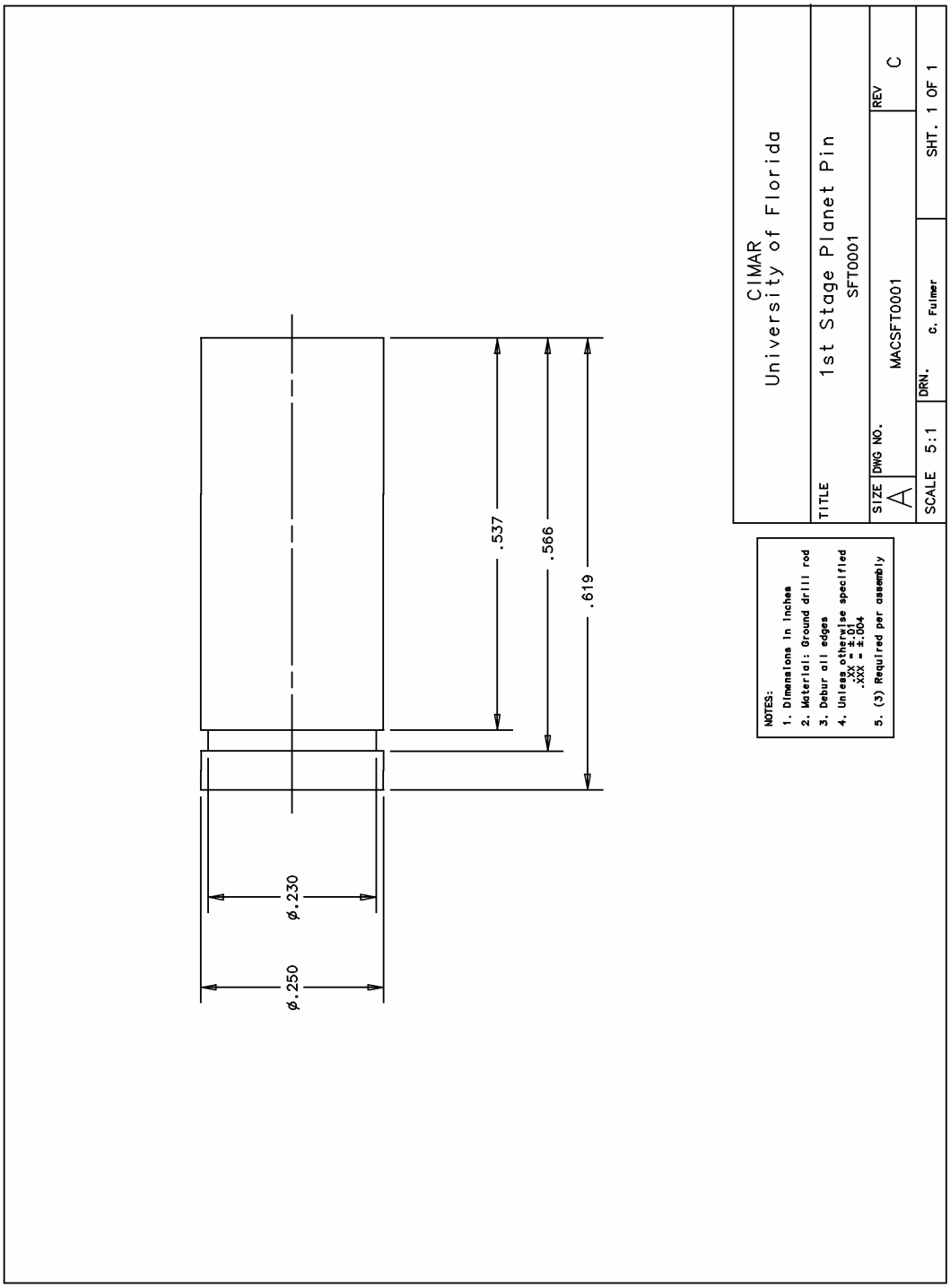

Figure A-28. 1st Stage planet pin

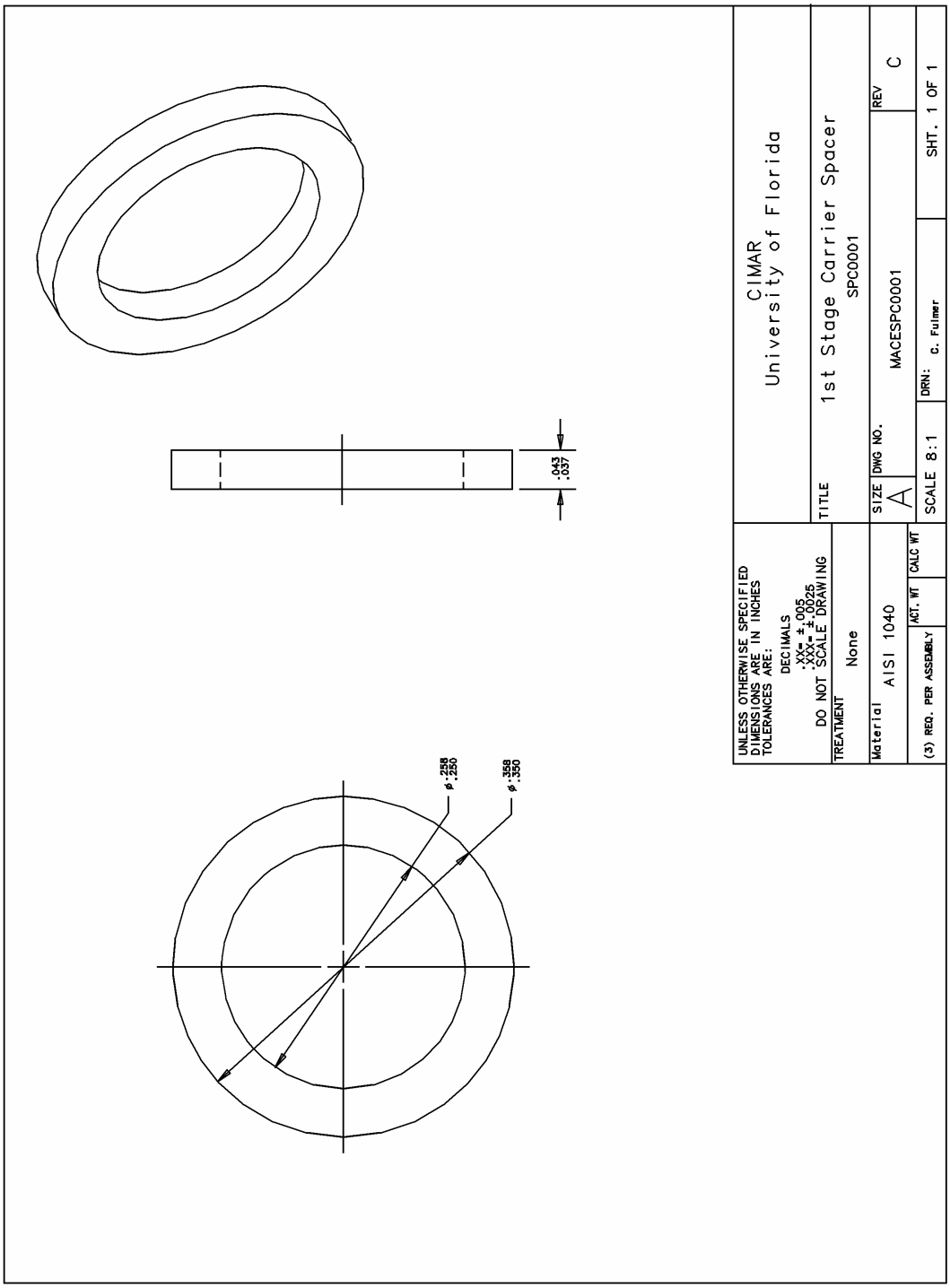

Figure A-29. 1st stage carrier spacer

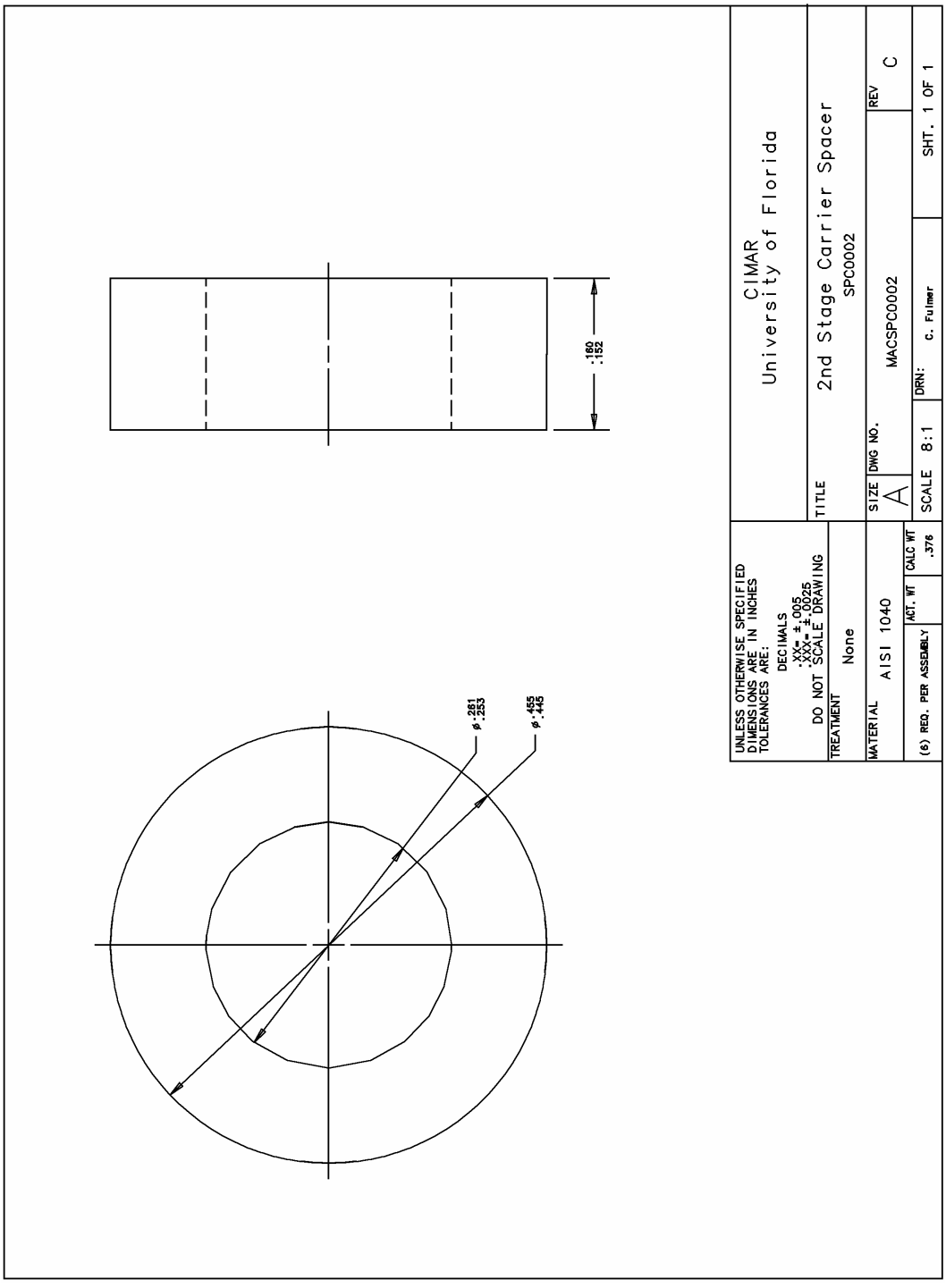

Figure A-30. 2nd stage carrier spacer

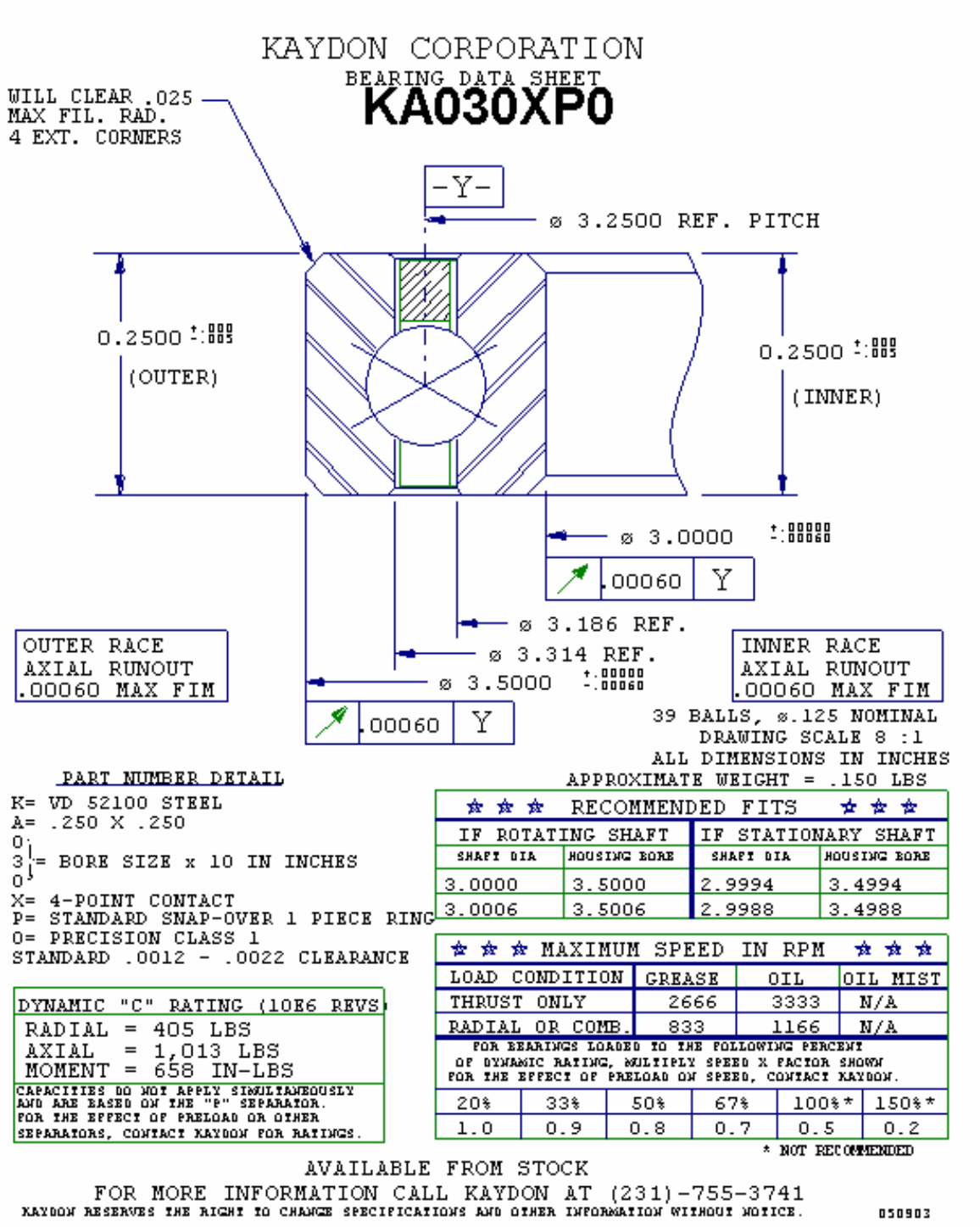

Figure A-31. Outside main bearing drawing

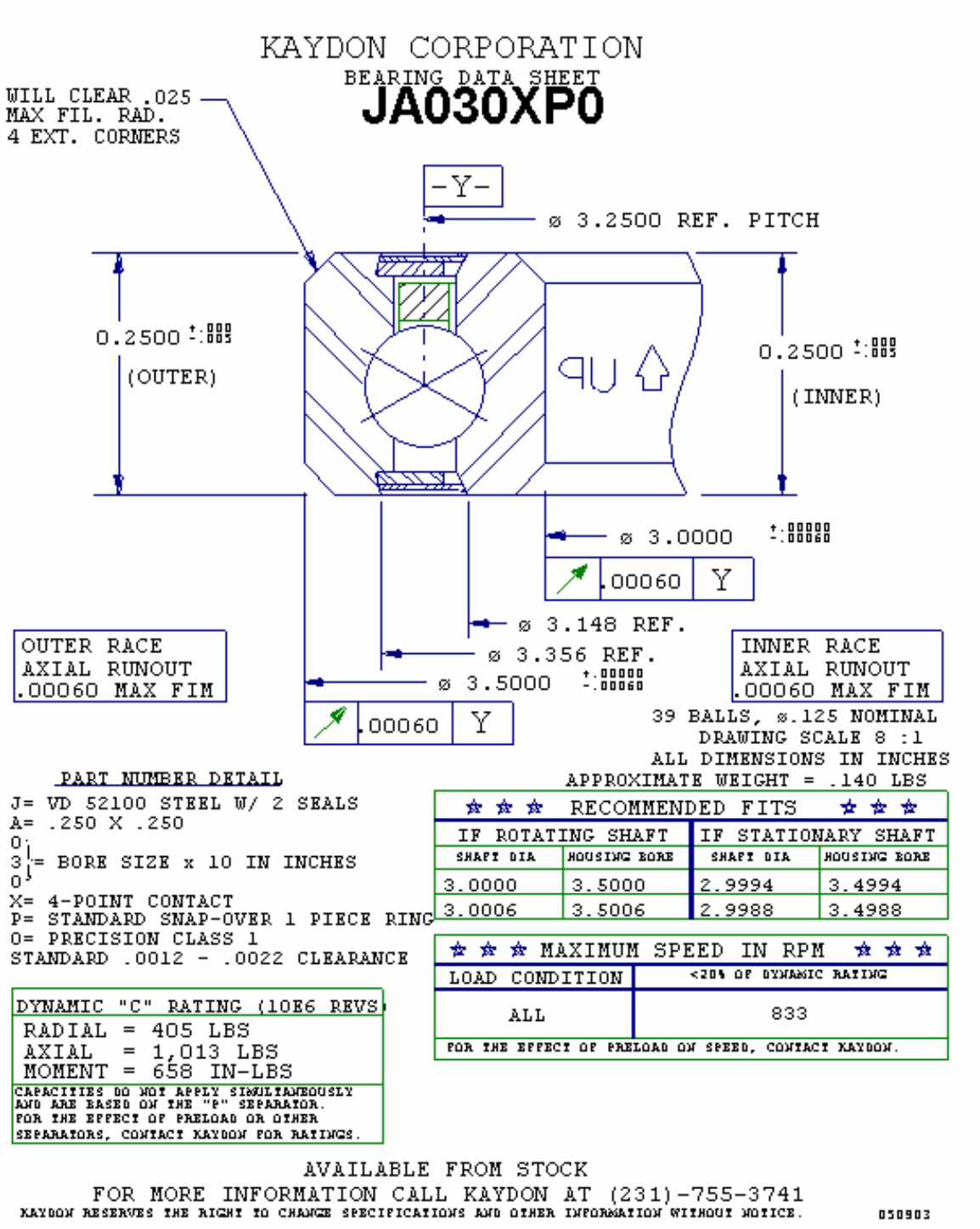

Figure A-32. Inside main bearing drawing

Table A-1. Bill of materials

Bill of Materials		
Part Name	Part Number	Quantity
Main Shaft	EXT3627	1
1st Stage Planet Gear	EXT3636	3
1st Stage Ring Gear	INT3699	1
1st Stage Carrier	EXT2420	1
2nd Stage Planet Gear	EXT2455	3
2nd Stage Ring Gear	INT24130	1
Carrier Cover	HOS0001	1
2nd Stage Carrier	HOS0002	1
Motor Housing	HOS0003	1
Motor Cover	HOS0004	1
Encoder Plate	HOS0005	1
Outside Plate	HOS0006	1
Inside Plate	HOS0007	1
Hub	HOS0009	1
Seal Plate	HOS0010	1
2nd Stage Carrier Spacer	SPC0002	6
1st Stage Carrier Spacer	SPC0001	3
Motor Housing / Ring Gear Gasket	GAS0001	1
Outside Plate Gasket	GAS0002	1
Seal Plate Gasket	GAS0003	1
Motor Retaining Sleeve	ELE0001	1
Motor Retaining Pin	ELE0002	1
Grommet	ELE0003	1
Wire Ring	ELE0004	1
Coolant Pin	COL0001	2
Kaydon Bearing ID=3" OD=3.5" open	KA030XP0	1
Kaydon Bearing ID=3" OD=3.5" sealed	JA030XP0	1
Bearing ID = .375 OD = .875 open	S3K	1
Bearing ID = .375 OD = .875 double sealed	S3PP	1
Bearing ID=.25 OD=.7500 open	S1K	5
Bearing ID=.25 OD=.625 open	S1K7	3
.25 X .5 inch Dowel Pin (Unbrako)	67876722	3
.25 X 1 inch Dowel Pin (Unbrako)	67876888	3
Socket head cap screw SS 4-40 X 5/8"	92196A112	4
Socket head cap screw alloy steel 6-32 X 1/2"	91251A148	6
Socket head cap screw alloy steel 8-32 X 5/8"	91251A196	6
Self locking Button head socket head screw 8-32 X .5 in. Alloy steel	92360A158	6
Socket head cap screw low profile SS 6-32 X 1/4"	93615A210	2
Socket head cap screw alloy steel 6-32 X 3/4"	91251A151	8
Socket head cap screw SS 8-32 X 1 1/4"	92196A201	8
Socket head cap screw SS 8-32 X 3/4"	92196A197	14

Table A-1 cont. Bill of materials

Self locking socket head screw 4-40 X .25 in. Alloy steel	91205A105	12
Retaining Clip Rings .25" shaft	67152801	3
1.5" oil seal	13125K11	1
.375" oil seal	13125K66	1
Encoder code wheel	HEDS 6140-B08	1
1000 count encoder	HEDS 9040	1
BUNA-N O-Ring	9452K15	2
Jam Nut Male Pin Bayonet Connector	M83723/75R2028N	1

APPENDIX B
GEAR DATA

Table B-1. Manufacturing data for 1st stage planetary arrangement

1st Stage Planetary Arrangement						
		Mesh 1		Mesh 2		
	Sun		Planets		Ring	
Manufacturing Data	EXT3627		EXT3636		EXT3699	
Diametral Pitch	36		36		36	
Number of Teeth	27		36		99	
Pressure Angle	20		20		20	
Pitch Diameter	0.75		1		2.75	
Tooth Form	Stand. Aden.		Stand. Aden.		Stand. Aden.	
Outer / Inner diameter	0.8056	0.8006	1.0556	1.0506	2.6944	2.6994
Root Diameter	0.6793		0.9293		2.8207	
Pin Diameter	0.0480		0.0480		0.0400	
Dimension over pins	0.8105	0.8085	1.0622	1.0602	2.7176	2.7196
Arc tooth thickness (norm)	0.0436		0.0436		0.0436	
Extra						
Addendum	0.0278		0.0278		0.0278	
Dedendum	0.0353		0.0353		0.0353	
Whole depth	0.0631		0.0631		0.0631	
Clearance	0.0076		0.0076		0.0076	
Circular pitch	0.0873		0.0873		0.0873	
Max and Min radial clearence	0.005	0.007	0.005	0.007	0.005	0.007
Operating Conditions (Reference)						
Mating gear part number	EXT3636	~~~~	EXT3627	EXT3699	EXT3636	
No. teeth in mating gear	36		27	99	36	
Center distance	0.873	0.877				
Pitch diameter	1		0.75	2.75	1	
Backlash	0.0036	0.0051	0.0036	0.0051	0.0036	0.0051
Gear Quality						
Gear Quality (AGMA)	8		8		8	
Total composite variation	0.0021		0.0022		0.0025	
Tooth to tooth composite error	0.0011		0.0011		0.0011	

Table B-2. Manufacturing data for 2nd stage planetary arrangement

2nd Stage planetary arrangement						
		Mesh 1		Mesh 2		
	Sun		Planets		Ring	
Manufacturing Data	EXT3627		EXT3636		EXT3699	
Diametral Pitch	24		24		24	
Number of Teeth	20		55		130	
Pressure Angle	20		20		20	
Pitch Diameter	0.8333		2.2917		5.4167	
Tooth Form	Stand. Aden.		Stand. Aden.		Stand. Aden.	
Outer / Inner diameter	0.9167	0.9117	2.3750	2.3700	5.3333	5.3383
Root Diameter	0.7293		2.1877		5.5207	
Pin Diameter	0.0720		0.0720		0.0600	
Dimension over pins	0.9269	0.9249	2.3861	2.3841	5.3618	5.3620
Arc tooth thickness (norm)	0.0655		0.0655		0.0655	
Extra						
Addendum	0.0417		0.0417		0.0417	
Dedendum	0.0520		0.0520		0.0520	
Whole depth	0.0937		0.0937		0.0937	
Clearance	0.0103		0.0103		0.0103	
Circular pitch	0.1309		0.1309		0.1309	
Max and Min radial clearence	0.006	0.008	0.006	0.008	0.0007	0.0009
Operating Conditions (Reference)						
Mating gear part number	EXT2455	~~~~	EXT2420	EXT24130	EXT2455	
No. teeth in mating gear	55		20	130	55	
Center distance	1.5605	1.5645				
Pitch diameter	2.2917		0.8333	5.4167	2.2917	
Backlash	0.0044	0.0058	0.0044	0.0058	0.0005	0.0007
Gear Quality						
Gear Quality (AGMA)	8		8		8	
Total composite variation	0.0025		0.0028		0.0032	
Tooth to tooth composite error	0.0013		0.0012		0.0012	

Table B-3. Backlash considerations for 1st stage of the epicyclic gear train

Backlash sources	Design Data	Sun	Mesh 1	Planets	Mesh 2	Ring	
	Pitch Diameter	0.75		1		2.75	
		Min. Rad. C.	Max. Rad. C.	Min. Rad. C.	Max. Rad. C.	Min. Rad. C.	Max. Rad. C.
Group I. Design Backlash Allowance							
1. Center Distance Allowance		0	0	~~~~~~	~~~~~~	~~~~~~	~~~~~~
2. Gear size allowance		0	0	0	0	0	0
Group II. Major Tolerance							
1. Center Distance		0.002	0.002	~~~~~	~~~~~~~	~~~~~~	~~~~~~~
2. Gear Size		0	0.0005	0	0.0005	0	0.0005
Group III. Secondary Sources							
1. Fixed - bearing eccentricities:							
a. Ball-bearing fixed race							
b. Sleeve - bearing runout							
2. Radial clearances:							
a. Ball-bearing radial play							
b. Clearance: Shaft and bearing bore							
(1) Shaft diameter tolerance		0.0001	0.0001	0.0001	0.0001		
(2) Bearing bore tolerance		0	0.00015	0	0.0015		
(3) Allowance		0	0.0001	0	0.0001		
c. Clearance: Bearing OD housing bore							
(1) Bearing OD tolerance		0	0.0002	0	0.0002		
(2) Housing bore tolerance		0.0001	0.0001	0.0001	0.0001		
(3) Allowance		0	0.0001	0	0.0001		
3. Component Error Sources							
a. Clearance: component mounting							
(1) Component - mounting pilot dia. Tolerance							
(2) Housing bore diameter tolerance							
(3) Allowance							
b. Component's mounting pilot eccentricity							
c. Component mounting pilot flatness and perp.							
d. Component shaft radial play							
Group IV. Sources Variable with rotation							
1. Total composite error		0.001	0.001	0.0011	0.0011	0.00125	0.00125
a. Runout							
b. Tooth-to-tooth composite							
Group V. Miscellaneous Sources							
1. Thermal		0.00022	0.00008	0.00029	0.00011	0.00025	0.00075
2. Deflections							
3. Other Sources							
	Row SUMS	0.00342	0.00383	0.00159	0.00331	0.0015	0.0025

	Mesh1		Mesh2	
	Min Rad C.	Max Rad C.	Min Rad C.	Max Rad C.
	0.00501	0.00714	0.00481	0.00409

ALL DIMENSIONS IN INCHES

Table B-4. Backlash considerations for 2nd stage of the epicyclic gear train

Backlash sources	Design Data / Pitch Diameter	Sun 0.833333333 Min. Rad. C.	Mesh 1 Max. Rad. C.	Planets 2.291666667 Min. Rad. C.	Mesh 2 Max. Rad. C.	Ring 5.416666667 Min. Rad. C.	Max. Rad. C.
Group I. Design Backlash Allowance							
1. Center Distance Allowance		0	0	~~~~~	~~~~~	~~~~~	~~~~~
2. Gear size allowance		0	0	0	0	0	0
Group II. Major Tolerance							
1. Center Distance		0.002	0.002	~~~~~	~~~~~~~	~~~~~	~~~~~~~
2. Gear Size		0	0.0005	0	0.0005	0	0.0005
Group III. Secondary Sources							
1. Fixed - bearing eccentricities:							
a. Ball-bearing fixed race							
b. Sleeve - bearing runout							
2. Radial clearances:							
a. Ball-bearing radial play							
b. Clearance: Shaft and bearing bore							
(1) Shaft diameter tolerance		0.0001	0.0001	0.0001	0.0001	0	0.0006
(2) Bearing bore tolerance		0	0.00015	0	0.0015	0.0003	0.0003
(3) Allowance		0	0.0001	0	0.0001	-0.00025	0
c. Clearance: Bearing OD housing bore							
(1) Bearing OD tolerance		0	0.0002	0	0.0002	0	0.0003
(2) Housing bore tolerance		0.0001	0.0001	0.0001	0.0001	0	0.0006
(3) Allowance		0	0.0001	0	0.0001	-0.00025	0
3. Component Error Sources							
a. Clearance: component mounting							
(1) Component - mounting pilot dia. Tolerance							
(2) Housing bore diameter tolerance							
(3) Allowance							
b. Component's mounting pilot eccentricity							
c. Component mounting pilot flatness and perp.							
d. Component shaft radial play							
Group IV. Sources Variable with rotation							
1. Total composite error		0.00125	0.00125	0.0014	0.0014	0.0016	0.0016
a. Runout							
b. Tooth-to-tooth composite							
Group V. Miscellaneous Sources							
1. Thermal		0.00025	0.00009	0.00065	0.00024	0.00145	0.00054
2. Deflections							
3. Other Sources							
	Row SUMS	0.0037	0.00409	0.00225	0.00374	0.00285	0.00444

Mesh1		Mesh2	
Min Rad C.	Max Rad C.	Min Rad C.	Max Rad C.
0.00595	0.00783	0.00659	0.00669

ALL DIMENSIONS IN INCHES

LIST OF REFERENCES

Advanced Motion Controls. PWM Servo Amplifiers Technical Manual. Author, Camarillo, 2000.

American Gear Manufacturers Association. AGMA Design Manual for Fine-Pitch Gearing. Author, 1973.

BEI. Brushless DC Motors An Applications Guide. BEI Technologies, Inc., San Marcos.

Davidson, M., Bahl, V., and Wood, C,. "Utah State University's T2 ODV Mobility Analysis, In Unmanned round Vehicle Technology II," SPIE, Vol 4024, 2000, pp. 96-105.

Diegel, O., Badve, A., Bright, G., Potgieter, J., and Tlale, S., "Improved Mecanum Wheel Design for Omni-directional Robots," Proceedings of the Australian Conference on Robotics Automation, Auckland, November 2002, pp.27-29.

Dooner, D.B., and Seireg, A. A., The Kinematic Geometry of Gearing, A Concurrent Engineering Approach. John Wiley & Sons, New York, 1995.

Dudley, D. W., Handbook of Practical Gear Design. Technomic Publishing Co. Inc., Lancaster, 1994.

Gieras, J. F., and Wing, M., Permanent Magnet Motor Technology: Design and Applications. Marcel Dekker, Inc., New York, 2002.

Hendershot, J. R. Jr., and Miller, T., Design of Brushless Permanent-Magnet Motors. Magna Physics Publishing and Clarendon Press, Oxford, 1994.

Histand, M. B., and Alciatore, D. G., Introduction to Mechatronics and Measurement Systems. McGraw-Hill, Boston.

Horton, H.L., and Ryffel H.H., Machinery's Handbook. Industrial Press Inc., New York, 2000.

Incropera, F. P., and DeWitt, D. P., Fundamentals of Heat and Mass Transfer. John Wiley & Sons, New York, 1996.

Shigley, J. E., and Mischke, C. R., Mechanical Engineering Design, McGraw-Hill Inc., New York, 1989.

South, D.W., and Mancuso, J.R., Mechanical Power Transmission Components. Marcel Dekker, New York, 1994.

Wood, C., Davidson, M., Rich, S., Keller, J., and Maxfield, R., "T2 Omni-Directional Vehicle Mechanical Design," SPIE Conference on Mobile Robots, Boston, Massachusetts, Vol. 3838, September,1999, pp. 69-77.

Wood, C., Rich, S., Frandsen, M., Davidson, M., Maxfield, R., Keller, J., Day, B., Mecham, M., and Moore, K., "Mechatronic Design and Integration for a Novel Omni-Directional Robotic Vehicle," Mechatronics Conference, Alanta, September 6-9, 2000.

Yamashita, A., Asama, H., Kaetsu, H., Endo, I. and Arai, T., "Development of Step-Climbing Omni-Directional Mobile Robot,"Proceedings of the 3rd International Conference on Field and Service Robotics (FSR2001), Espoo (Finland), June 2001, pp.327-332.

Yu, H., Dubowsky, S., and Skwersky, A., "Omni-directional Mobility Using Active Split Offset Castors," Proceedings ASME Design Engineering Technical Conferences, Baltimore, September 2000.

BIOGRAPHICAL SKETCH

Christopher Fulmer was born in Fort Pierce, Florida, where he received his Associate of Arts degree from Indian River Community College in 1998. He transferred to the University of Florida and graduated with a Bachelor of Science in Mechanical Engineering in the spring of 2001. He then graduated from the University of Florida in August of 2003 with a Master of Science degree in mechanical engineering.